HADRON-NUCLEUS COLLISION

強子－原子核碰撞

by

Ling Siu-ning

(凌兆寧)

A Thesis Submitted In Partial Fulfillment

of the Requirements for the Degree of

Master of Philopsophy in Physics

The Chinese University of Hong Kong

May 1984

Division of Physics

Graduate School

The Chinese University of Hong Kong

Thesis Title: Hadron-nucleus Collision

By: Ling Siu-hing

(凌兆興)

Abstract

The experimental data of the soft processes of hadron-hadron collisions and hadron-nucleus scattering are reviewed. Special attention is paid to the KNO scaling. In hadron-nucleus collisions, the universal KNO scaling at each impact parameter is proposed to explain the multiplicity distribution and the results compare favourably with the experimental data.

TABLE OF CONTENTS

LIST OF FIGURES

Acknowledgements

I would like to express my gratitude towards my supervisor, Dr. K. Young, for his patient and brilliant guidance.

I also wish to thank Prof. D. Kiang for his warm guidence during the course of this project.

The financial support of the Institute of Science and Technology of the Chinese University of Hong Kong is cordially acknowledged.

Abstract

The experimental data of the soft processes of hadron-hadron collisions and hadron-nucleus scattering are reviewed. Special attention is paid to the KNO scaling. In hadron-nucleus collisions, the universal KNO scaling at each impact parameter is proposed to explain the multiplicity distribution and the results compare favourably with the experimental data.

Chapter 1

Introduction

1.1 Scattering

Physics is the study of the structure of matter and their mutual interaction. Hadrons and their strong interaction is one major part in the physical world. Both theories and experimental data are needed in order to understand them. The most important tool to investigate the strong interaction of particles is by scattering. The object of this thesis is to review some basic experimental data and theoretical ideas about high energy hadron-hadron (h-h) collision and hadron-nucleus (h-A) collision. The rest of this chapter gives a brief review of the main tools and concepts in scattering theory. Chapter 2 reviews the h-h collision. Chapters 3 to 5 review the h-A collision where chapter 4 concentrates on the original work concerning universality in KNO scaling in h-A collision and chapter 5 reviews the inclusive h-A process. Chapter 6 will be the conclusion of the thesis.

A typical scattering experiment is as follows. A target (e.g. hydrogen) is struck by a beam of particles (e.g. electrons or protons). Let F be the incident flux, i.e the number of the incident particles crossing per unit time per unit area perpendicular to the direction of

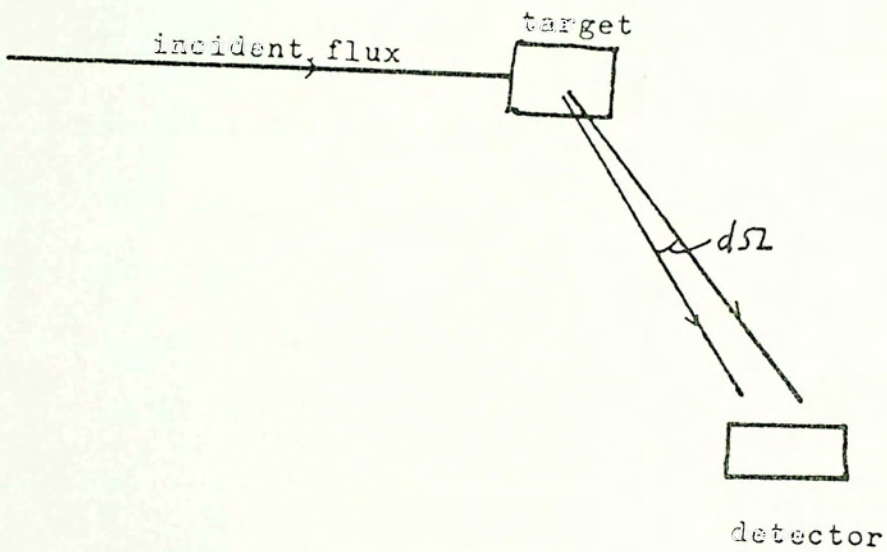

Fig.1.1.1 Typical scattering experiment.

propagation, in a frame at rest with respect to the target (i.e. in the lab frame). What the experimentalist measures is the number dN of particles scattered per unit time into the solid angle $d\Omega$. Obviously dN is directly proportional to the incident flux and the solid angle $d\Omega$ (Fig. 1.1.1).

$$dN = F(d\sigma/d\Omega)d\Omega$$

The proportionality constant $d\sigma/d\Omega$ is the received number per unit solid angle per unit incident flux and has the dimension of area. It is a convenient parameter measuring the probability of the particle being scattered by the target, and is called the scattering cross section of particle by the target in the direction, or for short, the differential cross section.

If there are many types of outgoing particles, $d\sigma/d\Omega$ can be further subdivided into different categories. We shall come back to this later. For the moment we assume that the scattered particle is the same as the incident one.

1.2 Total Cross Section

The total number of particles scattered per unit time is obtained by intergrating over angles.

$$\sigma_T \equiv \int d\sigma/d\Omega \, d\Omega \quad .$$

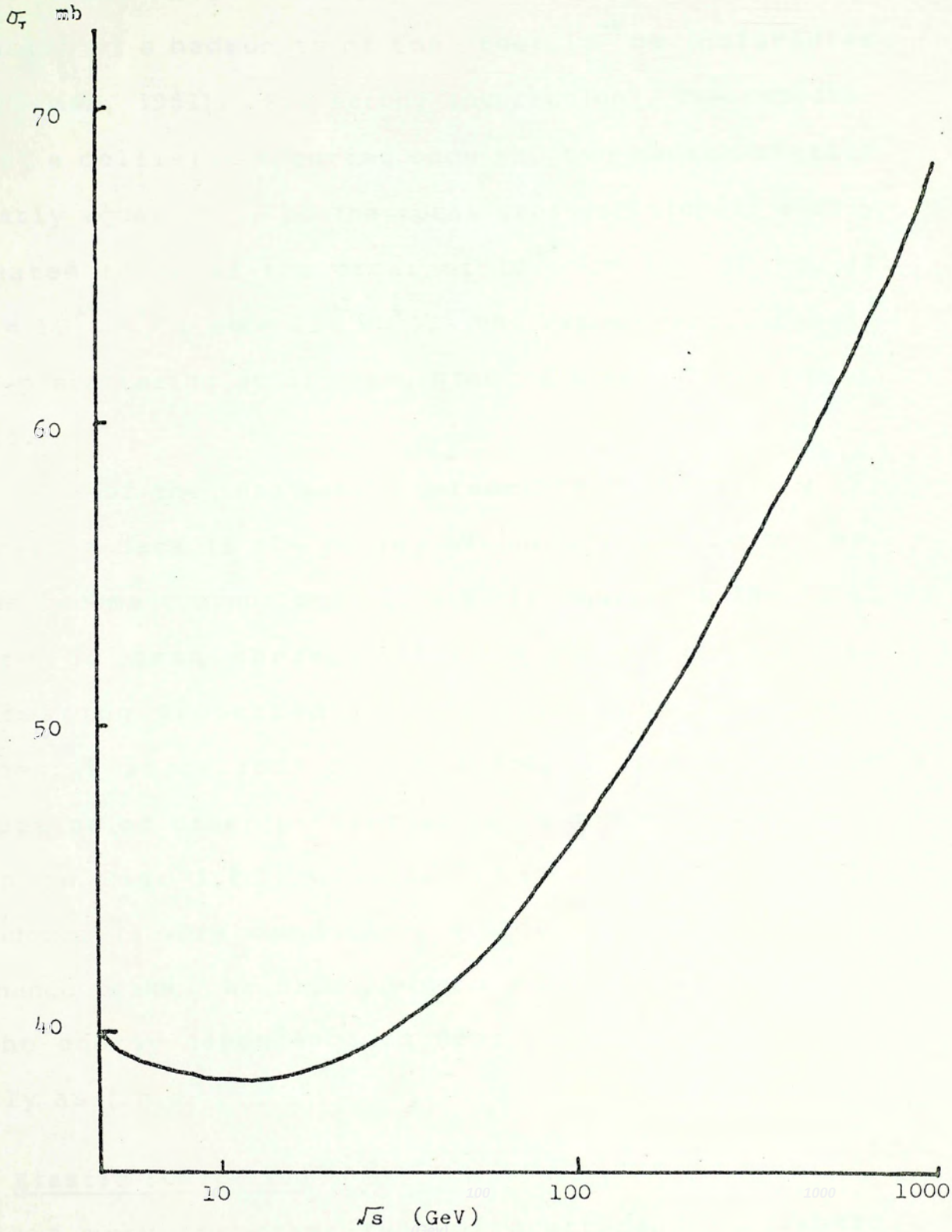

Fig.1.2.1 Experimental data for p-p scattering total cross section at high energies.

is the total cross section. The characteristic linear dimension of a hadron is of the order 10^{-13} cm (Hofstadter and Herman, 1961). For strong interactions, the probability of a collision occuring once the two hadron overlap is nearly equal to 1, so the total cross section is easily estimated to be of the order of 10^{-26} cm^2 i.e. 10 mb. (1 barn = 10^{-24} cm^2, 1 mb = 10^{-27} cm^2). The experimental result for p-p scattering at high energies is about 40 mb. (Fig. 1.2.1).

One of the interesting parameters in describing the scattering data is the energy of the scattering system. It has become conventional to use the square of the total centre of mass energy, denoted by s. It has two interesting properties: it is a Lorentz invariant; besides, $\sqrt{s}$ is related to the energy available for the production of other particles. The s dependence of σ_T is shown in Fig. 1.2.1. Generally speaking, the energy dependence is very complicated at low energies, including resonance peaks. At high energies (above 1 GeV) the curve of the energy dependence is nearly flat and increases slowly as $(\ln s)^2$.

1.3 Elastic Scattering

A very important type of scattering is elastic scattering, i.e. scattering during which the quantum numbers of the scatterer and the target do not change, and there is no energy tranfer to the internal degrees of freedom. For p-p collisions, at a centre-of-mass energy of

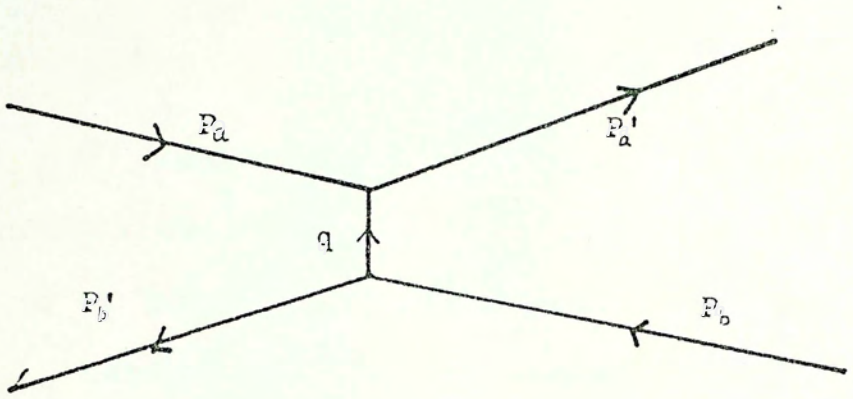

Fig.1.3.1 Kinematics of elastic scattering.

540 GeV the elastic cross section is about 13 mb (Battiston et al., 1982), i.e. about 20% of σ_T . To put it in another way, there is a 20% chance that the proton remains "intact" after a collision.

In general, an elastic collision may be written as

$$a + b \longrightarrow a + b$$

There are two independent parameters to characterize any elastic collision:s and the scattering angles $\Omega = (\theta,\phi)$ However, it is more conveinent to use a Lorentz invariant parament t, called the four momentum transfer square, to replace Ω . If the four momentum before collision are P_a and P_b and after the collision are P_a' and P_b' . (Fig.1.3.1), then the four momentum tranfer q is

$$q = P_a - P_a' = P_b' - P_b$$

and we define

$$t \equiv q^2 = (P_a - P_a')^2 = (P_b' - P_b)^2$$

In the centre of mass frame, we have

$$t = -2p_{cm}^2 (1 - \cos\theta_{cm})$$

where p_{cm} is the three-momentum in the centre of mass frame. Note that in elastic collisions, $t < 0$ because in

the centre of mass frame, there is momentum tranfer but no energy transfer, hence q is space-like, $t = q^2 < 0$. In the lab frame (b at rest), we have

$$t = -2 m_b (E_b' - m_b)$$

If $|t|$ is much smaller than m_b^2, the $E_b' - m_b$ is the kinetic energy in newtonian form, i.e. $p_b'^2 / (2m_b)$. Hence

$$t \cong - (p_b')^2$$

where p_b' is the three momentum of particle b in the lab frame after the scattering. Thus $\sqrt{-t}$ is the magnitude of the three-momentum tranfer.

By the uncertainty principle, $p' \Delta x \sim 1$, where Δx is the charecteristic linear dimension in the target b in the scattering. Therefore larger p_b' probes smaller Δx_b, so deeper structures can be seen. In other words, the "resolution" is controlled by t and is essentially independent of s. For this reason, it is convenient to introduce $d\sigma/dt$ in place of $d\sigma/d\Omega$. They have the followiong relation

$$d\sigma/dt = (\pi/p_{cm}^2) (d\sigma/d\Omega_{cm})$$

1.4 Scattering Amplitude

In quantum theory, a free particle moving in a

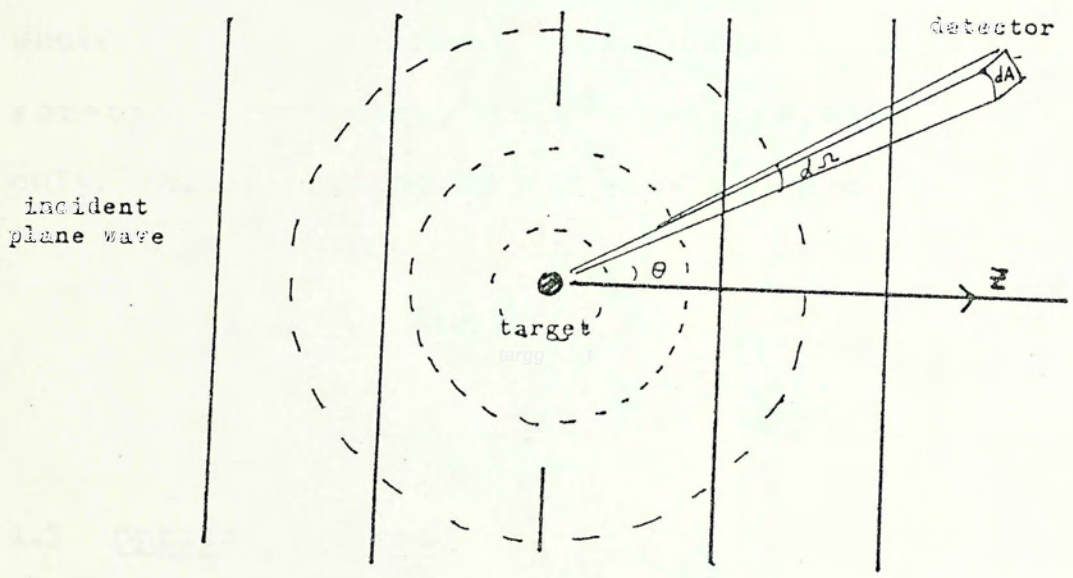

Fig.1.4.1 Scattering wave due to an incident plane wave.

direction, say along the z axis, is described by a plane wave: e^{ikz} . The scattered particles are described at large distances by an outgoing spherical wave $f(\theta,\phi)\, e^{ikr}/r$, as shown in Fig.1.4.1. This holds true in most scattering situations. The number of scattered particle dN in the $\Omega = (\theta,\phi)$ direction is

$$dN = F\left|f(\theta,\phi)/r\right|^2 dA$$
$$= F\left|f(\theta,\phi)\right|^2 d\Omega$$

where F is the incident flux. Usually, such a system has rotational symmetry in ϕ , so $f(\theta,\phi)$ is a function of θ only. After putting $dN / F = d\sigma$ we have

$$d\sigma / d\Omega = \left| f(\theta)\right|^2$$

1.5 Optical Theorem

There is a very important relationship between σ_T and the forward scattering amplitude $f(\theta)$, that is the optical theorem, which states:

$$\mathrm{Im} f(0) = (p/4\pi)\,\sigma_T .$$

Some relation between σ_T and $f(0)$ is expected because the forward scattering amplitude $f(0)$ is related to the probability of that the particle is not scattered, while the

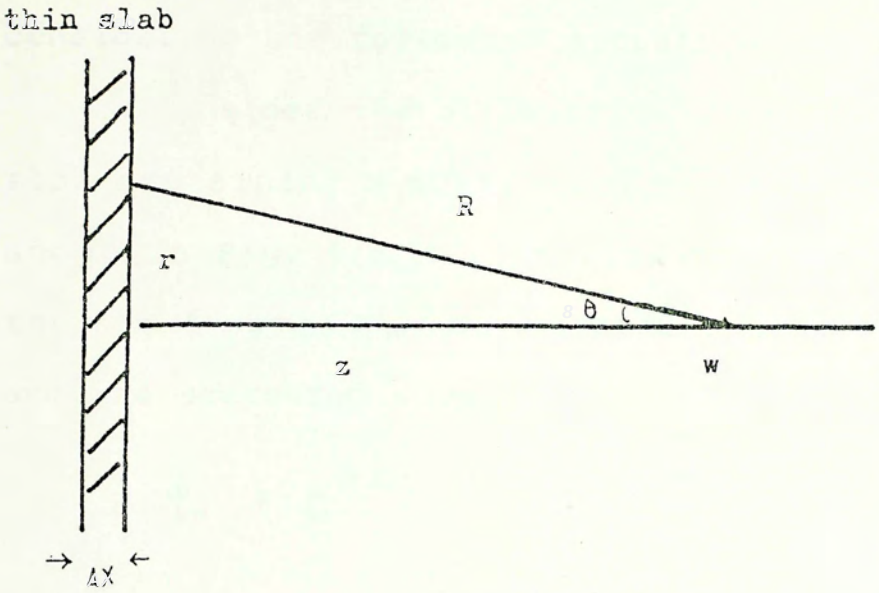

Fig.1.5.1 Geometry of a plane wave scattering by a thin slab.

σ_T measures the probability that the particle is scattered. Since the total probability of finding the particle is 1, hence knowing $f(\theta)$ gives us the information on σ_T. What may be unexpected is that only the imaginary part of $f(\theta)$ comes in. The reason for this can be understood by considering the following situation.

Consider the attenuation of a plane wave by a thin slab containing N scattering centres per unit volume as shown in Fig. 1.5.1. By the principle of superposition, the total wave ψ_w at w is the sum of the incident wave and the scattered wave.

$$\psi_w = e^{ikz} + \int_0^\infty f(\theta) \frac{e^{ikR}}{R} N \Delta x \, 2\pi r \, dr$$

$$= e^{ikz} + 2\pi N \Delta x \int_z^\infty f(\theta) e^{ikR} \, dR$$

For large z, $z \gg r$, $\theta \simeq r/z \ll 1$, we can expand $f(\theta)$ by a Taylor series

$$f(\theta) = f(0) + f'(0)\,\theta + \cdots\cdots$$

then

$$\psi_w \simeq e^{ikz} + 2\pi N \Delta x \int_z^\infty f(0) e^{ikR} \, dR$$

$$= e^{ikz} \left[1 + 2\pi i k^{-1} N \Delta x \, f(0) \right]$$

$$|\psi_w|^2 = 1 - 4\pi k^{-1} N \Delta x \, \mathrm{Im}\, f(0) + \mathcal{O}(\Delta x)^2$$

The attenuation of the amplitude is $1 - |\psi_w|^2$. This is given in term of σ_T as

$$1 - |\psi_w|^2 = \sigma_T N \Delta x$$

Comparing with the above equation, we have

$$\sigma_T = 4\pi k^{-1} \mathrm{Im}\, f(0)$$

which is the optical theorem.

The optical theorem is particularly useful in high energy elastic scattering because in this case, the scattering amplitude is nearly pure imaginary, so σ_T tells us everything about the forward scattering.

1.6 Relation between $\frac{d\sigma}{dt}$ and σ_T

Together with the optical theorem and the relation

$$\frac{d\sigma}{d\Omega} = |f(\theta)|^2$$

we have

$$\left(\frac{d\sigma}{d\Omega}\right)_{\theta=0} = |f(0)|^2 = |\mathrm{Im}\, f(0)|^2 [1 + \alpha^2]$$

where α = Ref(0)/Imf(0) is small. That is

$$f(0) = (i + \alpha)\, \mathrm{Im}\, f(0)$$

For $|\alpha| \ll 1$

$$\left(\frac{d\sigma}{d\Omega}\right)_{\theta=0} \sim |\mathrm{Im}\, f(0)|^2$$

$$\left(\frac{d\sigma}{dt}\right)_{\theta=0} = \frac{\pi}{P_{cm}^2}\left(\frac{d\sigma}{d\Omega_{cm}}\right)_{\theta=0}$$

$$\simeq \frac{\sigma_T^2}{16\pi}$$

Chapter 2

Hadron-hadron Collision

2.1 Elastic Scattering

In hadron-hadron collisions, the experimental result suggests that for small $|t|$, $|t| < 0.1$ (GeV/c), the cross section is well parametrized by

$$\frac{d\sigma}{dt} = A\, e^{-b|t|}$$

For p-p collision at $\sqrt{s}$ =53 GeV, A = 100 mb, b= 12.4 $(GeV/c)^{-2}$, as Fig. 2.1.1 shows. However the slope parameter b changes into 10.8 $(GeV/c)^{-2}$ at larger t (Giacomelli and Jabcob, 1979). Such double-slope structure is still not completely understood.

The dimension of the slope parameter b is $(GeV/c)^{-2}$. In units with $\hbar$=1, the dimension of b is that of area. Since in this system, the only characteristic dimension of area is the square of the linear characteristic dimension R of the target, so we can interpret $b = R^2$.

In quantum mechanics, particles have wave properties. In analogy to diffraction in optics, the incident particle can diffract into the shadow region of the target and form a diffraction pattern (Fig. 2.12). In diffraction, the angle for the first minimum is $\theta = \lambda / R$, so the momentum tranfer is $\theta p = \theta/\lambda = 1/R$, and the square of momentum tranfer is $1/R^2$. Now we return to the parametrization of $d\sigma/dt \propto e^{-b|t|}$ which shows a typical $t = 1/b$. Since $t = 1/R^2$,

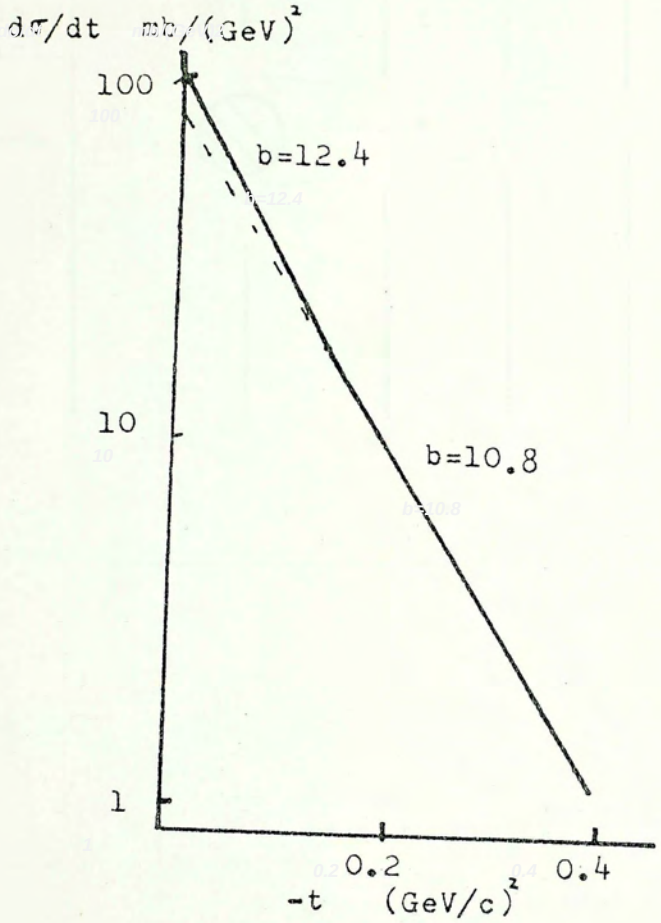

Fig.2.1.1 Elastic scattering for p-p at $\sqrt{s}$ = 53 GeV and b is in unit of GeV^{-2}

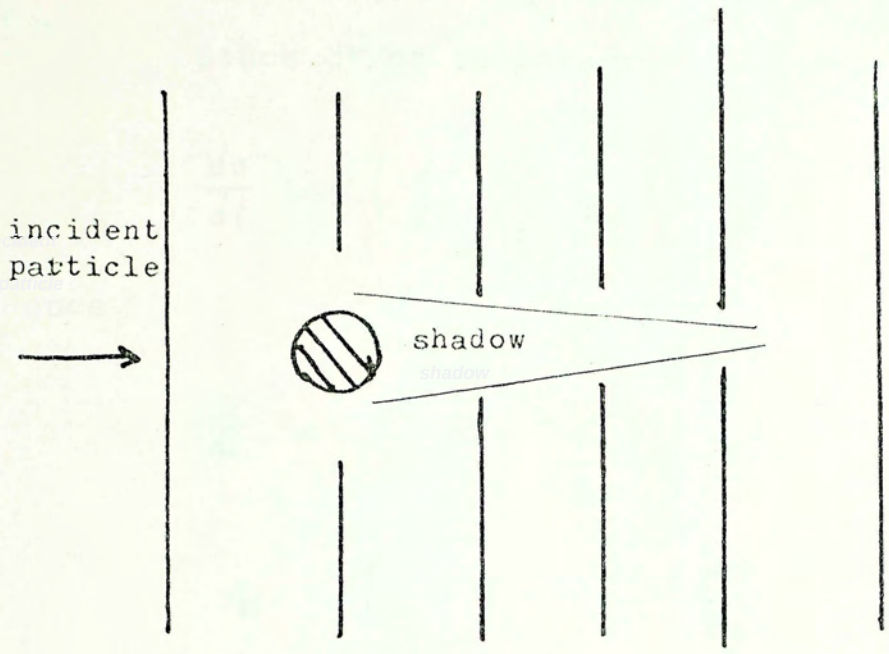

Fig.2.1.2 Shadow scattering

we have $b=R^2$, which justifies our dimensional argument. In general, the geometrical optical model gives us a satisfactory picture consistant with the experimental data of elastic scattering at high energies.

Since $d\sigma/dt$ is parametrized as

$$\frac{d\sigma}{dt} = \left(\frac{d\sigma}{dt}\right)_{t=0} e^{-b|t|}$$

Hence

$$\frac{d\sigma}{dt} = \frac{\sigma_T^2}{16\pi} e^{-b|t|} (1+\alpha^2)$$

$$\sigma_{el} = \int_0^{-\infty} \frac{d\sigma}{dt} dt = \frac{\sigma_T^2}{16\pi b} (1+\alpha^2)$$

This gives us an important constraint between σ_{el}, σ_T and b.

2.2 Energy dependence of σ_T, α, b, etc

The energy dependence of σ_T (s) in p-p collision is shown in Fig. 1.2.1 (Giacomelli and Jacob, 1979). The total cross section σ_T increases as

$$\sigma_T = 38.4 + 0.49 \ln^2\left(\frac{s}{122\,(GeV)^2}\right) \quad (mb)$$

In the framework of present theories, σ_T cannot rise faster than $(\ln s)^2$ at asymptotic energies. That is the so-called Froissart bound. The experimental data shows that σ_T reaches the bound.

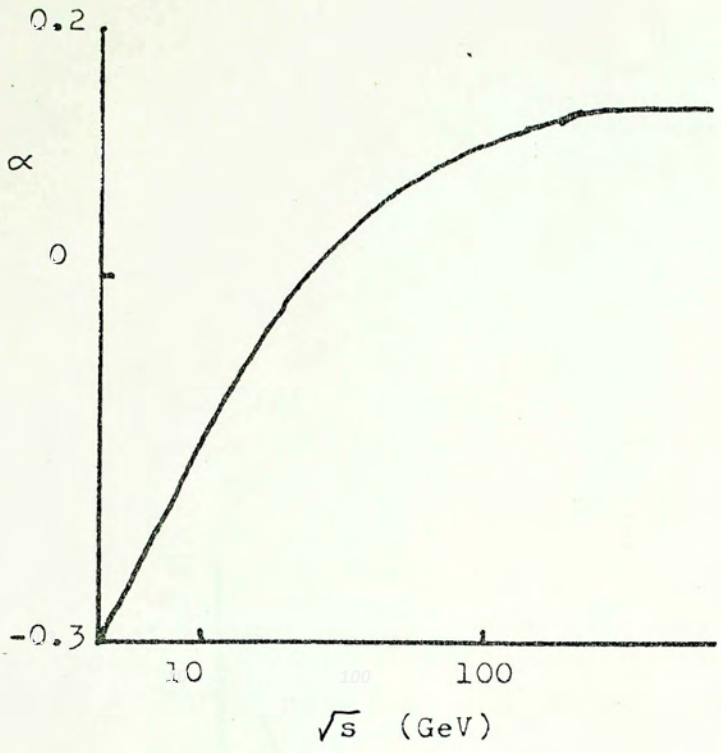

Fig.2.2.2 Energy dependence of ∝ for p-p collision

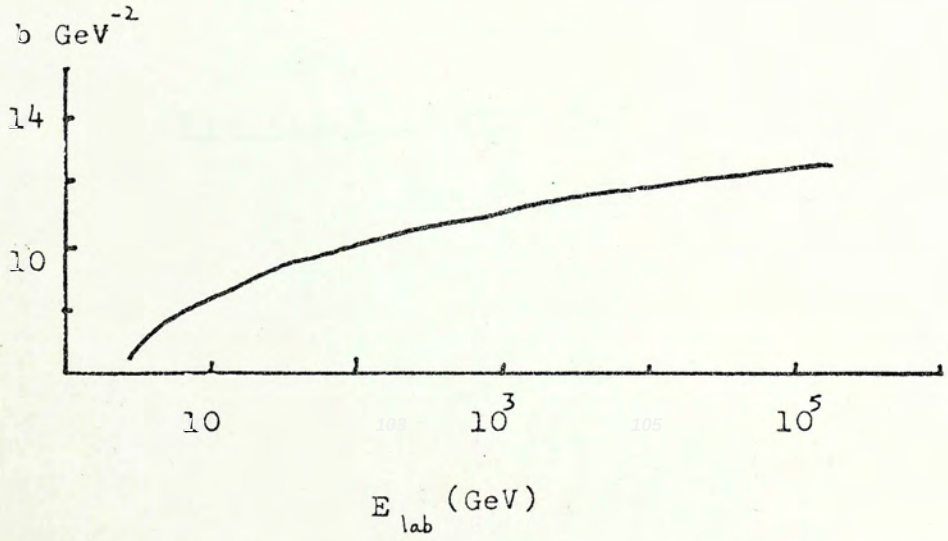

Fig.2.2.3 Energy dependence of slope parameter b for p-p collision.

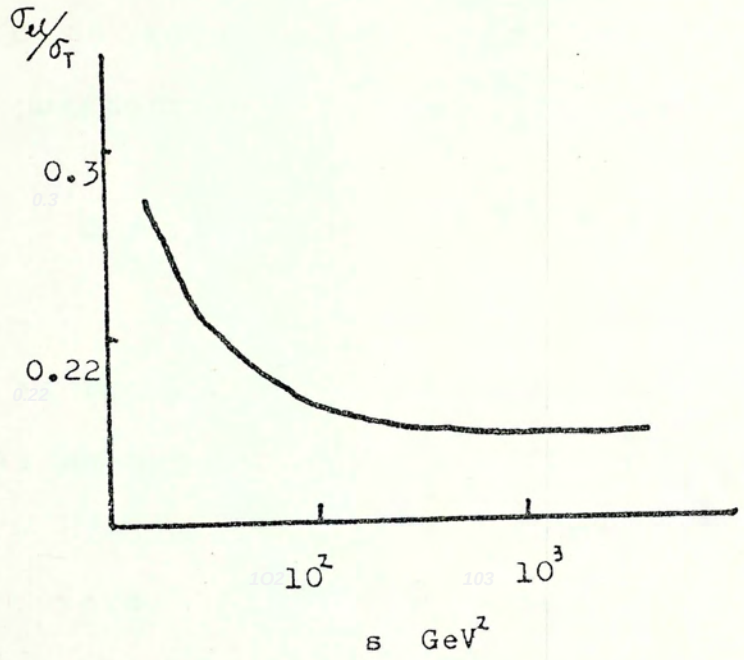

Fig.2.2.4 Energy dependence of σ_{el}/σ_T for p-p collision

As Fig. 2.2.2 shows $\alpha(s)$ increases with energy. It is fitted as (Giacomelli and Jacob, 1979)

$$\alpha_{pp} = -(0.490 \pm 0.034) + (0.076 \pm 0.006) \ln s$$

up to $\sqrt{s}$ = 53 GeV, where s is in $(GeV)^2$.

The energy dependence of the slope parameter b(s) is found to be logarithmic as shown in Fig. 2.2.3. It is usually parametrized as (Giacomelli and Jacob, 1979)

$$b = 8 + (0.556 \pm 0.026) \ln s$$

where s is in $(GeV)^2$, b is in $(GeV/c)^{-2}$.

At asymptotic energies, the analyticity and crossing symmetry of the forward scattering amplitude forces α to approach zero. Since $\sigma_{el} \cong \sigma_T^2/b$ and at present energies, experimental data show that $\sigma_T \propto (\ln s)^2$, $b \propto \ln s$, hence $\sigma_{el} \propto (\ln s)^3$ which will eventually be larger than σ_T, and this is impossible. Therefore we can see that we have not arrived at the asymptotic energy range yet.

It is interesting to observe the energy dependence of σ_{el}/σ_T. The behavior of σ_{el}/σ_T is shown in Fig. 2.2.4. It seems that σ_{el}/σ_T approaches a constant at high energy (Baksay et al., 1978). However, Yang (1983) claimed that σ_{el}/σ_T still increases with σ_T, hence increases with energy at the present energy range, as Yang's model predicts. Whether σ_{el}/σ_T is really a constant will be checked by further experiments.

2.3 Geometrical Model

A geometric model for hadron scattering was proposed by Chou and Yang (1967). The basic philosophy is that when two particles with small wavelengths collide at impact parameter b , the wave function is absorbed by a factor $e^{-\Omega(b)}$, where $\Omega(b)$ is called the blackness, a measure for absorption. Therefore the scattered wave for the elastic case is $1-e^{-\Omega}$. The scattering amplitide is then found to be

$$f(\theta,\phi) \simeq \frac{ik}{2\pi} \int e^{ik\cdot b} \left(1 - e^{-\Omega(b)}\right) d^2b$$

which is the so-called the eikonal approximation. Therefore the differential cross section is written as

$$\left(\frac{d\sigma}{dt}\right)_{el} = \frac{1}{4\pi} \left| \int e^{ik\cdot b} \left(1 - e^{-\Omega(b)}\right) d^2b \right|^2$$

In addition, $\Omega(b)$ is related to the matter distribution inside the particle. In p-p scattering, $\Omega(k)$ is written as $KG_E(k)$. where $\Omega(k)$ is the 2-dimensional Fourier transform of $\Omega(b)$ and $G_E(k)$ is the electric form factor of the proton. What $G_E(k)$ tells us is the charge distribution in the proton. Therefore the blackness is assumed to be simply related to the charge distribution. The parameter K is to be adjusted so that the total cross section σ_T is equal to the imaginary part of the forward scattering amplitude, as the result of optical theorem

$$\sigma_T = 2 \int \left(1 - e^{-\Omega}\right) d^2b$$

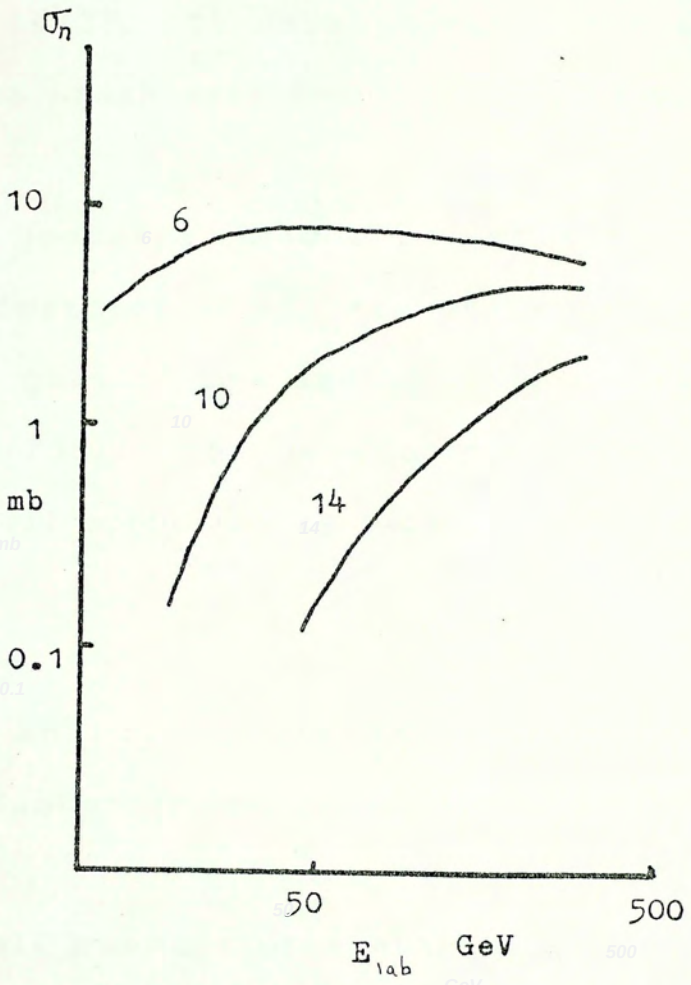

Fig.2.4.1 Energy dependence of the topological cross section (Whitemore, 1974).

since $\Omega(b)$ is assumed to be real.

With the discovery of the increasing total cross section the parameter K becomes a function of energy K(s).

Such a model provides a good description of the elastic differtial cross section in the small |t| region, $|t| < 1.2$(GeV/c)(Kac, 1973). It also predicts the existence of minima and maxima which were found in CERN experiments (Böhm et al., 1974).

Although geometric model is not the only model in describing the features of elastic cross section in hadron scattering, and many of its assumptions are controversial (Saleem et al., 1981), the geometrical aspects in hadron scattering are well supported by experiments.

2.4 Multiplicity

In high energy collisions, many particles are produced. The number of particles produced increases with energy.

In a bubble chamber or spark chamber, it is easy to observe the number of charged particles coming out after the collsion. The number of charged prongs is called the charge multiplicity, n. The probability for the production of final states with n charged prongs is called the topological cross section σ_n. The energy dependence of the topological cross sections is shown in Fig. 2.4.1. As the energy increases, σ_n for large n rise comparative quickly and flatten out. That is, as energy grows, the inelastic cross

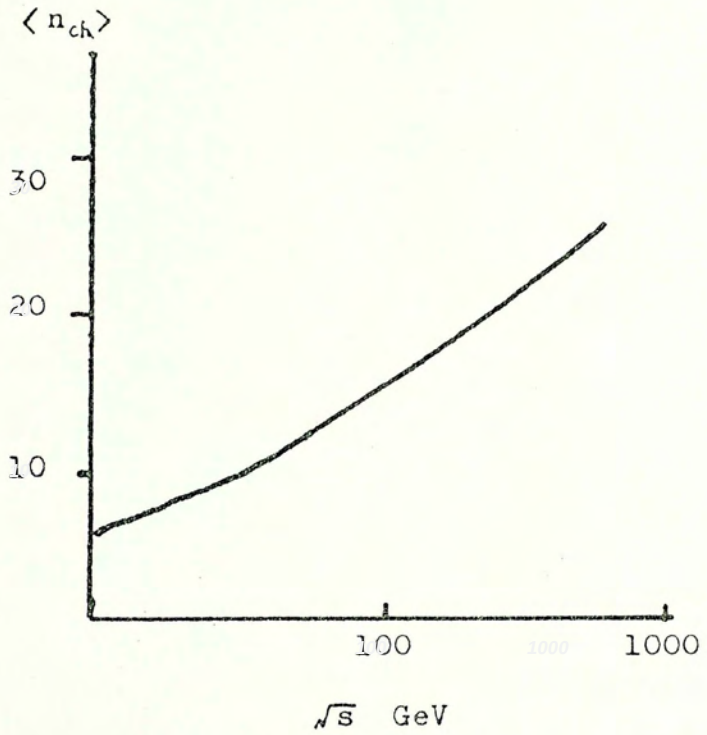

Fig.2.4.2 Energy dependence of average charge multiplicity for p-p collision

section is mainly made up by larger n topological cross sections.

One may define the average multiplicity as

$$\langle n \rangle \equiv \frac{1}{\sigma_T} \sum n \sigma_n$$

but it is more common to use

$$\langle n \rangle = \frac{1}{\sigma_{in}} \sum_{in} n \sigma_n$$

where $\sigma_{in} = \sigma_T - \sigma_{el}$ is called the inelastic cross section and the sum extends only over inelastic events. The difference is that one excludes from σ_T the elastic contribution and normalizes to the inelastic cross section. The energy dependence of $\langle n \rangle$ for p-p collision is shown in Fig. 2.4.2, and parametrized as (Thomé et al., 1977)

$$\langle n \rangle = (0.88 \pm 0.10) + (0.44 \pm 0.05) \ln s + (0.118 \pm 0.006) (\ln s)^2$$

where s is in $(\text{GeV})^2$.

2.4.1 Multiplicity Distribution

What we want to learn in the multiplicity distribution is the probability distribution of n particle production. It is common to define

$$P_n = \frac{\sigma_n}{\sigma_{in}}$$

as the probability for n particle production. It is easy to check that

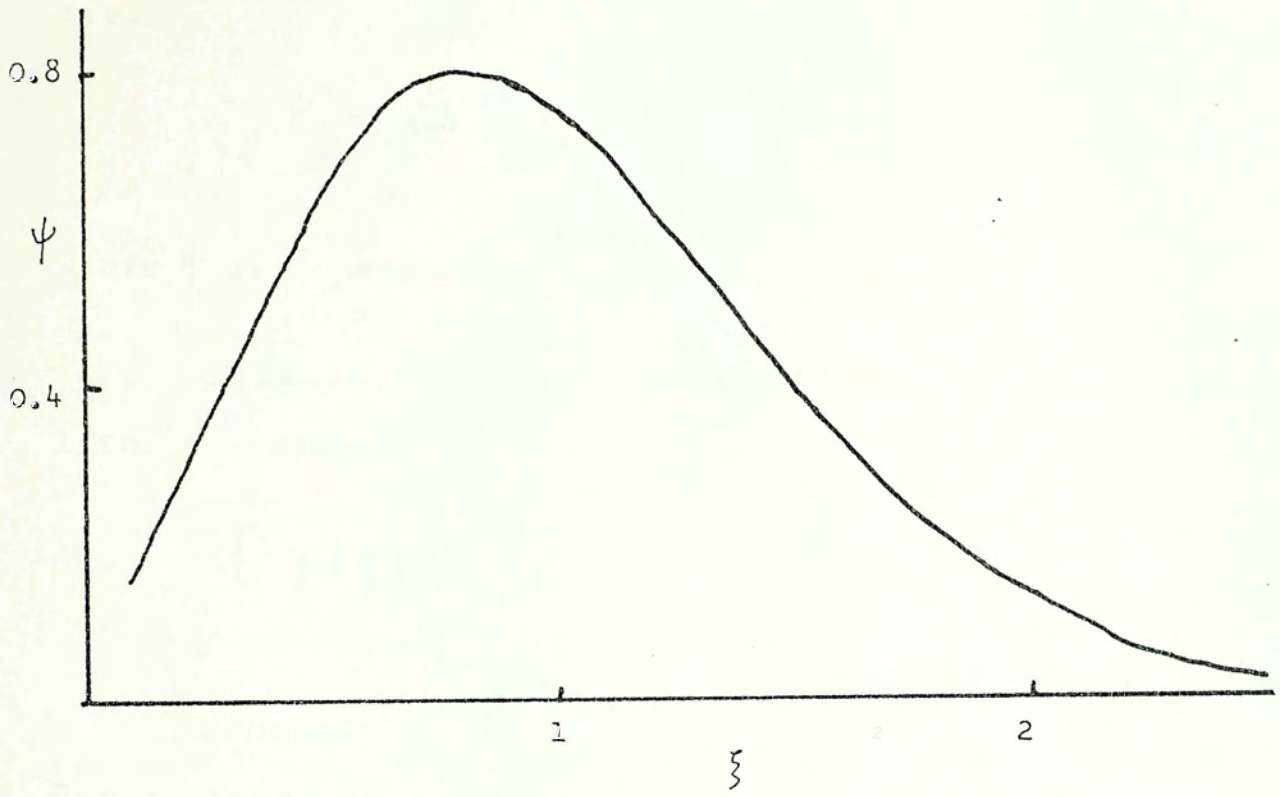

Fig.2.4.3 Shape of KNO function.

$$\sum_{n}^{n} P_n = \frac{\sum^{n} \sigma_n}{\sigma_{in}} = 1$$

Koba, Nielsen and Olesen (1972) proposed that in the high energy limit, $s \to \infty$, $\langle n \rangle P_n$ is only a function of $n / \langle n \rangle$ i.e.

$$P_n = \frac{1}{\langle n \rangle} \Psi \left(\frac{n}{\langle n \rangle} \right)$$

where Ψ is independent of s

This is what so-called "KNO scaling". The factor $1/\langle n \rangle$ is inserted such that

$$\int \Psi(\xi) \, d\xi = 1$$

Recently experiments at the ISR ($\sqrt{s}$ = 53 GeV) and the $\bar{p}$-p collider at CERN ($\sqrt{s}$ = 540 GeV) seem to support the KNO scaling. The graph of Ψ is shown in Fig. 2.4.3. (Slattery,1972). The theoretical ground for such scaling is still unclear and whether such scaling really exists as an exact statement is still in question. However it is beneficial to consider photon emission cases parallel to the hadron emission cases. In some photon emission cases (Lam and Walton, 1983), the photons are emitted independently. The probability of producing one extra photon is $\lambda(E)dE$, and the probaility of producing two or more photons is zero. Hence the increment of $P_n(E)$, $\Delta P_n(E)$, is due to $\lambda(E) P_{n-1}(E) \Delta E$ and the decrease of $P_n(E)$ is due to $\lambda(E) P_n(E) \Delta E$. Therefore

$$\Delta P_n(E) = \lambda(E)\,\left(P_{n-1}(E) - P_n(E)\right)\Delta E$$

$$\frac{d P_n(E)}{d E} = \lambda(E)\,\left(P_{n-1}(E) - P_n(E)\right)$$

With inital condition $P_n(0) = \delta_{n0}$, the solution is the Poisson distribution, that is

$$P_n(E) = e^{-\langle n\rangle}\,\frac{\langle n\rangle^n}{n!}$$

In the high energy limit, $\langle n\rangle \to \infty$, the distribution has the KNO form

$$P_n = \frac{1}{\langle n\rangle}\,\psi$$

but ψ has zero width

$$\psi = \delta\left(1 - \frac{n}{\langle n\rangle}\right)$$

Such a behaviour is due to the fact that at large $\langle n\rangle$, the probability of fluctuations with $\Delta n \sim \langle n\rangle$ is very small.

In hadronic processes, the KNO distribution is much wider. It is suggested that each gluon emits new gluons. Thus fluctuations with $\Delta n \simeq 1$ at the early stage of the cascade development will give birth to large n and lead to a wider KNO fuction (Gribov et al., 1983; Lam and Walton, 1983).

After considering such effect, Lam and Walton (1983) tried to generalize the stochastic equation of the photon emission cases for large n as

$$\frac{dP_n(E)}{dE} \simeq \sum_{k=1} \lambda_k(E) \left[(n-k) P_{n-k}(E) - n P_n(E) \right]$$

The main difference between the photon cases and the hadron cases is that in hadron cases, there is multiplicity n associated with $P_n(E)$. Hence the physics of cascade development is put in.

However further experiment is required to verif whether such scaling really exists as an exact statement.

2.5 Inclusive Processes

Although the many body final states is one major part of high energy collision, the individual final states are harder to analyse because it is difficult to determine experimentally that the final state particles observed in the detectors are in fact the only particles produced.

Because of the above problem, it has become useful to concentrate on processes in which a given particle or set of particles is found to occur in the final state, but nothing is asked about all the other particles which may also be present in this final state. Such processes are called inclusive processes. For example, the reaction

$$P + P \longrightarrow P + X$$

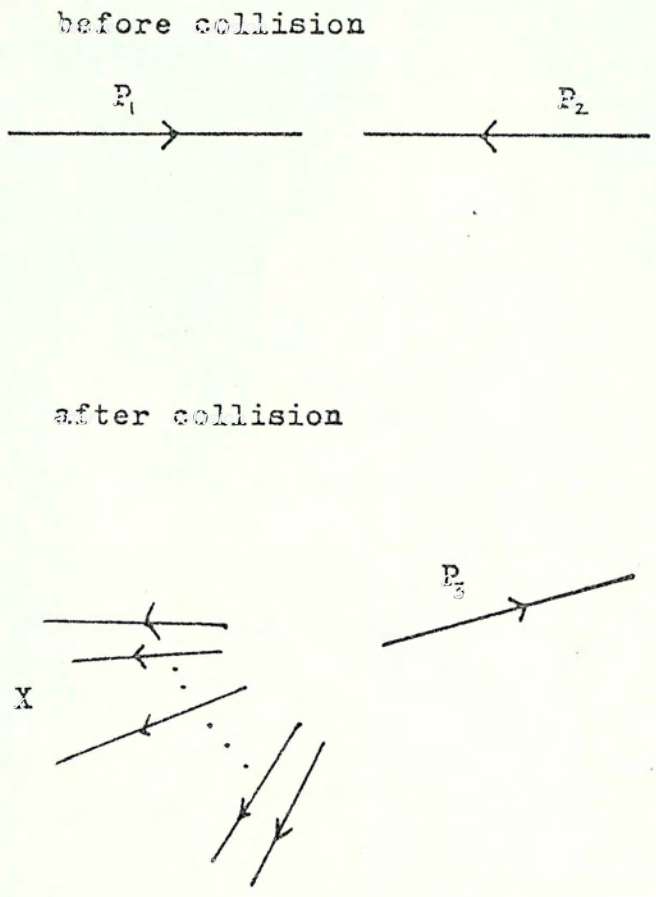

Fig.2.6.1 Kinematics of one particle inclusive process.

2.6. Some Kinematic Variable of One Particle Inclusive Process

We consider the process shown in Fig. 2.6.1. There are two frequently used variables. One of these is the Feynman variable x (Feynman, 1969)

$$x \equiv \frac{P_L^*}{P_{L\,max}^*} \simeq \frac{2P_L}{\sqrt{s}}$$

where * indicates that the value is taken in the centre of mass frame and $P_{L\,max}^*$ is the maximum momentum that particle 3 can have. Thus the range of x is obviously

$$-1 \leqslant x \leqslant 1$$

The other commonly employed variable is the rapidity y defined by DeTar (1971).

$$y \equiv \frac{1}{2} \ln \left(\frac{E + P_L}{E - P_L} \right)$$

Then

$$\sinh y = P_L / m_T \quad , \quad \cosh y = E / m_T$$

where m_T is the tranverse mass of particle 3

$$m_T^2 = m^2 + P_T^2 C^2$$

so the 3-momentum of particle 3 is

$$P = (m_T \cosh y \, , \; P_T \, , \; m_T \sinh y)$$

This variable has the advantage that under a longitudinal Lorentz boost by v = c, y is increased by a constant.

$$y' = y + \frac{1}{2} \ln \left(\frac{1+\beta}{1-\beta} \right)$$

If $\beta << 1$

$$y' = y + \beta$$

so in the non-relativistic limit, $\beta << 1$, rapidity is just velocity. But unlike velocites, rapidities simply add even relativistically. This means that in different inertial frames, the final state particle distributions in rapidity have the same shape, only the origin shifts. Therefore it is very convenient to use rapidity to analyse data.

Unlike Feynman x, the range of rapadity is not fixed at different energies. In the centre of mass frame

$$y = \frac{1}{2} \ln \left(\frac{E + P_L}{m_T^2} \right)$$

The extreme values are $E \sim \sqrt{s}/2$, $P \sim \pm \sqrt{s}/2$. Hence

$$Y_{max} = (1/2) \ln (s/m_T^2)$$

The range of y is simply $2y_{max} = \ln (s/m_T^2)$. Therefore the range of y is linear in ln s.

For small transverse momenta in high energy processes, $E \sim P$, $m_T^2 \sim p^2$

$$y \sim \ln (2P_L / P_T) = - \ln (\tan \theta^*/2) \equiv \eta_3$$

where η_3 is called the pseudo-rapidity and θ^* is the angle

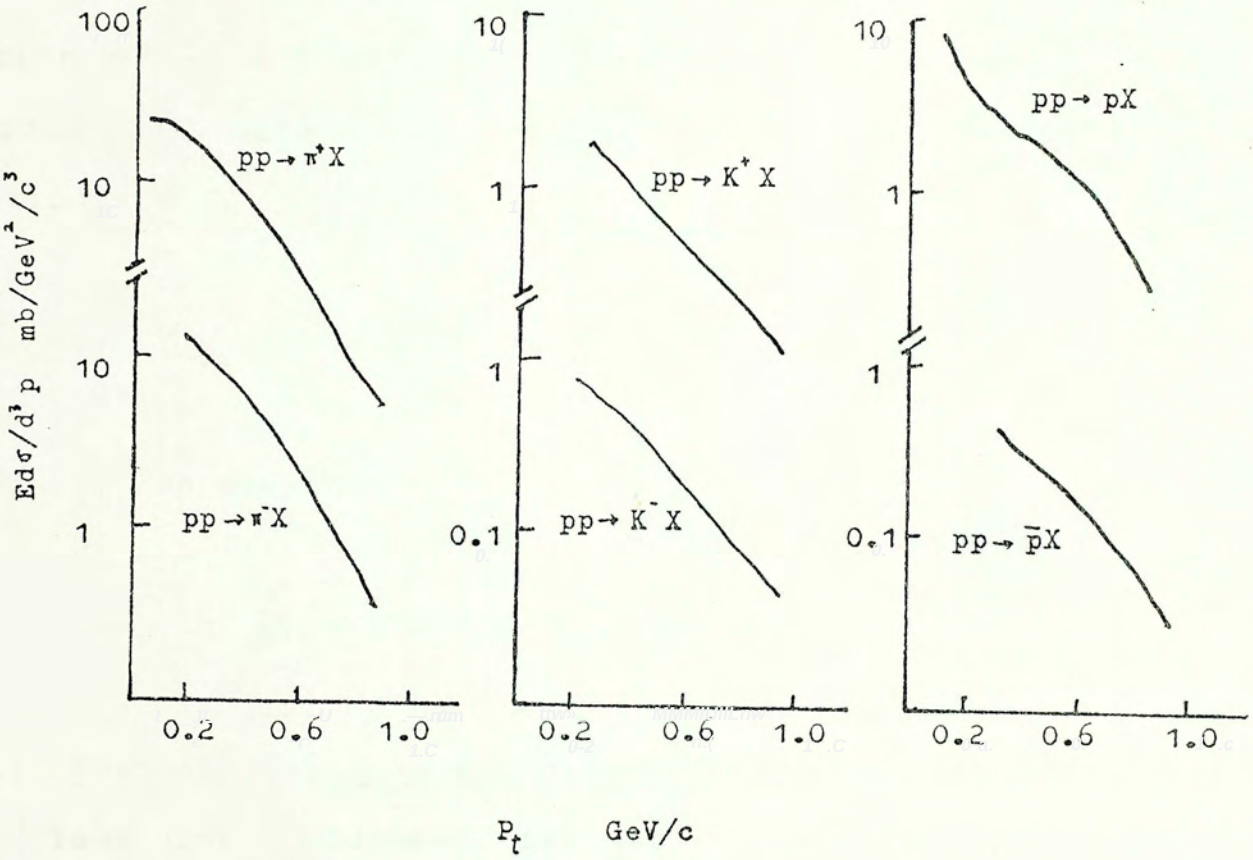

Fig.2.7.1 The invariant cross section vs P_t at $x=0.15$, for different channels and energies ($\sqrt{s}$: 23 to 53 GeV), which indicate approximate Feynman scaling and limited transverse momentum.

where η_3 is called the pseudo-rapidity and θ_3^* is the angle in centre of mass frame.

This representation of y in terms of angle is convenient for experimentalists who can measure the angle but not the momentum. For many cases, rapidity and pseudorapidity are regarded as the same thing.

2.7 The One Particle Inclusive Cross Section

It is well known that the differential cross section $d\sigma$ and d^3P/E are Lorentz invariants so it is natural to define a Lorentz invariant momentum distribution

$$f(p_\perp , p_\parallel , s) = E\, d\sigma /d^3p = E\, d\sigma / \pi\, dp_T^2\, dp$$

Using Feynman variable x

$$f(p_\perp , x, s) = E\, d\sigma /\pi\, p^*_{max}\, dp_\perp^2\, dx$$

2.7.1 Feynman Scaling and Limiting Fragmentation

Yang (1969) proposed that the emitted particles are the result of the fragmentation of two original particles; the target fragmentation and the projectile fragmentation. The probability of producing particle 3 with momentum p is independent of s for sufficiently high s. This is called limiting fragmentation. Therefore the inclusive distribution reaches a limiting value for fixed x as s increases. That is

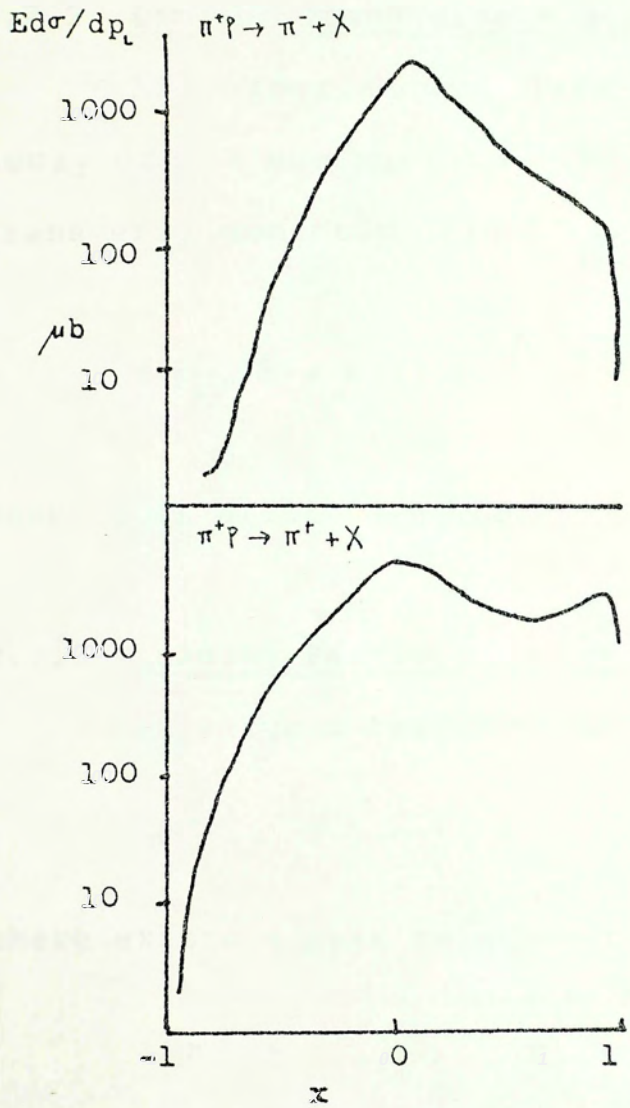

Fig.2.7.2 Edσ/dp$_L$ vs x for leading particle channel $\pi^+p \rightarrow \pi^+X$ and other channel $\pi^+p \rightarrow \pi^-X$. Leading particle effect is well illustrated.

$$f(p_\perp, x, s) \cong f(p_\perp, x)$$

This is called Feynman scaling. Experimental data show that at high energies, the scaling roughly holds when the ln s dependence is ignored (Fig.2.7.1)(Bertin et al., 1972; Thomé et al., 1979).

2.7.2 Limited Transverse Momentum

All experimental data show a strong exponential decay of the one particle inclusive cross section in the transverse momentum (Fig.2.7.1)so $f(p_\perp, x)$ is written as

$$f(p_\perp, x) = A(x)\, e^{-a p_\perp}$$

where a is around 4-6 $(GeV)^{-1}$ (Bertin et al., 1972).

2.7.3 Leading Particle Effect

In large x region of the collision,

$$\pi^+ + P \longrightarrow \pi^+ + X$$

there exists a peak relative to

$$\pi^+ + P \rightarrow \pi^- + X$$

This implies that the incident particle tends to preserve its inital momentum. Hence there tends to be a particle in the final state identical to the particle in the inital state. This is called the leading particle effect. It is well illustrated in Fig. 2.7.2 (Beaupre et al., 1971).

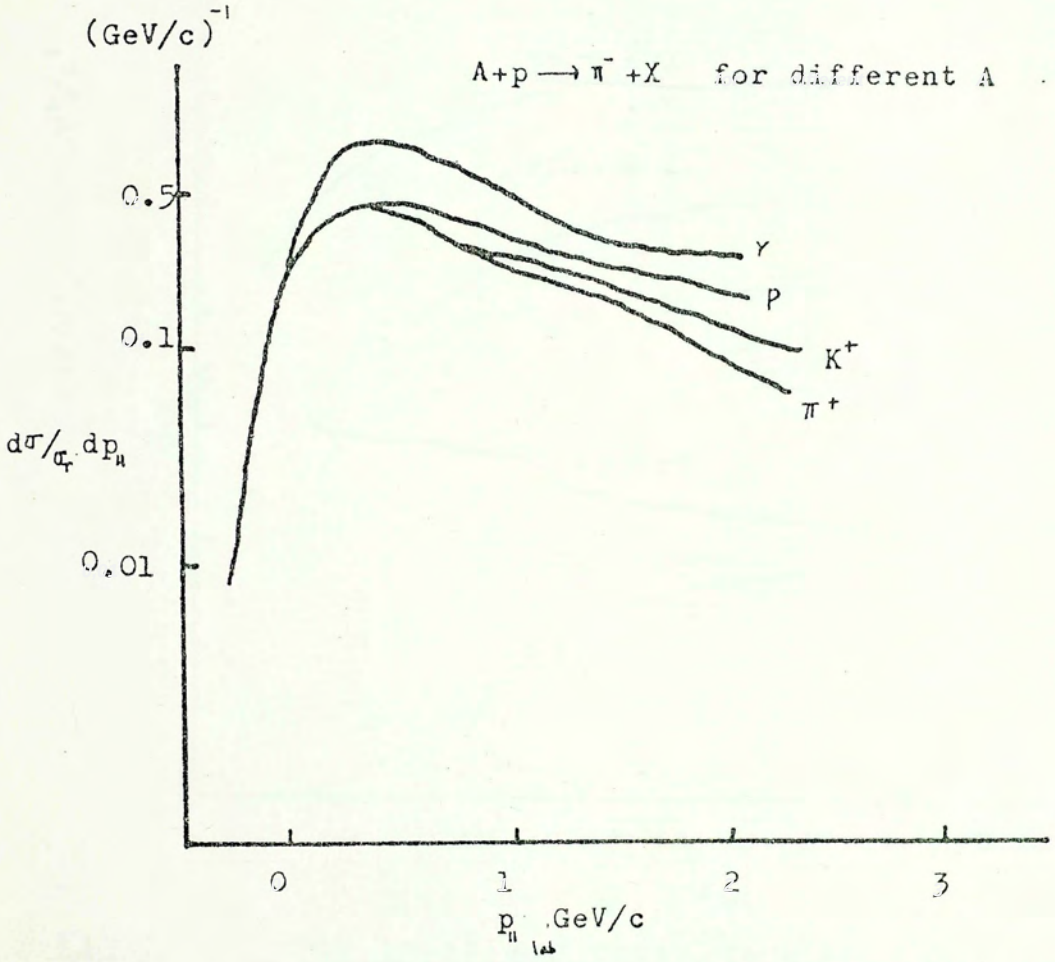

Fig.2.7.3: The inclusive distribution vs $p_{\parallel lab}$ showing that the target fragmentation region is independent of the projectile

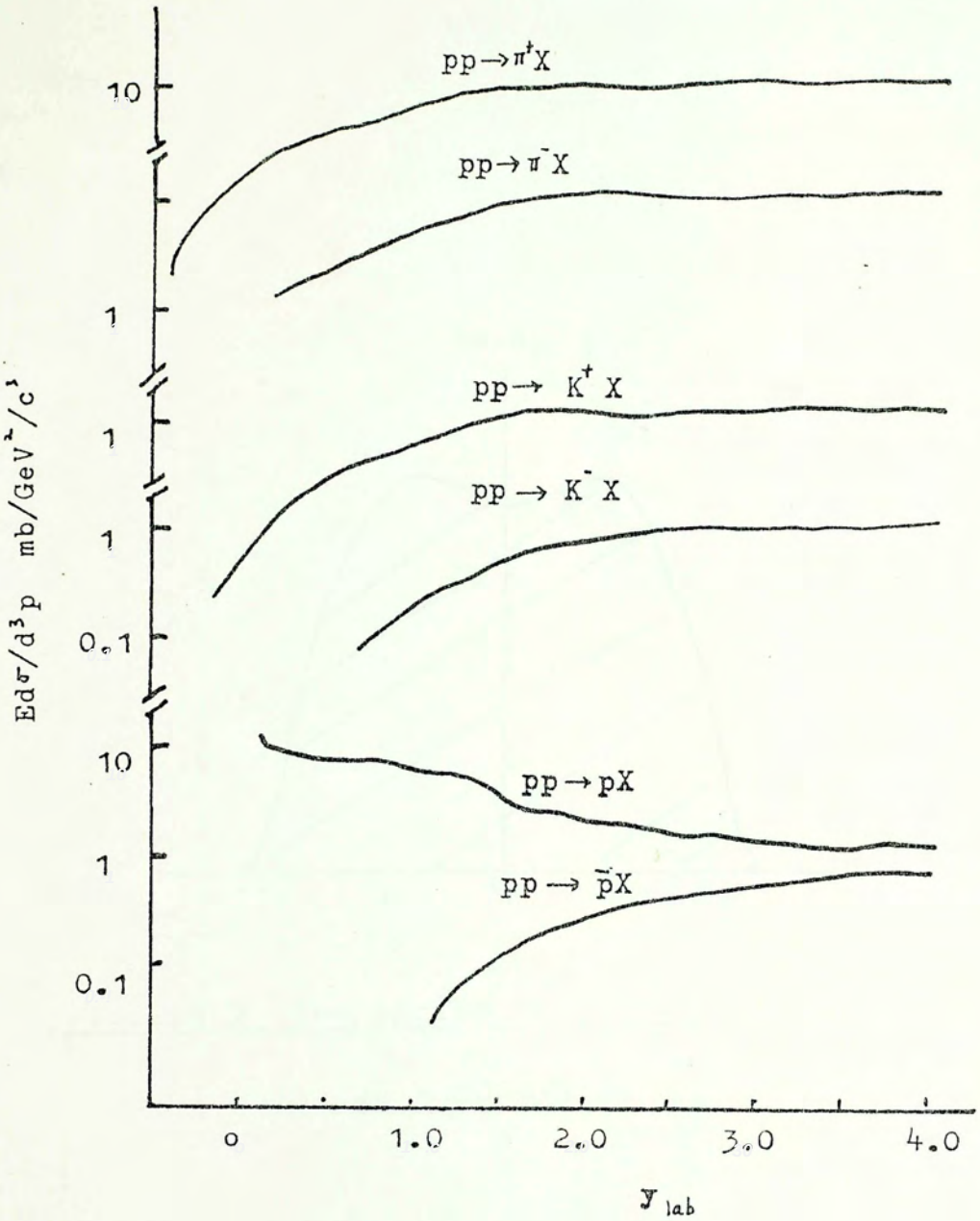

Fig.2.8.1 The invariant cross section for π^+, π^-, K^+, K^-, p and $\bar{p}$ production vs y at p_t = 0.4GeV/c.

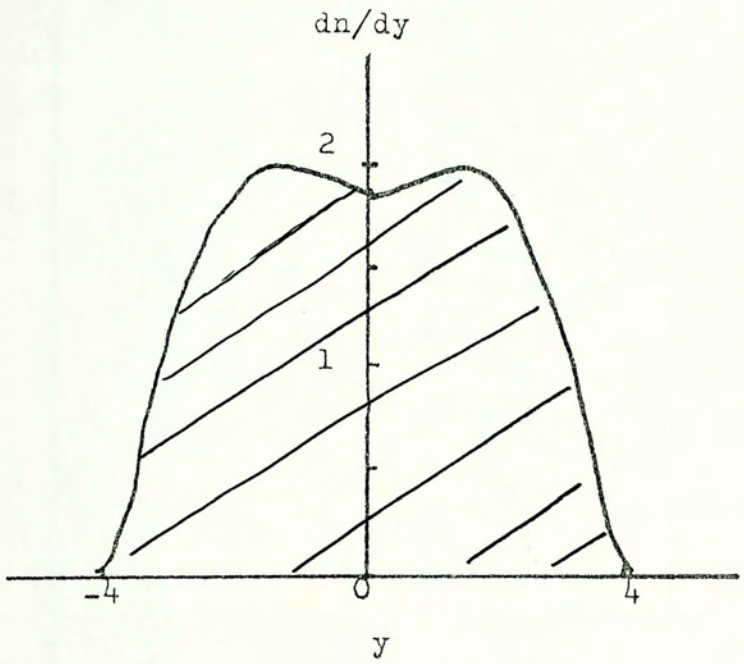

Fig.2.8.2 The inclusive rapidity distribution for $\sqrt{s}$ = 53GeV.

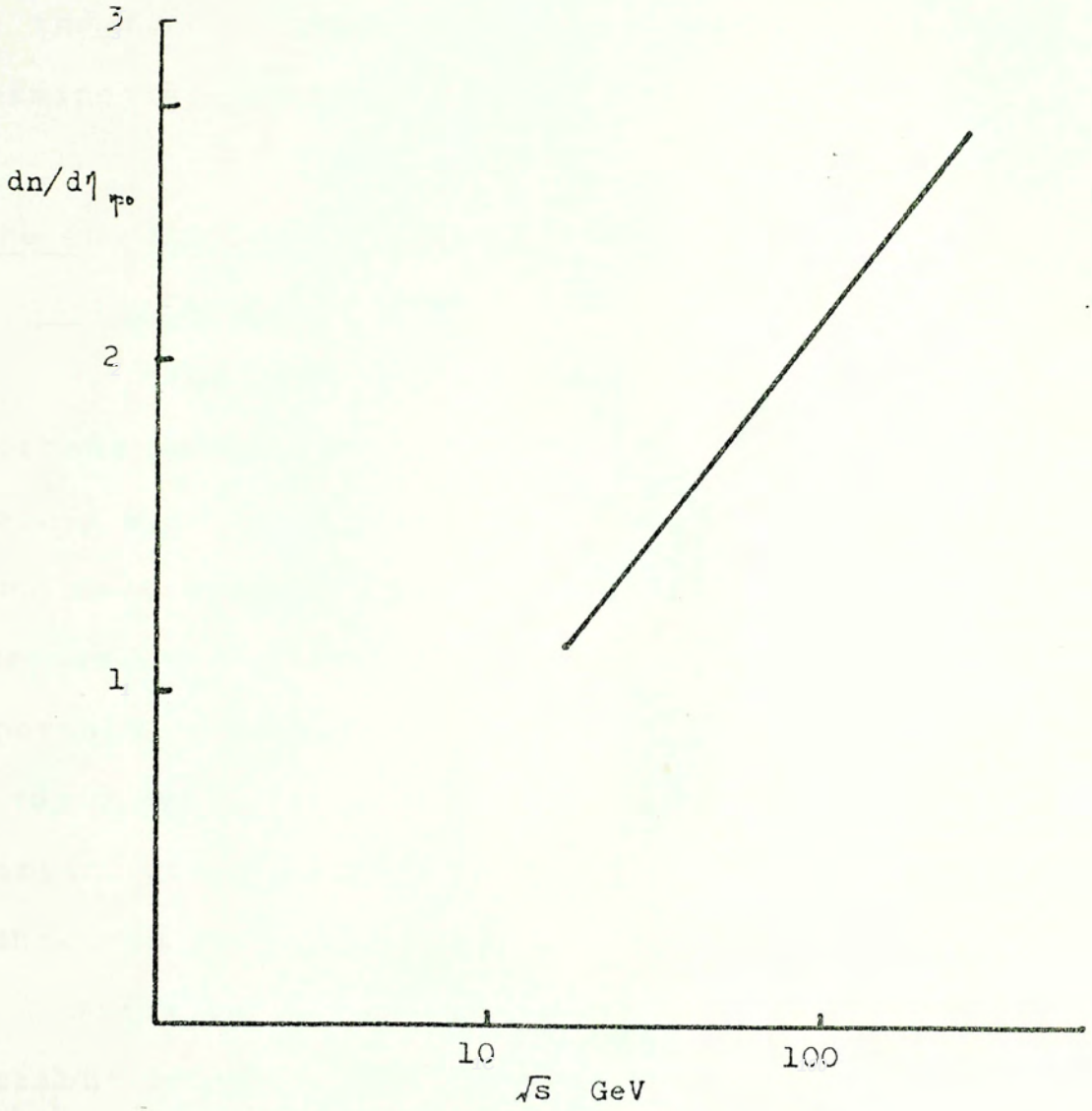

Fig.2.8.3 The energy dependence of the height of the plateau.

2.7.4 Factorization

In the target fragmentation region, $p_{Lab} = 0$, the inclusive distribution is independent of the projectile Fig.2.7.3 (Moffeit et al., 1972). Such a feature implies that the fragmentation in target fragmentation region is determined by the target only.

2.8 The One Particle Inclusive Spectra

in Rapidity Distribution

In high energy collisions, the $x = 0$ region is important because $x = p/\sqrt{s}$ is scaled down by $\sqrt{s}$ and every finite p will end up at $x = 0$ as s increases. Therefore it is more convenient to use a variable whose range increases with s. For this reason and other adventageous properties, e.g. additivity in Lorentz transformations, the rapidity is frequently used to present the data. The invariant cross section vs the rapidity in the lab frame is shown in Fig. 2.8.1 (Giacomelli and Jacob, 1979).

Since $\langle n \rangle$ is equal to $\int (dn/dy)\, dy$. The dn/dy distribution (Thomé et al., 1979) is shown in Fig. 2.8.2. THe average multiplicity $\langle n \rangle$ is equal to the area of the shaded region. Since the range of y increases with ln s, so dn/dy must increase as ln s such that $\langle n \rangle$ increases as (ln s). The data (UA5 Collaboration, Alpgård, 1981) is shown in Fig. 2.8.3. The height of the plateau seems to increase as ln s.

2.9 Two Particle Inclusive Reaction

The studies involve the reaction

$$h + h \longrightarrow c_1 + c_2 + X$$

The number of independent variables with fixed energy are y_1 , y_2 , p_{T_1} , p_{T_2} and ϕ_{12} ; only the relative azimuthal angle ϕ_{12} is relevent if polarization effect are not measured. At present, most of the data refer to charged particles, which are mainly pions.

In studying the two particle inclusive reaction, the individual physical properties which are being studied in the one particle inclusive reaction are not the most interesting. The major role is to study the correlation between them.

The conservation of energy- momentum automatically produces some sort of correlations among the particles in the final state. These kinematic effect have to be removed before one attempts to study the dynamics of the process observed.

2.9.1 Rapidity Correlation

The one particle distribution is defined as

$$\rho(y) \equiv \frac{1}{\sigma_{in}} \frac{d\sigma}{dy}$$

The two particle distribution is likewise defined as

$$\rho(y_1, y_2) \equiv \frac{1}{\sigma_{in}} \frac{d^2\sigma}{dy_1 dy_2}$$

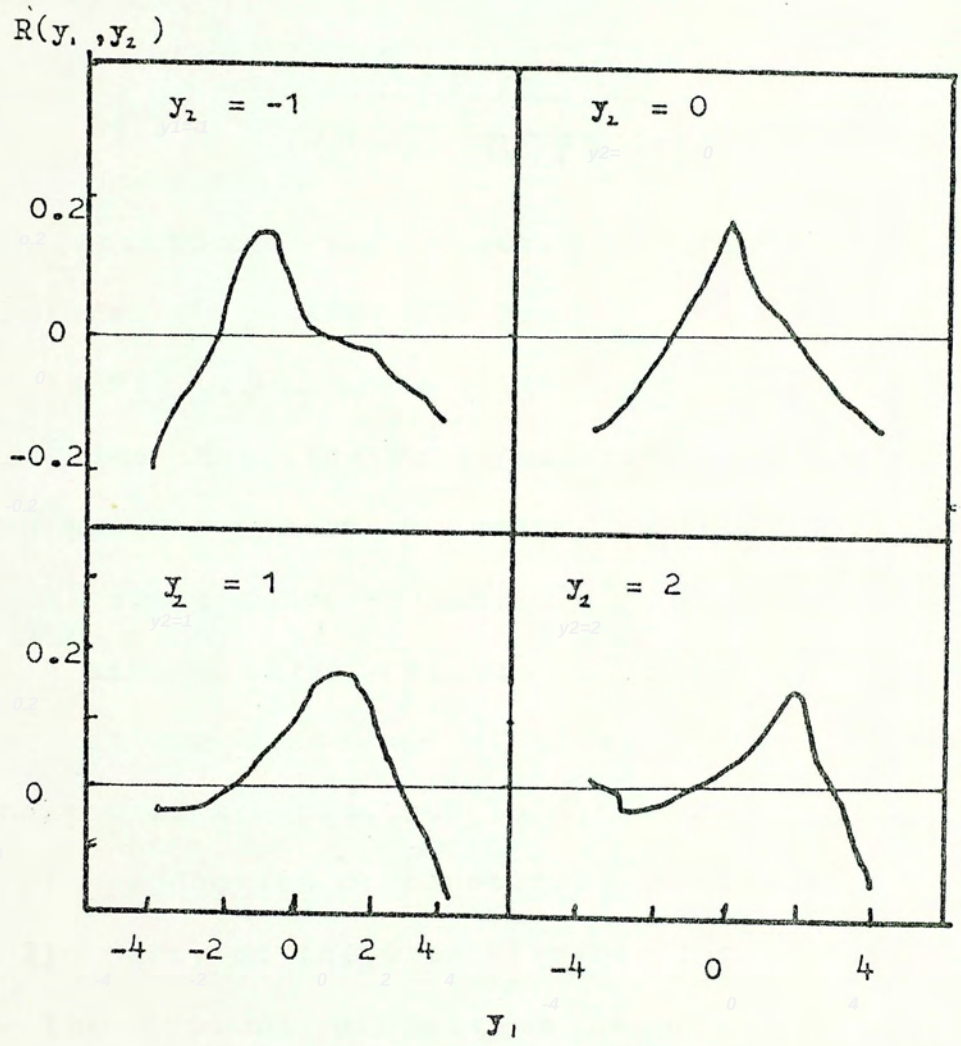

Fig.2.9.1 The normalized two particle rapidity correlation

For two kinds of particles c_1, c_2, the two particle correlation function is defined as

$$C(y_1, y_2) \equiv \langle n_{c_1} n_{c_2} \rangle \rho(y_1, y_2) - \langle (n_{c_1} - \delta_{c_1 c_2}) n_{c_2} \rangle \rho(y_1) \rho(y_2)$$

The normalized two particle correlation function is defined as

$$R(y_1, y_2) \equiv \frac{C(y_1, y_2)}{\langle (n_{c_1} - \delta_{c_1 c_2}) n_{c_2} \rangle \rho(y_1) \rho(y_2)}$$

This definition just ensures $R(y_1, y_2) = 0$ for particles uncorrelated in y (Appendix A).

As Fig. 2.9.1 shows, $R(y_1, y_2)$ has a peak at $y_1 = y_2$. This implies that finding a particle makes it more likely to find another one in the nearby rapidity range. This is a typical short range effect.

A simple interpretation of the short range effect is given in the framework of cluster models which states that particles are produced in a two step process:

1) production of clusters.

2) decay of the clusters into final state particles.

The typical properties of one cluster are the following:

1) width in rapidity of cluster decay = 0.67

2) density of cluster = 1/unit rapidity

3) average mass = 1.3 GeV /c

4) average charge = 0.65

5) average transverse momentum = 0.65 GeV/c

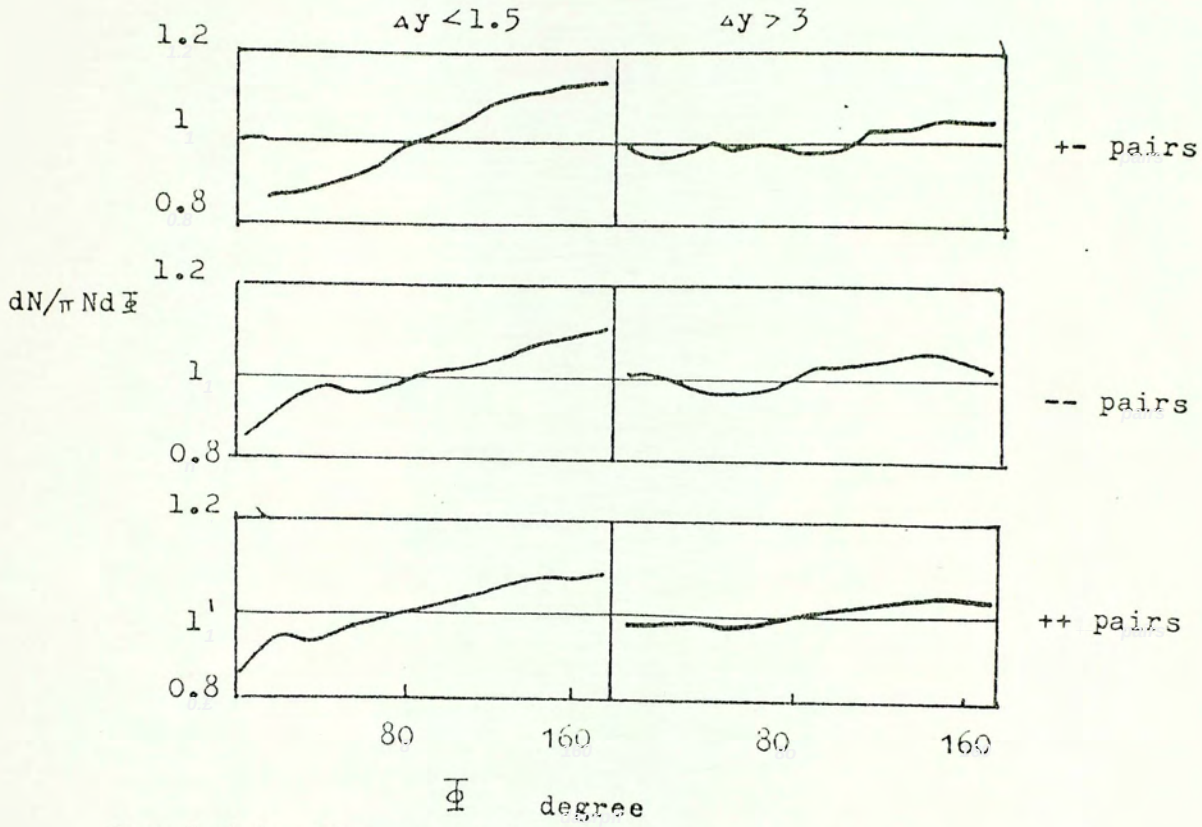

Fig.2.9.2 The normalized two particle azimuthal function for two different rapidity range showing short range transverse momenta compensation.

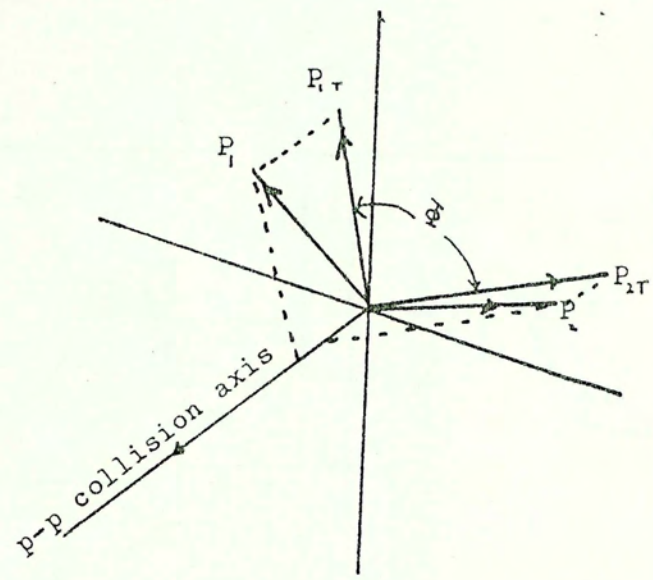

Fig.2.9.3 Definition of Φ .

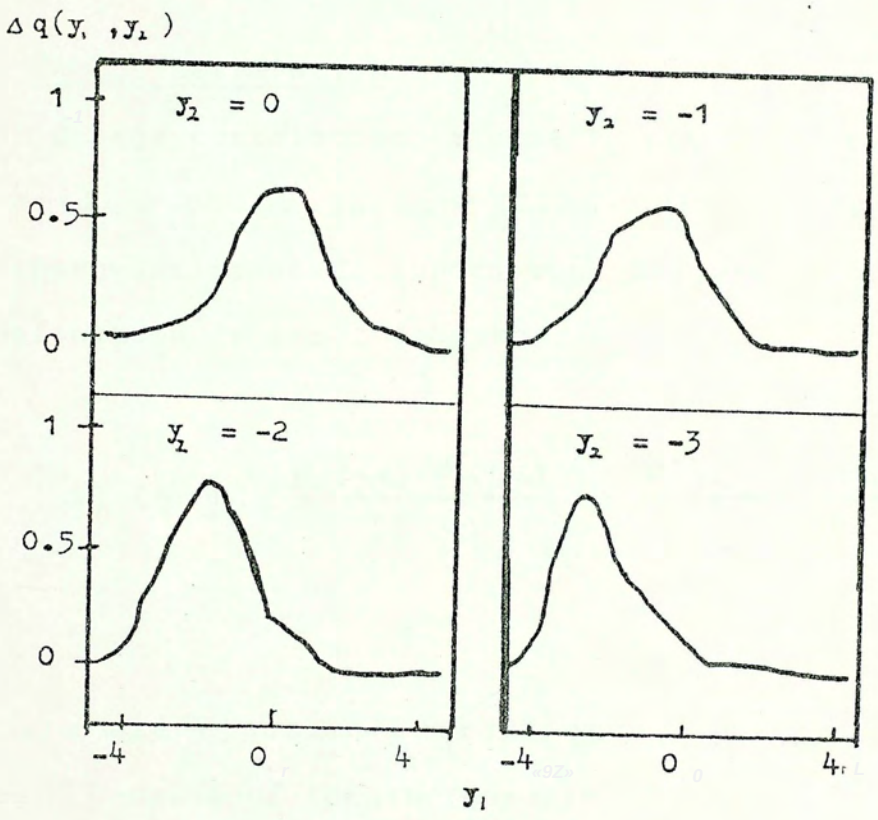

Fig.2.9.4 The charge compensation function.

2.9.2 Azimuthal Correlation

Fig. 2.9.2 shows the normalized azimuthal distribution $dN/d\Phi$ for two rapidity intervals where Φ is defined in Fig.2.9.3. The data show that there are strong asymmetries for $\Delta y < 1.5$ and negligible ones for $\Delta y > 3$. That means that the transverse momenta compensate each other.

2.9.3 Charge Correlation

Charge correlation is usually described in terms of the charge compensation (CERN-College de France-Heidelberg-Karlsruhe Collaboration, Drijard et al., 1980). The definition is the following.

$$\Delta q\,(y_1, y_2) \equiv \frac{\rho^{-+}(y_1,y_2) - \rho^{++}(y_1,y_2)}{\rho^{+}(y_2)} + \frac{\rho^{+-}(y_1,y_2) - \rho^{--}(y_1,y_2)}{\rho^{-}(y_2)}$$

If there are opposite charges in y_1 and y_2, Δq will increase because of the increase in ρ^{-+} or ρ^{+-}. That means a large charge compensation. As Fig. 2.9.4 shows, Δq has a maximum when $y_1 = y_2$, indicating local charge compensation (CERN-College de France-Heidelberg-Karlsruhe Collaboration, Drijard et al., 1980).

2.9.5 Correlation of Cocconi-Kopylov-Podgoresky

The normalized correlation function $R(p_1, p_2)$ when

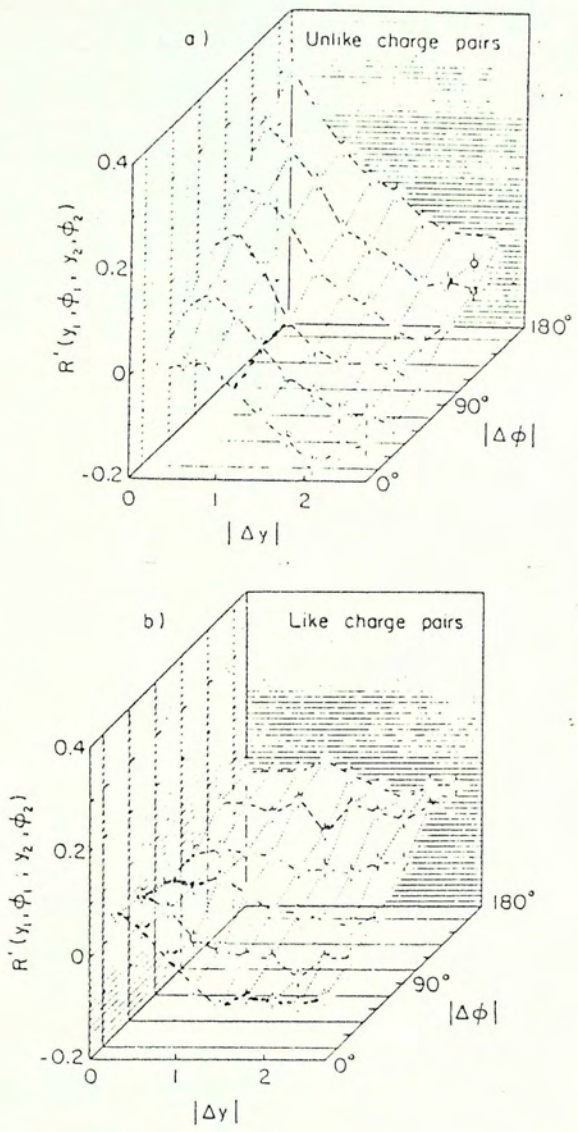

Fig.2.9.5 Normalized 2-particle correlation function vs Δy and $\Delta\phi$ for (a) opposite charge pairs; (b) same charge pairs.

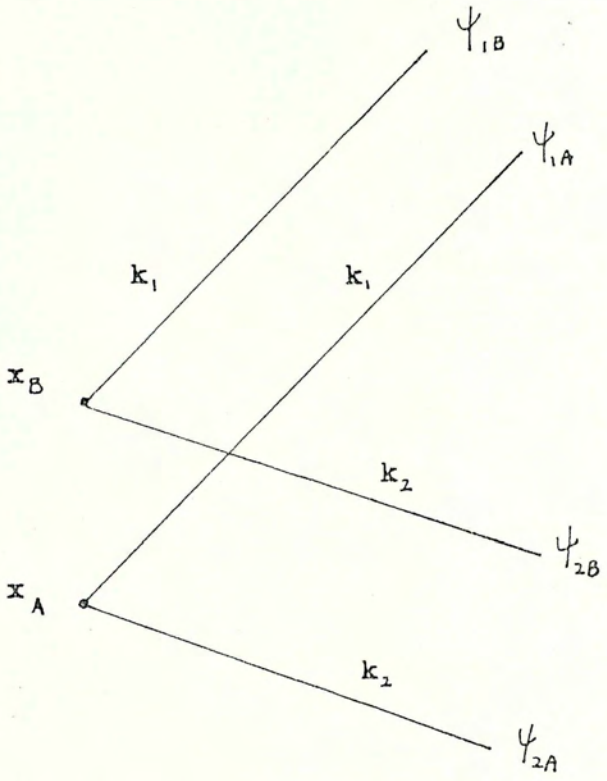

Fig.2.9.6 The interference by two sources.

plotted as function of $\Delta y = |y_1 - y_2|$ and $\Delta\phi = |\phi_1 - \phi_2|$ shows significant difference between like charge, (π^-,π^-), (π^+,π^+) and unlike charge, (π^+, π^-), at small $\Delta\phi$ and Δy, as Fig. 2.9.5 shows.

For like charge particles $R(p_1, p_2)$ shows a maximum when the $\Delta\phi = \Delta y = 0$. This has been interpreted as Bose-Einstein condensation of two pions system (Kopylov, 1974; Cocconi, 1974).

Consider the production of two identical pions with momenta k_1 and k_2, arising from two sources A and B with coordinates x_A and x_B, as Fig. 2.9.6 shows. The pion wave function in plane wave approximation are

$$\psi_{1A} \sim e^{i k_1 x_A}$$
$$\psi_{1B} \sim e^{i k_1 x_B}$$
$$\psi_{2A} \sim e^{i k_2 x_A}$$
$$\psi_{2B} \sim e^{i k_2 x_B}$$

In the $\Delta\phi = 0$ region, the sources A, B are too close to be distinguished. In this case we have to add the amplitude before squaring. For Bose particles, symmetrization leads to the amplitude

$$A = \psi_{1A}\psi_{2B} + \psi_{1B}\psi_{2A}$$

The corresponding intensity is

$$|A|^2 \sim 2 + 2\cos\left[(k_1 - k_2)(x_A - x_B)\right]$$

which is maximum at $\Delta k = 0$. That is $\Delta y = 0$.

Usually, the variables q_t and q_{11} are used, where q is the component of $q = \vec{p}_1 - \vec{p}_2$ in the direction of $\vec{p}_1 + \vec{p}_2$ and q_t is the component in the direction perpendicular to it. The correlation R is parametrized as (Kopylov, 1974)

$$R(p_1, p_2) \equiv R(q_{11}, q_t) = \beta \left\{ 1 + \alpha \frac{J_1^2(q_t \Delta x)}{(q_t \Delta x)^2} \frac{1}{(1 + q_{11}\tau)^2} \right\}$$

where β is a normalized constant, J_1 is the Bessel function of first order, $\Delta x, \tau$ are the measures of the radius and lifetime of the pion source. These values are experimentally fitted to be 1.34 fm and 1.34 fm/c respectively.

2.9.6 Forward-backward Multiplicity Correlation

We now consider the correlation between the multiplicity of particles emitted in one hemisphere defined with respect to the direction of the projectile and the multiplicity in the opposite hemisphere. This is called the forward-backward multiplicity correlation. Let n_B be the multiplicity in the backward hemisphere and n_F be the multiplicity in the forward hemisphere.

As Fig. 2.9.7 shows (UA5 Collab., Alpgård et al., 1983), $\langle n_F \rangle$ for a given n_B, $\langle n_F \rangle$ exhibits an approximately linear rise as a function of n_B as

$$\langle n_F \rangle = a + b\, n_B$$

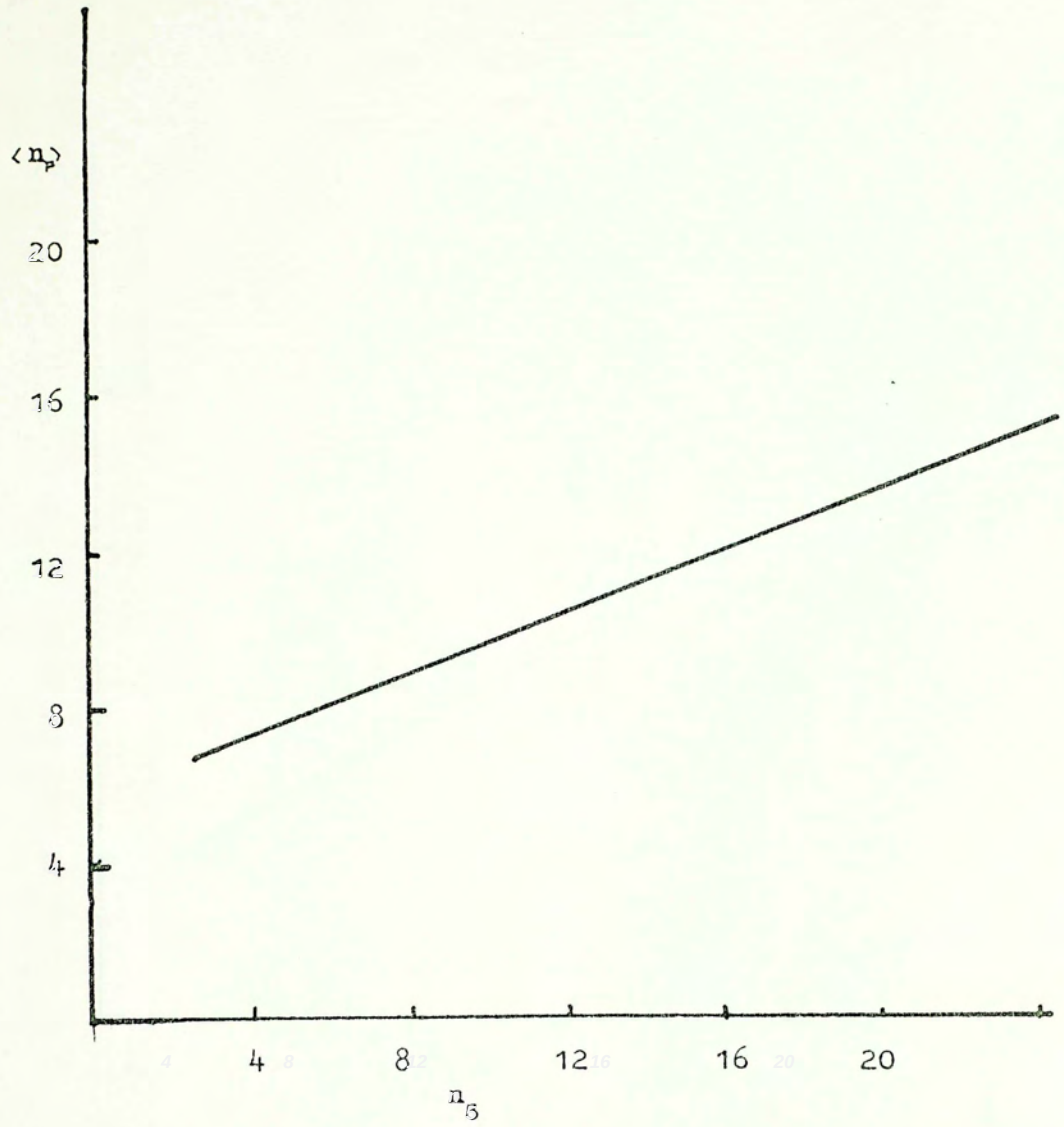

Fig.2.9.7(a) $\langle n_F \rangle$ vs n_B for long rapidity range $(1 < |\eta| < 4)$.

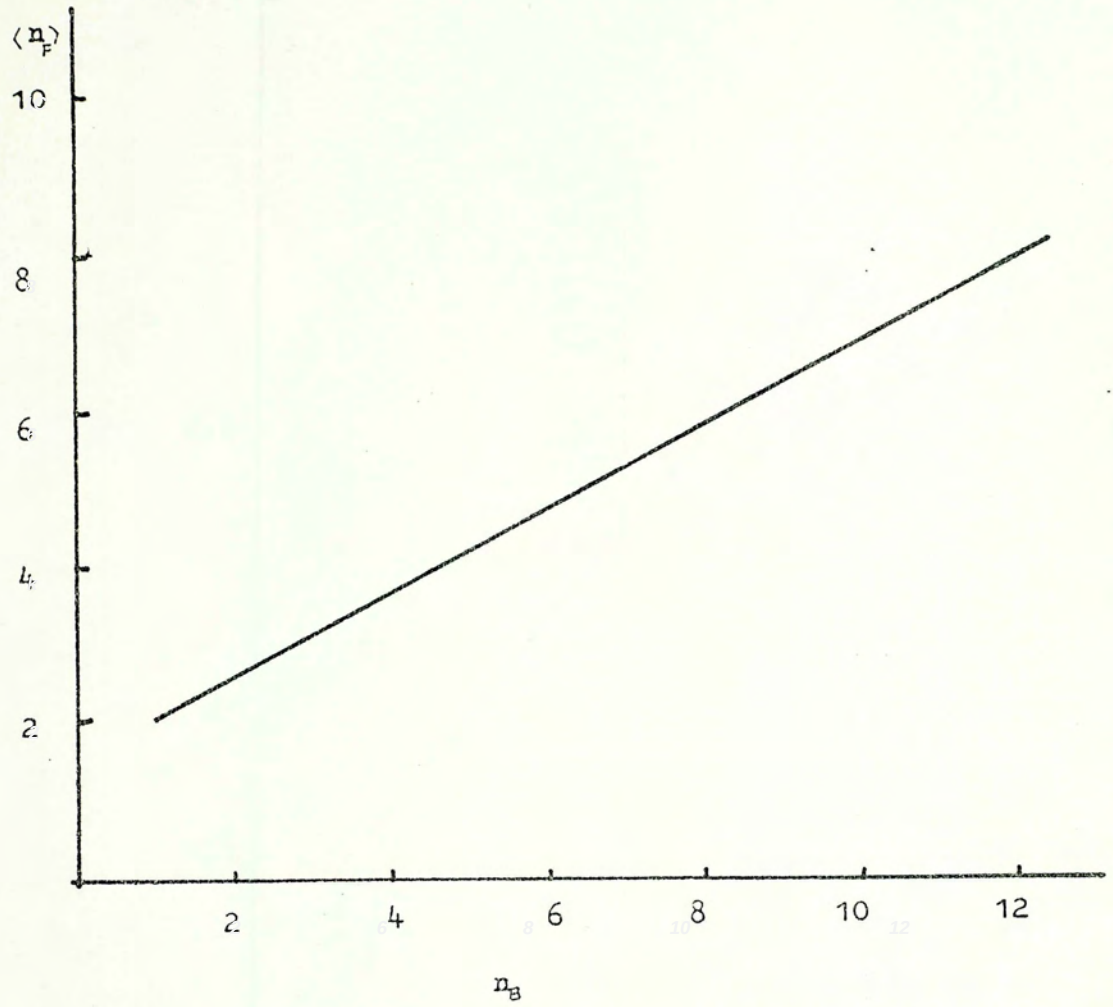

Fig.2.9.7(b) $\langle n_F \rangle$ vs n_B for short rapidity range ($1 > |\eta|$).

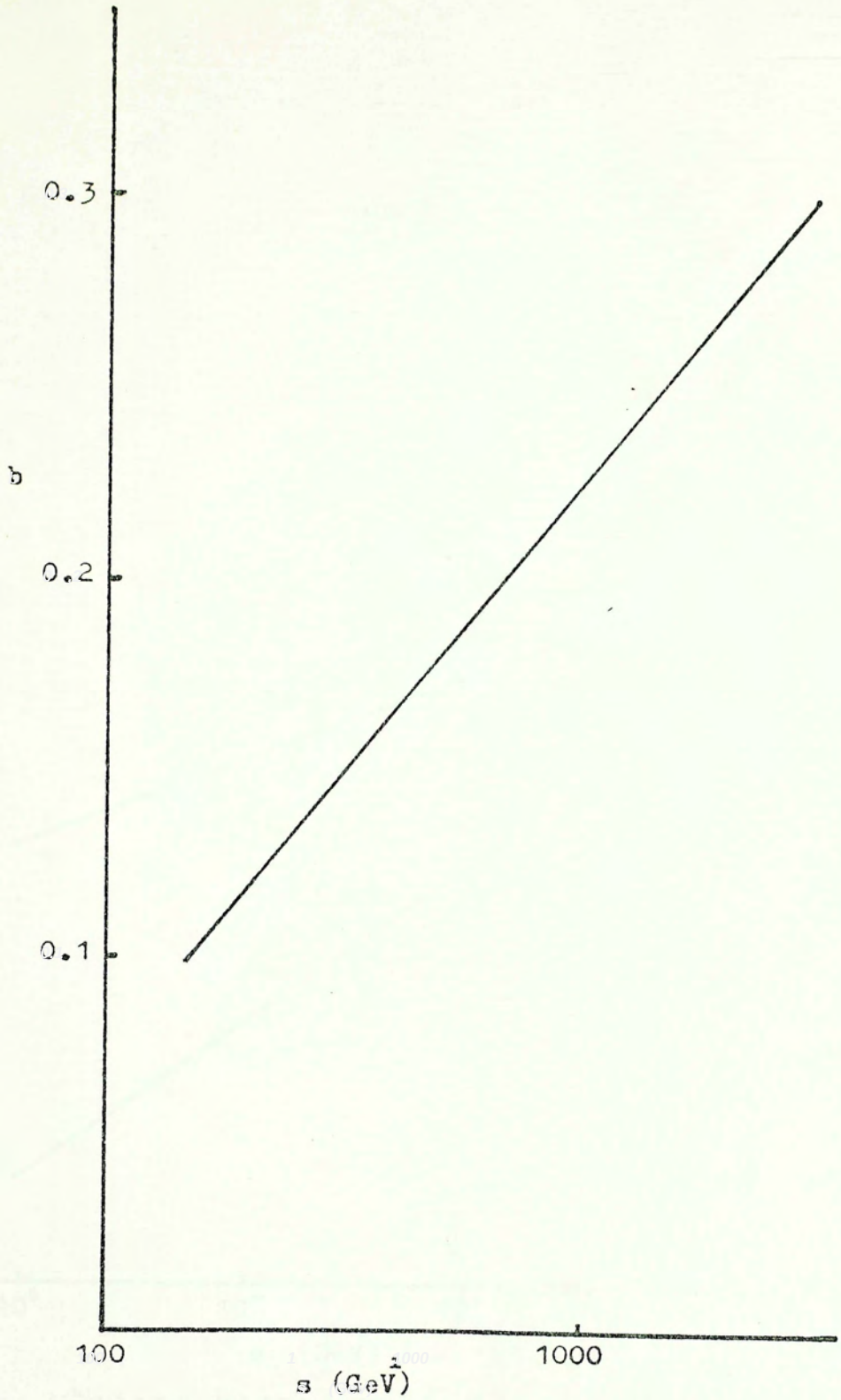

Fig.2.9.8 Energy dependence of b.

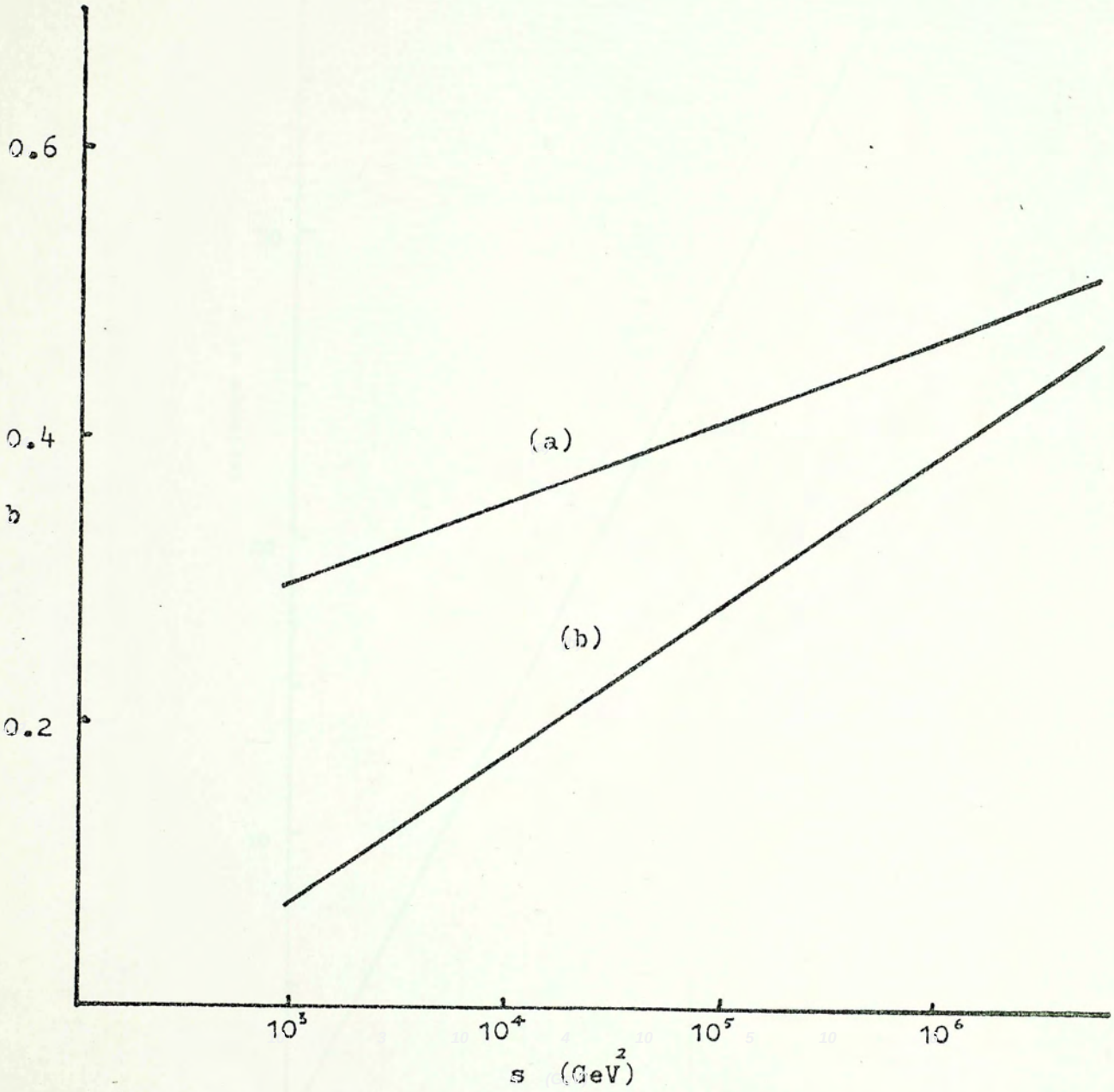

Fig.2.9.9 Energy dependence of b: (a) short range; (b) long range.

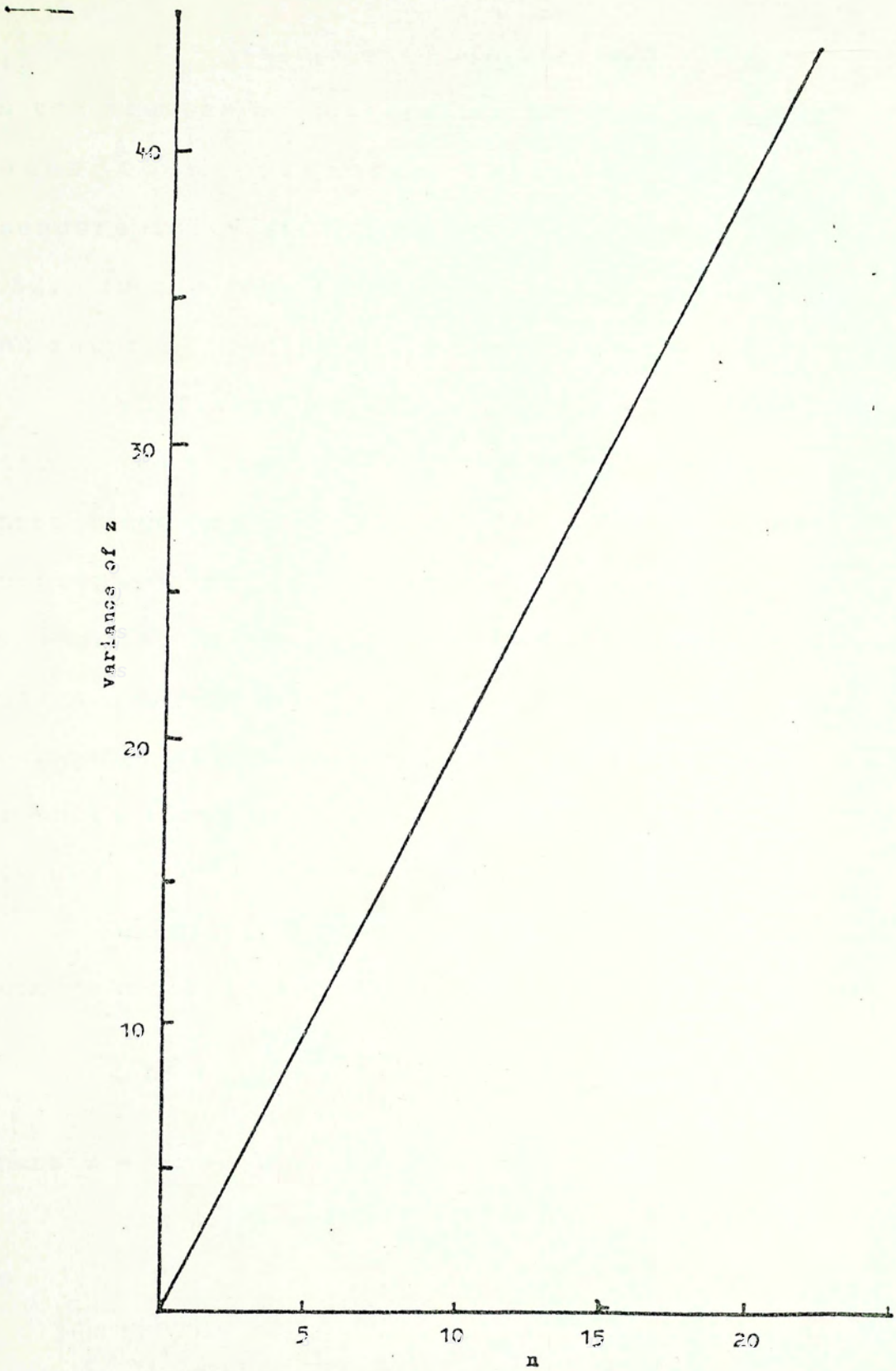

Fig.2.9.10 Variance of z vs n.

$$b = (\langle n_F n_B \rangle - \langle n_F \rangle \langle n_B \rangle) / (\langle n_F^2 \rangle - \langle n_F \rangle^2)$$

is the measure of correlation between n_F and n_B. In the cases that particles fall in the interval of pseudorapidity $|\eta| < 1$ (the short range case), a = 1.2, b = 0.52. In the long range case, i.e. only the particles in the interval $1 < |\eta| < 4$ are considered, a = 5.3, b = 0.42.

Wroblewski (Koch, 1983) observed a linear rise of b with ln s as displayed in Fig. 2.9.8. In Fig. 2.9.9, the short range and long range correlations are compared as a function of s. The short range correlation is already substantial at low energies, and increases only slightly with s. On the other hand, the long range correlation is negligable at low energies and reaches almost the strength of short range correlation at $\bar{p}p$ collider energies $\sqrt{s}$ = 540 GeV.

Recently, Chou and Yang (1984) discovered that the data is well fitted as (Fig.2.9.10)

$$\langle z^2 \rangle_{fix\ n} = 2n \qquad (2 \cdot 9 \cdot 6 \cdot 1)$$

where $z = n_F - n_B$

The probability distribution P(n, z) is proposed as

$$P(n,z) = \psi\left(\frac{n}{\langle n \rangle}\right) C_{(n+z)/4}^{n/2} \; B(n)^{-1} \qquad (2 \cdot 9 \cdot 6 \cdot 2)$$

where B^{-1} is the normalization factor. $\psi(n/\langle n\rangle)$ is the KNO scaling function, C_a^b is the number of combinations of b objects chosen in a objects, i.e.

$$C_a^b = \frac{b!}{a!\ (b-a)!}$$

The physical picture is that many low multiplicity (= 2) clusters are emitted at random along the rapidity plateau and each cluster fragments into two charged particles. The positive charges, about n/2 in number, are distributed in the forward and backward sides in a binomial distribution $C_m^{n/2}$, where m is the number of positive charges on the forward side. The total charge is assumed to be neutral on each side (local charge compensation), so that $n_F = 2m$ and $z = n_F - n_B = 4m - n$, i.e.

$$m = (n + z)/4$$

which yields (2.9.6.1) and (2.9.6.2). If both sides of (2.9.6.1) are averaged over all n, we get

$$\frac{\text{average of } \langle z \rangle}{\text{average of } n} = 1$$

$$\frac{\text{variance of } z}{\text{variance of } n} = \frac{1-b}{1+b} = \frac{2n}{\text{variance of } n} \equiv \alpha$$

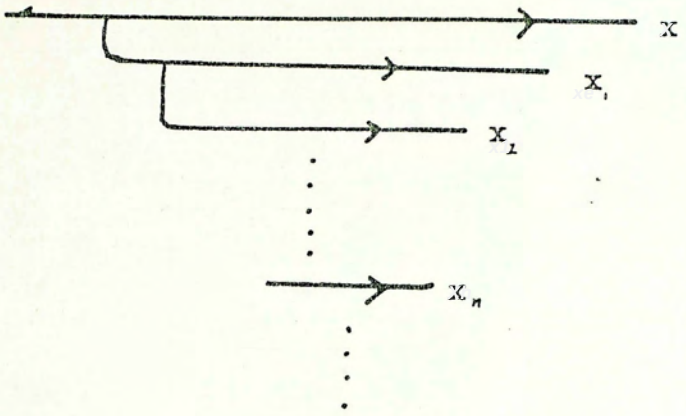

Fig.2.10.1 Parton cascades

Acording to KNO scaling, $\alpha \tilde{=} 1/\langle n \rangle \rightarrow 0$ as $E \rightarrow \infty$ so that the population becomes a narrow band in the $n_F - n_B$ plane.

2.10 Parton Model in Hadron-hadron Collision

As proposed by Feynman, a hadron is composed of particles called partons. The incoming hadron is like a box of free parton sharing the momentum of the hadron.

The momentum of a parton is ξp, where p is the momentum of hadron. If $\xi p < 1$ GeV/c, we then call it a wee parton. In analogy to bremsstrahlung, particles are generated in a dx/x distribution so the small x region contains large and nearly equal numbers of particles and antiparticles. In other words many particles fill in the central region in rapidity space with net quantum numbers equal to zero; and further that the low x region is generated from higher momenta by a series of cascades. (Fig. 2.10.1).

Feynman argued that partons interact only if their relative 4-momentum is not too large, because if their relative momentum is too large, they will have no time to interact. In rapidity language, parton 1 and parton 2 interact only if $|y_1 - y_2| < 1$. Therefore the interaction in rapidity space is short ranged.

As proposed by Yang (Feynman, 1972), in hadron collisions, particles having finite momenta in the centre of mass frame is indistinguishable as being target or beam fragments because longitudinal transformations with a

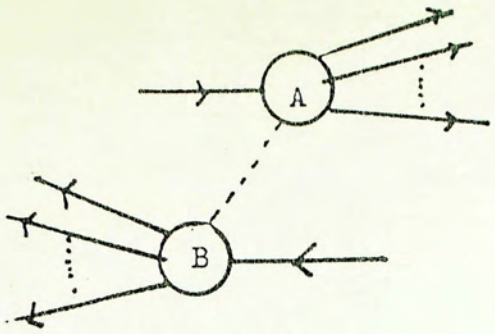

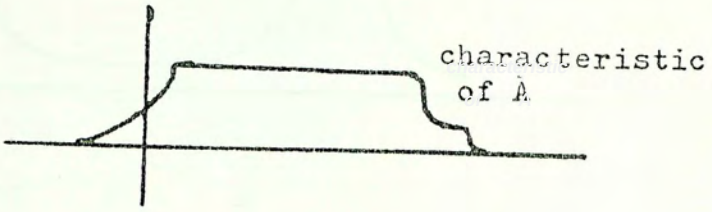

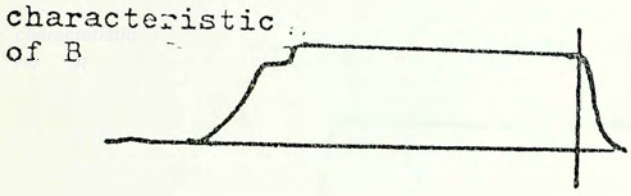

final state

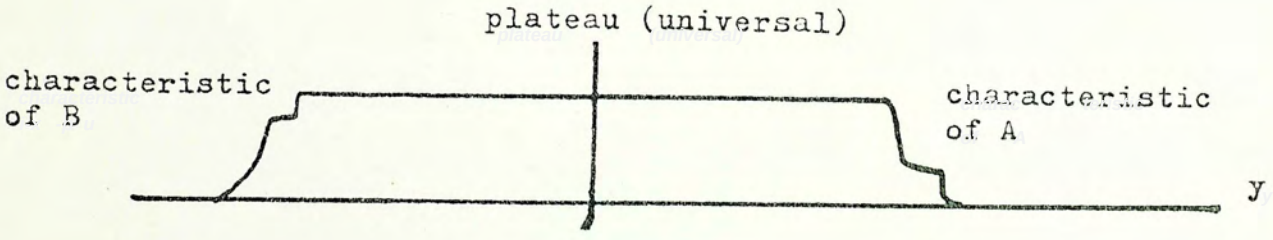

Fig.2.10.2 Illustration of particle poduction in parton model.

Yang:

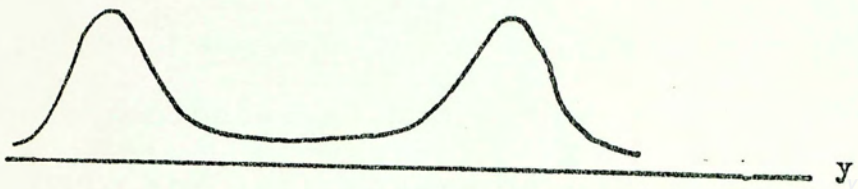

Feynman:

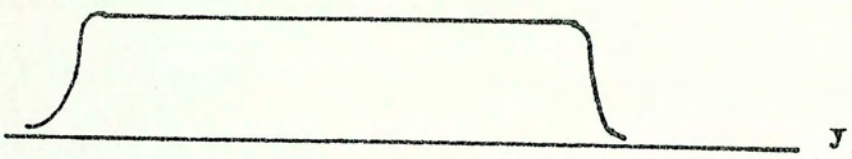

Fig.2.10.3 Difference between Yang and Feynman in existence of plateau.

velocity v not too close to c leave the distribution of such particles unchanged. There is a universal plateau, as Fig.2.10.2 shows.

In the high energy limit for a scattering A + B, the rapidity range between A and B is so large that there is no interaction between them. The right movers depend only on A while the left movers depend only on B. It is also called limiting fragmentation by Benecke et al.(1969). However at that time it was supposed that these regions are seperate and no central plateau exists. The difference between the pictures of Yang and Feynman is shown in Fig.2.10.3.

Partons are sometimes identified as quarks and gluons participating in interaction of quantum chromodynamics (QCD). A hadron is thought of as being composed of valance quark which carry its quantum number, and of a neutral sea of gluons and quark-antiquark pairs corresponding to the wee partons. It is called the quark-parton model.

Because of asymptotic freedom in QCD (Gross and Wilczek, 1973; Politzer, 1973), large momentum transfer phenomenen, $p_\perp$ > 1 GeV/c can be calculated perturbatively and compared with the data. However, processes which involve large momentum tranfers have very small cross section and hadron production is completely dominated by small $p_\perp$ events. Such soft process in QCD require a non-perturbative approach which is still lacking. It has not

been possible so far to use it to explain the bulk of the expermental data in hadron-hadron collision.

Chapter 3

Hadron-nucleus Scattering

3.1 Introduction

After a quick look at hadron-hadron interactions, we now come to hadron-nucleus (h-A) collisions.

A nucleus consists of loosely bound protons and neutrons, so to a certain extent, we may regard hadron-nucleus collisions as hadron colliding with a collection of independent protons and neutrons.

At high energies, details of the nuclear structure can be largely ignored because the wavelength of the incident particle is much smaller than the nuclear radii and the energy is much higher than the excitation energy between the energy levels of the nucleus, which have charecteristic magnitudes in MeVs, thousands of times smaller than the relevant energy range of several GeV. With structural details ignored, the nucleus can then be regarded as nucleons distributed with a density which extends to the nuclear size $R = R_0 A^{1/3}$, $R_0 = 1.2$ fm. Therefore the study of high energy h-A collisions provides insight into the dynamics of hadron-nucleon (h-N) collisions, especially in short-time hadronic production and space-time evolution of hadronic process.

Let τ be a charecteristic time of a pp collision in the centre of mass frame. In the target rest frame,

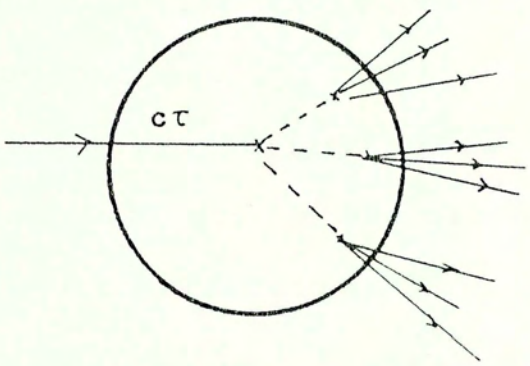

Fig.3.1.1 Intranuclear cascade.

it is dilated to $\tau' = \tau(E/2m)^{1/2}$, where E is the incident energy in the centre of mass frame. If E is sufficiently large, τ will exceed the nuclear mean free path λ where $\lambda = 1/\rho\sigma$ where $\rho = (4\pi R_0^3/3)$ is the mean nucleon density (no. of nucleons per unit volume) and σ is the total cross section. Thus λ = 2 fm. For $c\tau < \lambda$, the particle will undergo a second collision etc before it is finally detected (Fig. 3.1.1). In such processes cascade effect will be observed. For $c\tau > \lambda$, the particle will not undergo a second collision so there is lack of cascade. Hence hadron-nucleus collisions yield information that cannot be inferred directly from h-h collisions. Hadron-nucleus collisions are good analysers in hadronic space-time evolution, which was pointed out by Gottfried (1974).

Like h-h collisions, the important experimental data are the cross sections and the multiplicity distribution. These will be discussed in more detail in the following sections.

The A dependence and the energy dependence of cross sections in high energy collisions are in argeement with geometric ideas, as expressed by say the Glauber model (Glauber,1959).

On the other hand, the A dependence of the multiplicity is surprisingly weak. It is interpreted as the lack of cascading in h-A collisions and is often said to show that hadrons are formed outside the nucleus. Hwa (1981) estimated the radiation length for fast quarks in nuclear matter as 100 fm. Busza (1977) also claimed that

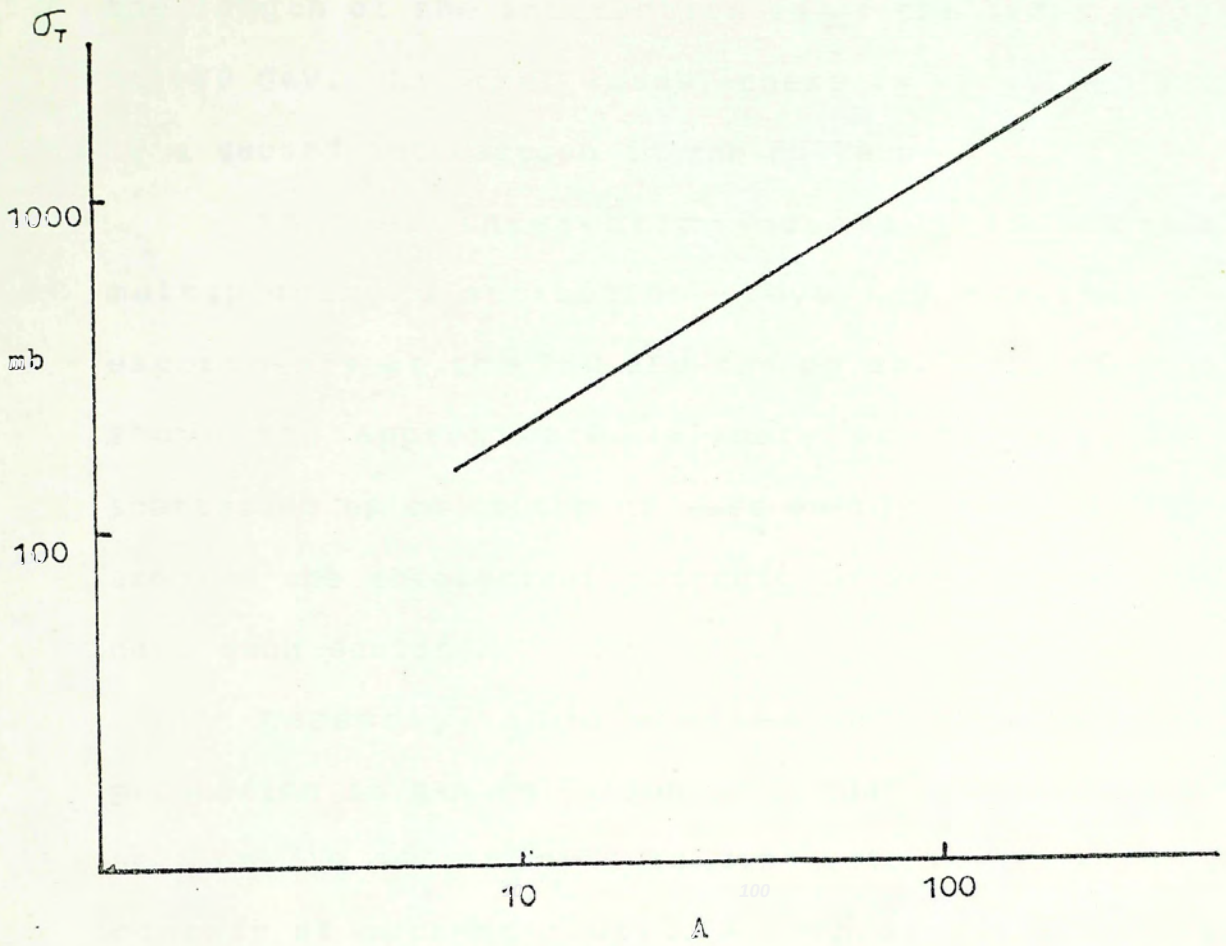

Fig.3.2.1 The A dependence of the total cross section in n-A collision around E:30-300 GeV.

the length of the interaction is of the order of 1000 fm at 100 GeV. In other words, there is very little chance of a second interaction in the nucleus.

Another interesting question is whether the multiplicity distribution obeys KNO scaling. Recent experiments at the ISR and the pp collider at CERN have shown the approximate validity of KNO scaling in hN scattering up to centre of mass energy $s = 540$ GeV. This arouses the theoretical interest in whether h-A collision have such scaling.

Recently, some studies on inclusive particle production in h-A collision show that the inclusive cross sections in A-dependence is difficult to interpret in the context of current models. All those questions will be discussed below.

3.2 Hadron-nucleus Cross Section

3.2.1 Total Cross Section

Some data on total cross section are shown in Fig. 3.2.1. The A dependence and the energy dependence are both interesting. For A dependence, the total cross sections are often parametrized as $\sigma = \sigma_0 A^{\alpha}$, σ_0 need not be the h-p total cross section, i.e. the parametrization does not hold for A = 1. As Fig. 3.2.1 (Busza, 1977) shows, in h-A collision around energy 30-300 GeV, $\sigma_0 = 50$ mb, $\alpha = 0.77$.

The value of α ($2/3 < \alpha < 1$) is a measure of

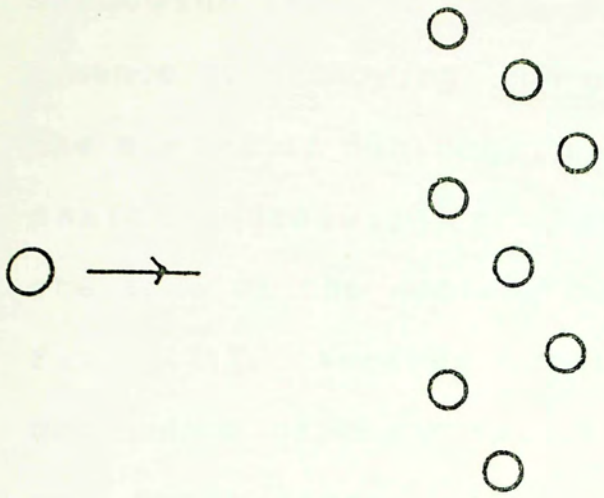

(a)

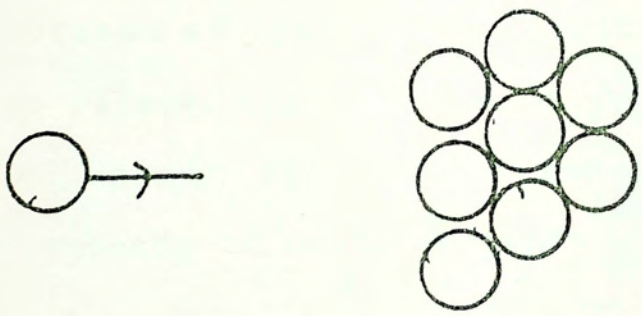

(b)

Fig.3.2.2 Shadowing affects the A dependence of cross section: (a) absence of shadowing gives $\alpha = 1$; (b) maximum shadowing gives $\alpha = 2/3$.

shadowing in h-A collision, with $\alpha \sim 1$ in the absence of shadowing and $\alpha \sim 2/3$ for maximum shadowing. In the absence of shadowing, the cross section is proportional to the number of nucleons, so it is proportional to A. For maximum shadowing, the cross section is proportional to the area of the nucleus hence to $A^{\frac{2}{3}}$. This is shown in Fig. 3.2.2. Another interesting feature is the energy dependence of the total cross section. At high energies, the total cross section only increases slightly with energy. Compared to the case of hN scattering, the energy dependence is very weak. Such weakness may be explained as follows. As the energy increases, σ^{hN} increases, then σ_0 increases. However α decreases because of the increase of the shadowing due to the larger σ^{hN}. These two effect: the increase of σ_0 and the decrease of α would compensate each other and hence weaken the energy dependence of cross sections.

3.2.2 Absorption Cross Section

Another interesting cross section is the probability of absorption of the incident particle. For elastic scattering, only the momentum of the incident particle changes so there is no absorption. Usually the absorption cross section is identified as the inelastic cross section. That is $\sigma_a = \sigma_T - \sigma_{el}$.

3.2.3 Elastic Differential Cross Section

Hadron-nucleus collisions have similar structure as

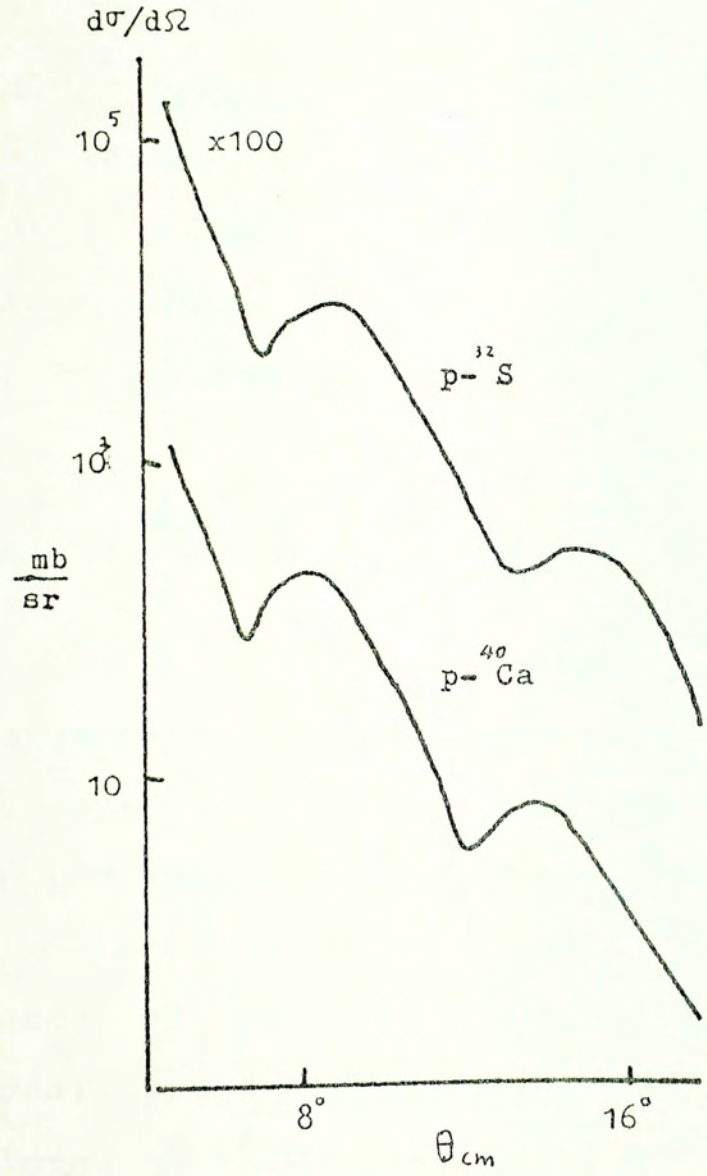

Fig.3.2.3 Differential cross section for 1 GeV p-A scattering. The theorectical calaulations match the data in the same line.

h-h collisions. In Fig. 3.2.3 the differential cross section of elastic h-A scattering is shown; it behaves like a diffraction pattern. The wave property of the incident particle diffract into the shadow region of the nuclei hence the diffraction pattern is formed.

3.2.4 The Geometric Model

The main experimental features of the cross section can be well explained by geometric ideas like the Glauber model (Glauber, 1959). One adopts the eikonal approximation for the scattering amplitude

$$f(\Omega) \simeq \frac{ik}{2\pi} \int e^{ik\cdot b} \left(1 - e^{-\Omega(b)} \right) d^2b$$

At high energies, the incident particle goes through the nucleus in such a short time that it is a very good approximation to assume that the nucleons do not rearrange themselves until the incident particle has left, the so-called frozen approximation. In addition, if the nucleons of the target do not overlap, then the total eikonal is the sum of the individual contributions of nucleons $\Omega = \sum_{i=1}^{A} \Omega_i$ so the eikonal Ω can be expressed in terms of hadron-nucleon phase shifts. This is called the dynamical approximation. Such theories are frequently applied to calculate the cross section of h-A collisions and have shown great success. The comparsion of theoretical calculation and the data is shown in Fig.

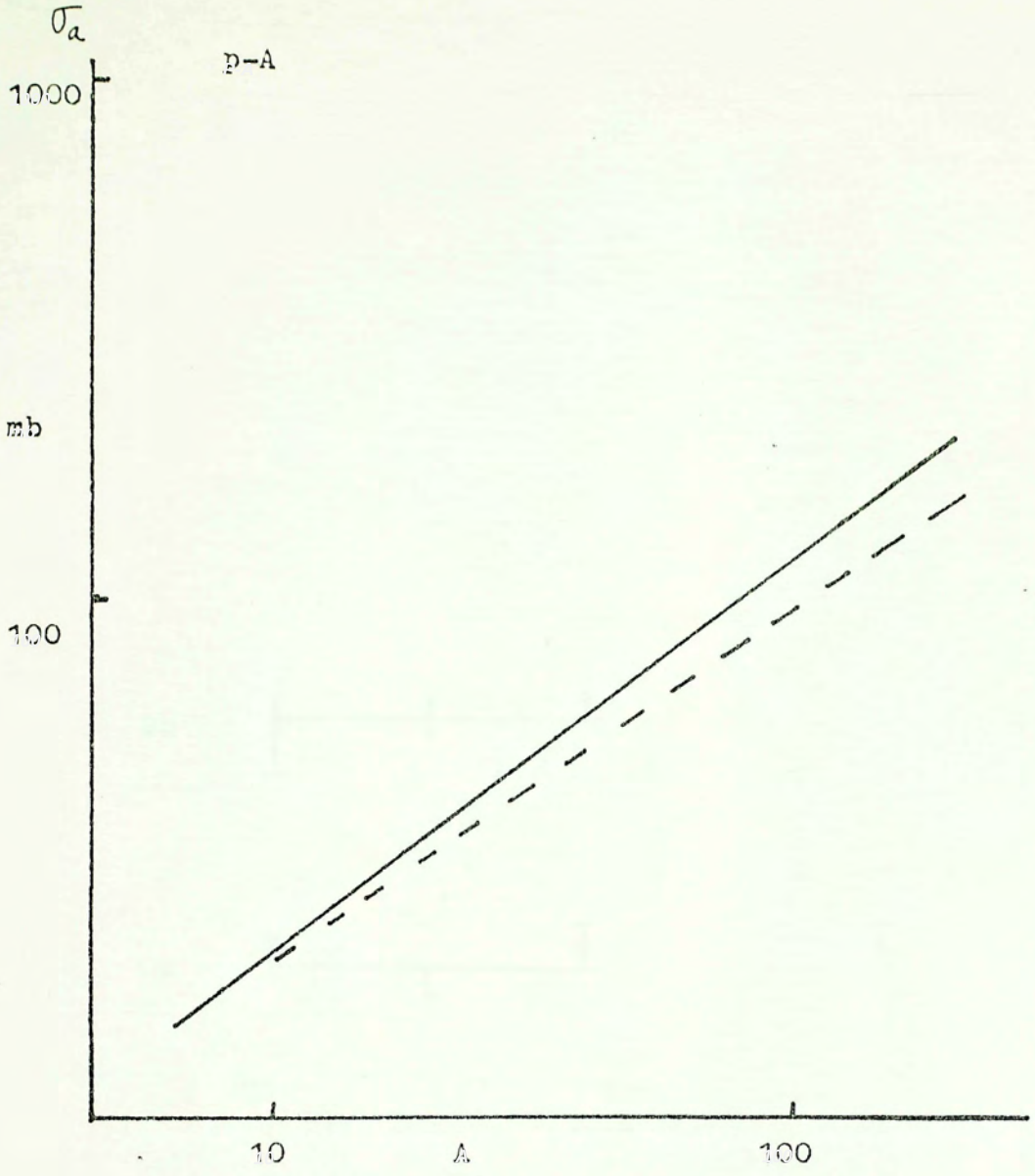

Fig.3.2.4 Absorption cross section for p-A collision average over the range 20-60 GeV. The solid line represents the data and the dash line is the theorectical calaulation.

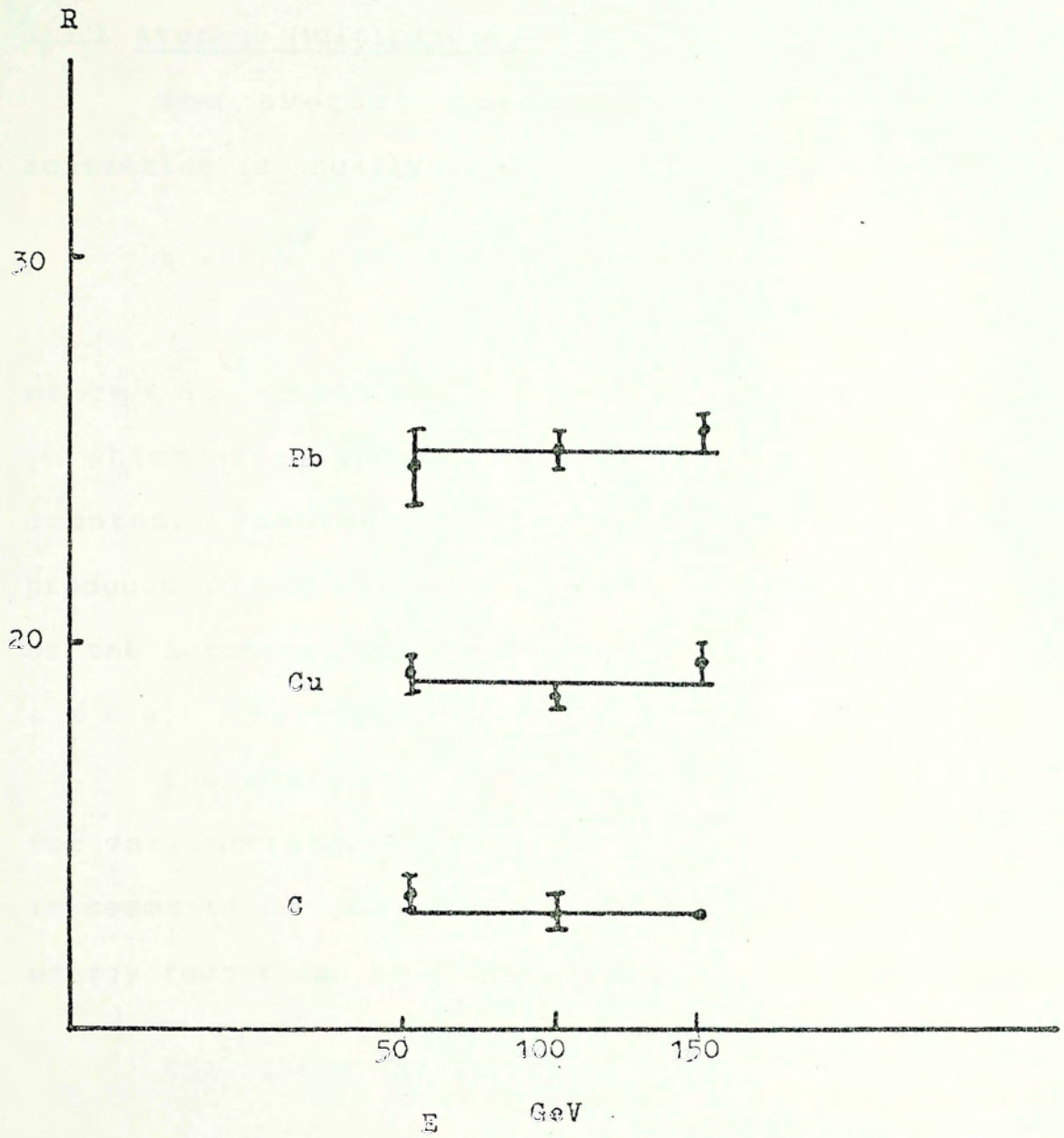

Fig.3.3.1 Energy dependence of R for various target.

3.2.3 and 3.2.4 (Alkhazov et al., 1975; Busza, 1977).

3.3 The Multiparticle Production

3.3.1 Average Multiplicity

The average multiplicity in hadron-nucleus scattering is usually reported in terms of the ratio

$$R = \langle n \rangle^{hA} / \langle n \rangle^{hN} = R(E, A)$$

where $\langle n \rangle^{hA}$ is the average multiplicity in hA scattering, in which usually only the shower particles ($\beta > 0.7$) are counted. The reason is following: only the particles produced in the collision are interesting. The evaporated or the knock-out nucleons which are usually quite slow ($\beta < 0.7$) must be ruled out.

The energy dependence of R is shown in Fig. 3.3.1 for various targets (Elias et al., 1980). At E > 100 GeV, it seems to be independent of energy. That means that the energy factor can be factorized out and written as

$$\langle n \rangle^{hA}(E) = \langle n \rangle^{hN}(E)\ f(A)$$

Other kinds of definition of R are discussed in Appendix B.

The A dependence of R is also interesting. It is well established that R increases slowly with A (Fig. 3.2.2). That means little intra-nuclear cascading is observed. That indicates that the distance of particle formation is rather long compared with nuclear radius.

This give us some information about the space-time evolution of hadronic process.

3.3.2 Number of Collisions in h-A Collision

Another usual parameter in describing the data is the average number of inelastic collisions of the incident hadron in the nucleus, which is the ratio of the number of hN inelastic collisions over the total number of inelastic events in hA collisions. The total number of inelastic events is proportional to the inelastic hA cross section. The number of hN collisions is proportional to σ^{hN}, the nucleus thickness and the area facing the projectile beam. The nucleus thickness is proportional to $A^{1/3}$ whereas the area is proportional to $A^{2/3}$. Hence

$$\langle \nu \rangle \equiv \frac{A\,\sigma_{in}^{hN}}{\sigma_{in}^{hA}}$$

is usually defined. The proportional constant is found by setting $\langle \nu \rangle = 1$ when $A = 1$. In the limit of abscence of shadowing, $\langle \nu \rangle$ would approach a constant. In the limit of severe shadowing, it would increase as $A^{1/3}$, which is the strongest possible A dependence.

In recent years, it seems to have become possible to assign a value of ν to each event, which measures how many times the incident hadron interacts with the target nucleus. In other words, ν is related to the nuclear thickness as the projectile goes through. More interest

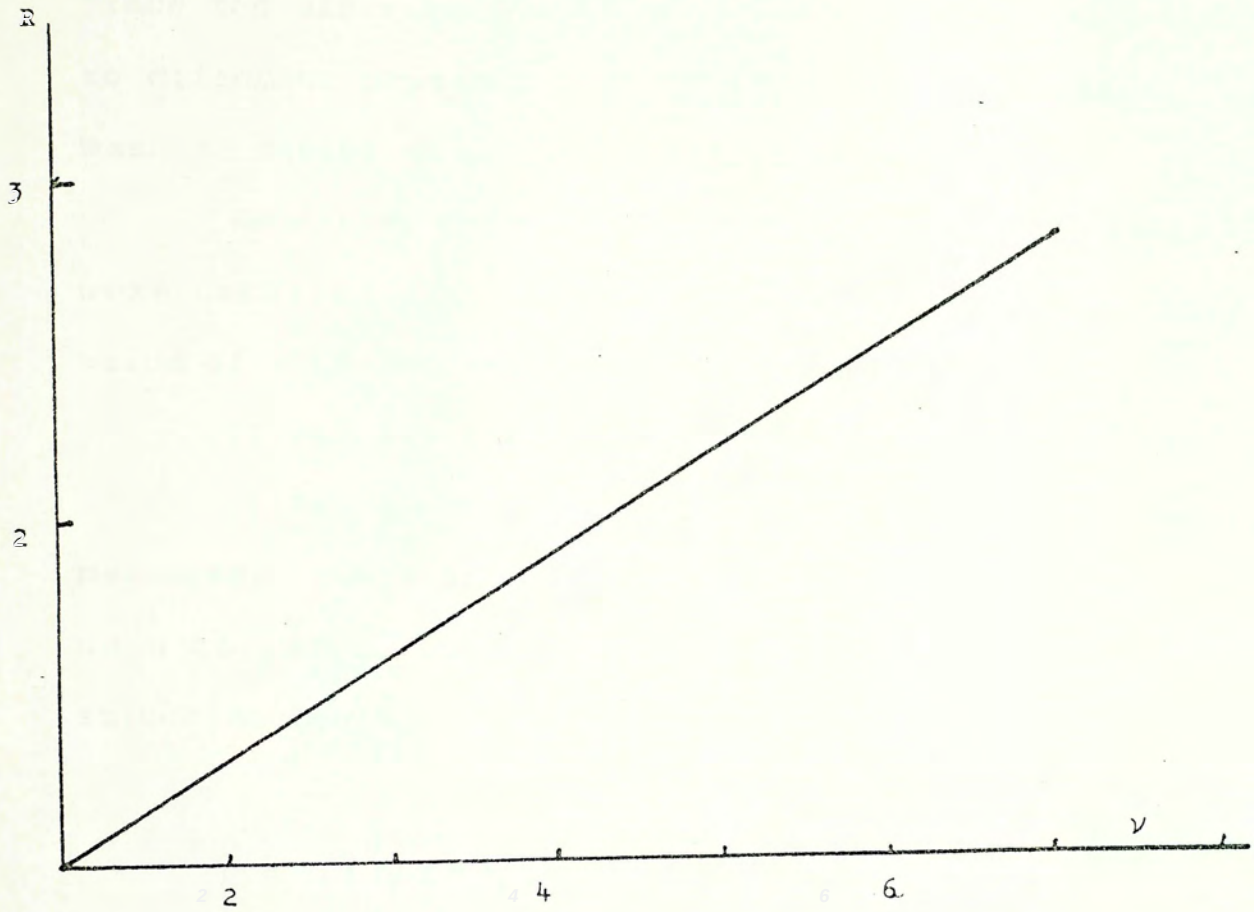

Fig.3.3.2 ν dependence of R for h-A with different projectile and energies.

is paid to ν then to A because the information about ν gives us a more detail knowlege than A only. Besides, it seems more natural to ask what is the multiplicity in collision because of the universality of nuclear matter. Since the distribution of nuclear matter in nuclei belongs to different physics, it is not so natural to connect the mass of nuclei with the multiplicity directly.

Recently, Chao et al.(1983) presented the data in a more detailed way. They plot R vs ν rather than A. The value of ν is determined in two different ways.

1) For fix target A, $\nu = \langle\nu\rangle_A$ is taken.

2) For Cu and Pb, the number of grey tracks N_g is measured. There are various empirical and semi-empirical ways to relate the observed number N_g to the number of struck nucleons, e.g. (Hegab and Hufner, 1981)

$$\nu = (1.02 \pm 0.12)\,\langle\nu\rangle_A \sqrt{\frac{N_g}{\langle N_g\rangle_A}}$$

where N_g is the observed number of grey particles of a particular event and $\langle N_g\rangle_A$ is the average over all events for the particular target nucleus.

The result, shown in Fig. 3.3.2, shows that R vs ν falls on the same straight line, independent of energy, in agreement with the absence of cascades. Besides, various ways to define ν are consistent. They all fall on the same straight line and justify the introducing of

ν . Chao et al. (1983) parametrized R as

$$R = 1 + \beta (\nu - 1)$$

with R = 1 when ν = 1. In principle, β may depend on the projectile; however it seems to be a universal constant according to experiment (Chao et al., 1983) (Fig. 3.3.2).

3.3.3 Angular and Rapidity Dependence

The angular dependence of R is also interesting. The interesting feature is the increase of R occurs entirely at large angles. That is, no multiplication is seen in the forward direction (Busza, 1975). It is because the particles are deflected by some angle in every collision so the forward particles are absorbed and redistributed to larger angles. We can also put it into the pseudo-rapidity language. As in h-h collsion, the pseudo-rapidity η is defined as

$$\eta \equiv - \ln \tan \left(\tfrac{1}{2} \theta \right)$$

Small angles correspond to large η . A ratio r is defined as

$$r \equiv \frac{d \langle n \rangle_A (\eta; E, \nu)}{d\eta} \Big/ \frac{d \langle n \rangle_A (\eta, E; \nu=1)}{d\eta}$$

The information of r gives us the structure of R in pseudo-rapidity space. The pseudo-rapidity dependence of r is shown in Fig. 3.3.3. It shows that r decreases with

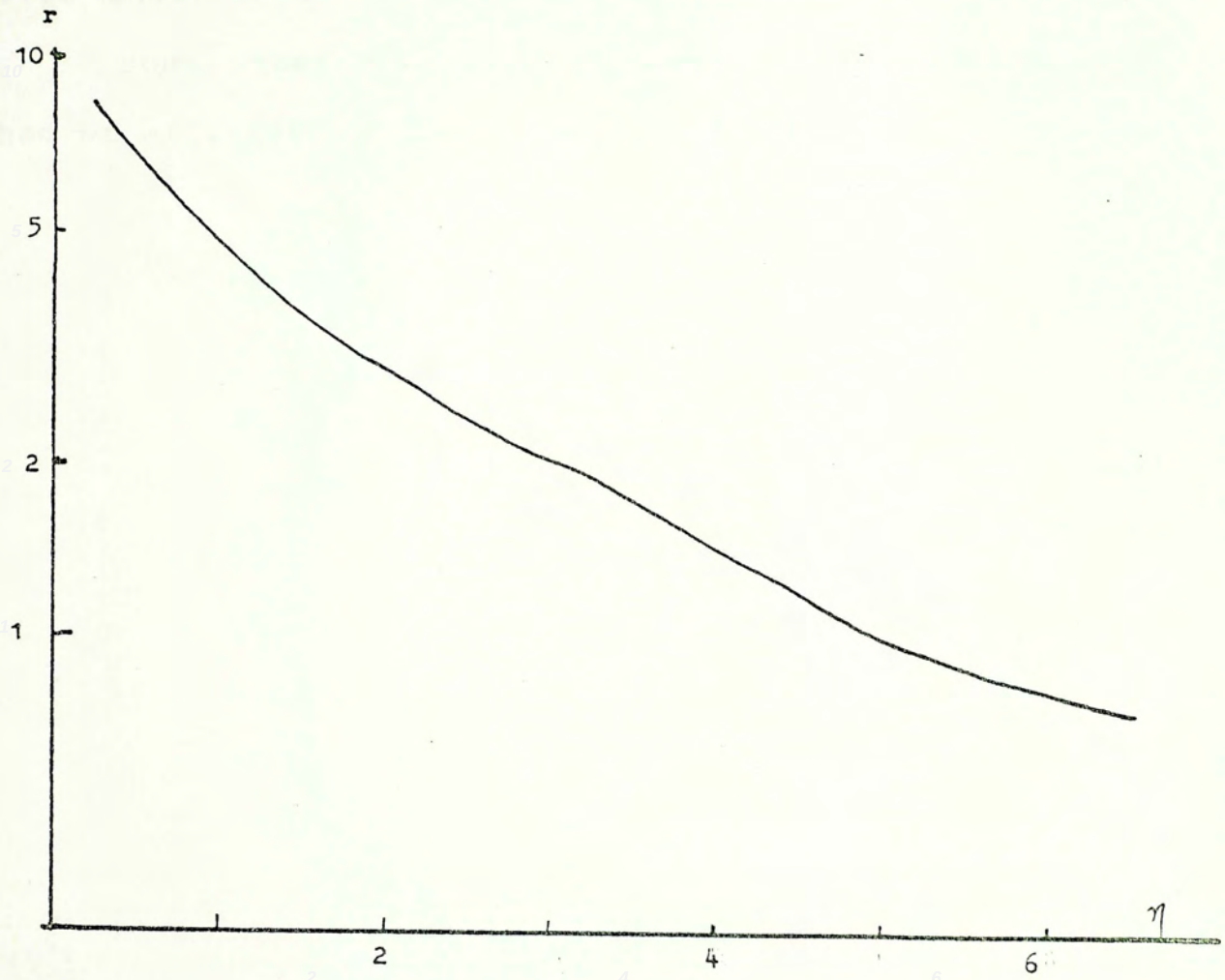

Fig.3.3.3 Rapidity dependence of r at 200 GeV for h-Em.

the increase of η i.e. with the decrease of angle. For ν =3.1, at large angles, the ratio of multiplicity is about 10, hence large multiplicity is observed. At small angles, r is smaller than 1 so the fast forward particles are absorbed. The detail explanation of such feature is still unclear.

Some other interesting parameters are discussed by Chao et al.,(1983). They are put in the Appendix C.

Chapter 4

The Multiplicity Distribution in h-A Collision

4.1 Introduction

It has been known for a long time that the multiplicity distribution for h-h collision seem to obey KNO scaling. That is the function

$$\langle n \rangle \frac{\sigma_n}{\sigma_{in}} \equiv \langle n \rangle P_n \equiv \psi$$

is independent of energy and is only a function of variable n / < n > in the high energy limit, where σ_n is the topological cross section of producing n particles and <n> is inserted so that $\psi\left(\frac{n}{\langle n \rangle}\right)$ is normalized. It is claimed that KNO scaling seems also valid in e^+e^- scattering (Beger et al., 1980) and in lepton-nucleon collisions (Zieminska et. al., 1983). Recent experiments at ISR and pp collider at CERN seem to support KNO scaling up to $\sqrt{s}$ = 540 GeV. Therefore it is natural to see whether such scaling holds for a nuclear target, and whether such scaling is universal across nuclei.

Recently high statistic data in multiplicity distribution in h-A collisions have been presented (De Marzo,1982). Since only the produced particles due to the collision are interesting, the evaporated and the knock-out nucleons must be eliminated. Those particles are mainly with the momentum below 600 MeV/c. The particles with momentum larger than 600 MeV/c are treated as produced particles. Most of them are pions. Produced

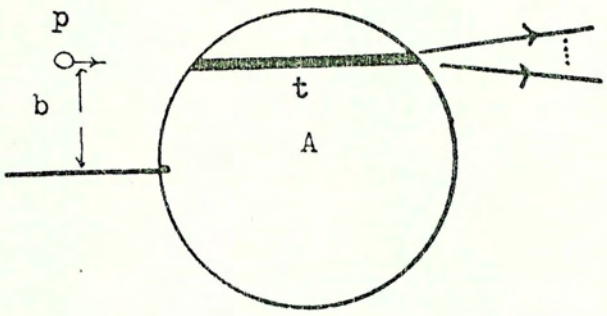

Fig.4.2.1 Geometric picture for p-A collision.

particles with β larger than 0.7 are called the shower particles. In the following only the shower particles are concerned. The experimental data show that the universal KNO scaling over the nuclei breaks down. For larger nuclei the peak of the scaling function ψ shifts to the smaller values of $n/\langle n\rangle$; the normalized dispersion and skewness increase. As proposed by Kiang et. al.(1983), if the multiplicity distribution in h-N collision obey universal KNO scaling at each impact parameter, then the above properties can be explained in this model, which is sketched below.

4.2 Formalism

At high energies, the wavelength of the projectile is much smaller than the nuclear radii and the beam fragments are confined within a narrow forward cone because of the limitation on transverse momenta. Hence it is reasonable to say that the collision occurs at a specific impact parameter b, Fig.4.2.1. What the experiments measure is the average contribution due to different impact parameters. This is the so-called geometric picture. For each b, the nuclear thickness t(b) is

$$t(b) = \int dz\, \rho(r) \qquad r = [z^2 + b^2]^{1/2}$$

where the nuclear density is taken to be of Woods-Saxon form for A > 12.

$$\rho(r) \propto \left[1 + \exp\left(r - \frac{R}{S} \right) \right]^{-1} \qquad R = R_0 A^{\frac{1}{3}}$$

$$R_0 = 1.12 \qquad S = 0.545$$

in unit of fm, and normalised to

$$\int d^3r \, \rho(r) = A$$

The probability of an elastic reaction is 1-exp(- σ t(b)), where $\sigma = \sigma_{in}^{hN}$ is the inelastic h-N cross section. By frozen approximation, the target is taken to be a tube of hadronic matter of area d^2b,(the rest of the nucleus are spectators), and the inelastic cross section is

$$d\sigma_{in} = d^2b \left[1 - e^{-\sigma t(b)} \right]$$

The total inelastic cross section is then

$$\sigma_{in}^{hA} = \int d^2b \left[1 - e^{-\sigma t(b)} \right]$$

This formula fits σ_{in}^{hA} for A > 12 to a few percent.

It is an experimental fact that the average multiplicity <n> increases linearly with the number of inelastic collisions.

$$\langle n \rangle (E, \nu) = \langle n \rangle^{hN}(E) \left[1 + \beta (\nu - 1) \right] \qquad (4.2.1)$$

where $\langle n \rangle^{hN}(E)$ is the hadron-nucleon multiplicity at incident energy E and $\beta = 0.5$ (Chiu et al, 1982). The factor β describes the degree of intranuclear cascading where $\beta = 0$ implies no secondary multiplicity, larger β

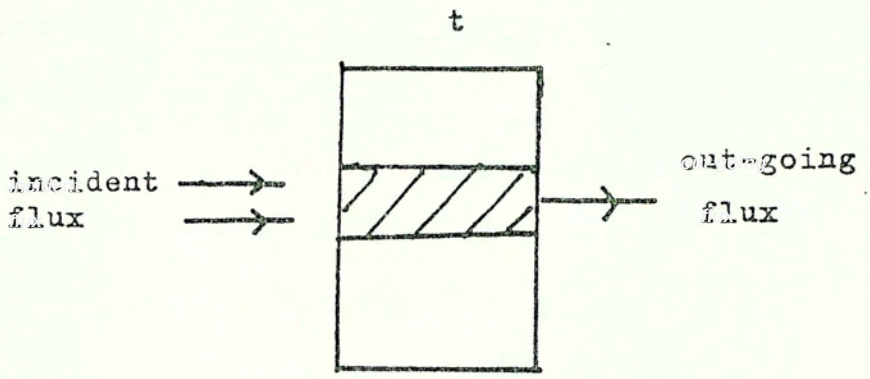

Fig.4.2.2 Absorption of incident flux by nuclear target with thickness t.

leads to higher secondary multiplicity.

Theoretically, one can define the number of collisions in every impact parameter b. Different b gives different nuclear thickness t for the projectile to go through and different multiplicity produced. Let us consider the projectile goes through a thickness. The inelastic cross section is assumed to be constant during the whole journey. It is reasonble to say that the number of collision is proportional to σt, however when the incident flux goes through the nuclear matter, it will be absorbed. The out-going flux is $e^{-\sigma t}$ (Fig.4.2.2). The number of scattered particles per time per area is $1-e^{-\sigma t}$, hence the average ν for fixed thickness is

$$\nu(b) = \frac{\sigma t}{1 - e^{-\sigma t}}$$

Such expression for $\nu(b)$ has following good properties:

1) $\nu(b) > 1$

2) $\langle\nu\rangle = \int d^2b \ (1-e^{-\sigma t}) \ \nu(b) \ / \int d^2b \ (1-e^{-\sigma t})$

$$= \frac{A\sigma}{\sigma_{in}^{hA}}$$

which is the usually accepted definition of $\langle\nu\rangle$.

3) $\langle n\rangle^{hA} / \langle n\rangle^{hN}$ is 1 for $t \sim 0$ and $\beta\sigma t$ for large t

4) equation 4.2.1 leads to

$$\langle n\rangle^{hA}(E) = \langle n\rangle^{hN}(E) \ [1 + \beta(\langle\nu\rangle - 1)] \qquad (4.2.2)$$

The general features of the results really depend

only on these properties, and are insensitive to the detailed assumptions on ν .

Having found the average multiplicity $\langle n \rangle (b,E)$ at each impact parameter b and energy E, the average multiplicity of the whole nucleus can be calculated. In analogy with hadron-hadron scattering, one expects $\langle n \rangle (b,E)$ to have KNO scaling. Besides, the homogeneity of nuclear matter implies that a tube is characterized only by its thickness t(b), and no information on A is needed (Fig.4.2.1), so the KNO function for each tube is expected to be universal across nuclei. This hypothesis of universal KNO scaling at each impact parameter is the basis of the model.

With these assumptions, the n-prong cross section on a nucleus A at incident energy E is

$$\sigma_n^{hA}(E) = \int d^2b \left[1 - e^{-\sigma t(b)}\right] \psi\left(\frac{n}{\langle n \rangle (b,E)}\right) \frac{1}{\langle n \rangle (b,E)} \qquad (4.2.3)$$

To determine ψ, note that for A = 1, $\nu(b) = 1$ for all b, and $\langle n \rangle (b,E) = \langle n \rangle^{hN}(E)$ is independent of b. Hence it gives

$$\sigma_n^{hN}(E) = \sigma_{in}^{hN} \psi\left(\frac{n}{\langle n \rangle^{hN}}\right) \frac{1}{\langle n \rangle^{hN}}$$

so ψ is recognized as the KNO function for hadron-nucleus scattering. If the hadron is a proton then ψ is parametrized by Slattery (1972) :

$$\psi(\xi) = \frac{1}{2}\left(3.79\,\xi + 33.7\,\xi^3 - 6.64\,\xi^5 + 0.312\,\xi^7\right) e^{-3.04\xi}$$

where $\xi = n/\langle n \rangle$

The philosophy is to regard h-h scattering as elementary, and build up h-A scattering via (4.2.3).

It is convenient to rewrite (4.2.3) in terms of scaling variables:

$$\psi_A(\xi, E) = \langle n \rangle^{hA}(E) \quad \frac{\sigma_n^{hA}(E)}{\sigma_{in}^{hA}(E)}$$

$$= \int d^2b \left(1 - e^{-\sigma t}\right) \psi\left(\frac{\xi}{g}\right) \frac{1}{g} \Big/ \int d^2b \left(1 - e^{-\sigma t}\right) \quad (4.2.5)$$

where

$$g(b) = \frac{1 + \beta\,(\nu(b) - 1)}{1 + \beta\,(\langle \nu \rangle_A - 1)}$$

has an average value of unity when weighted by the interaction probability:

$$\int d^2b \left(1 - e^{-\sigma t}\right) g(b) \Big/ \int d^2b \left(1 - e^{-\sigma t}\right) = 1$$

4.3 Result

4.3.1 Energy Dependence

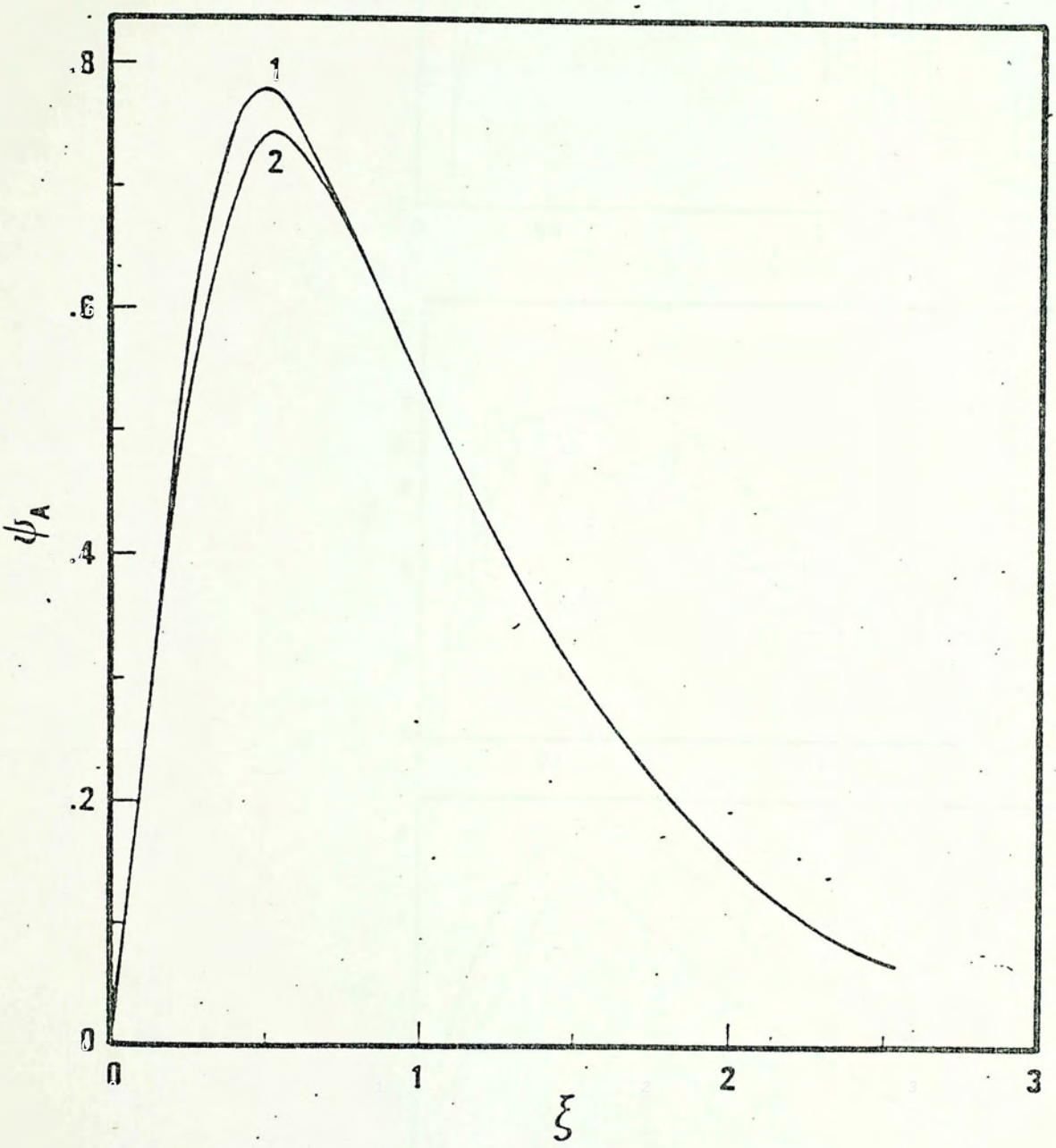

Fig.4.3.1 The calaulated Ψ_A for U^{235} at 300 GeV(curve 1) and 30 GeV(curve 2).

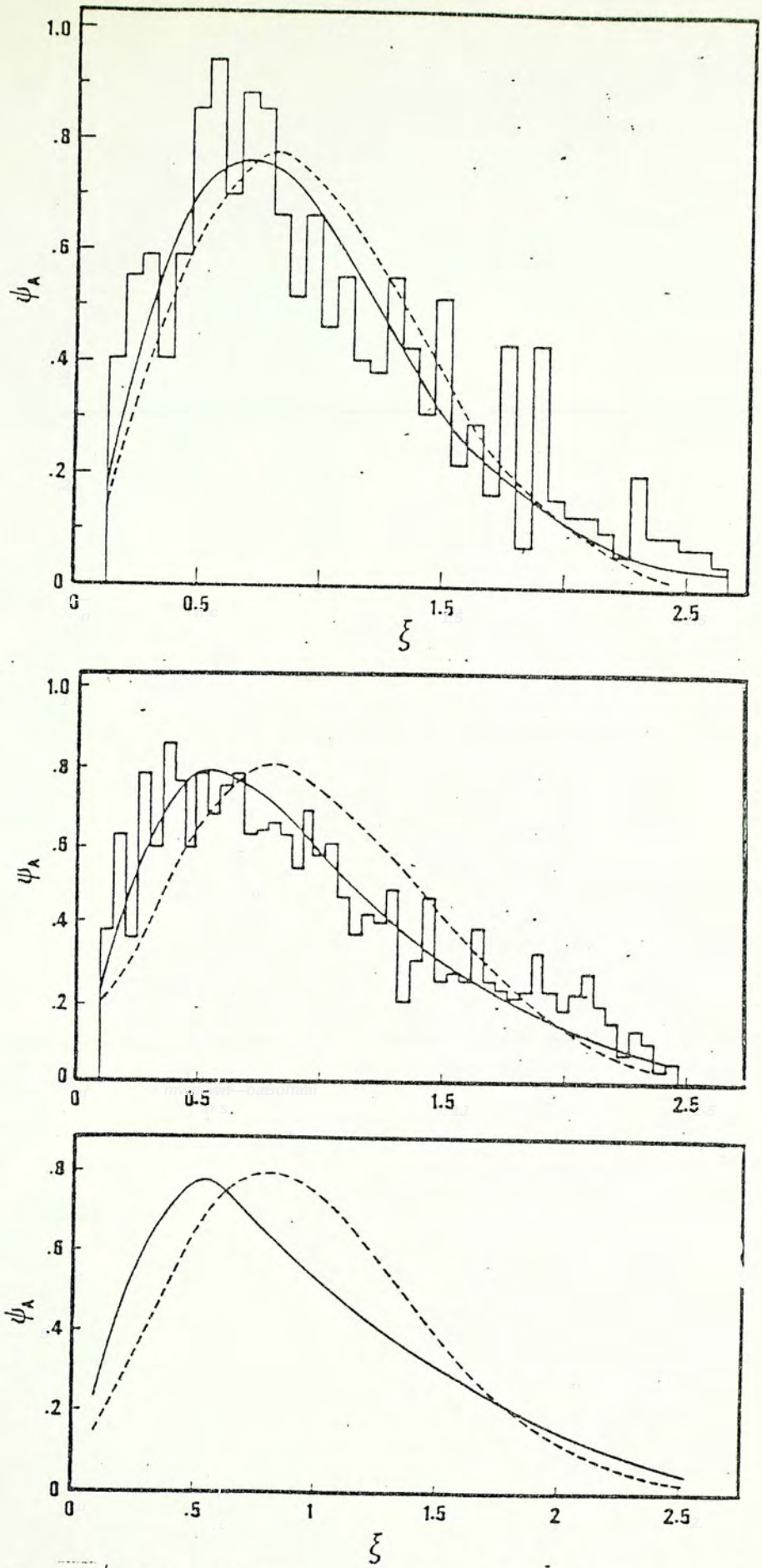

Fig.4.3.2 Ψ_A for 200 GeV: (a) p-Ar, (b) p-Xe, (c) p-U. The histograms are data from De Marzo. The solid lines are calculated values and the dash lines are the Slattery curve.

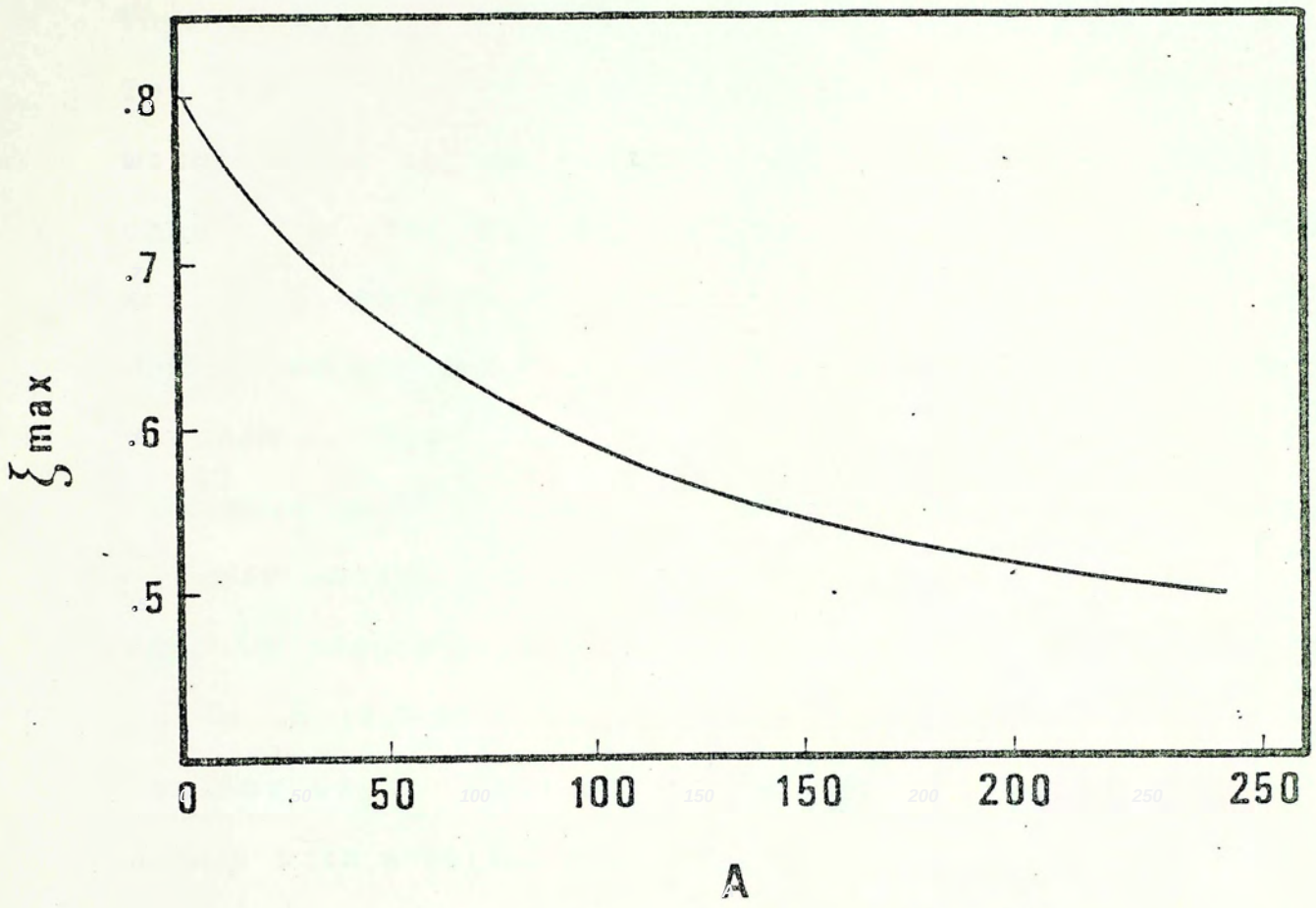

Fig.4.3.3 A dependence of ξ_{max}.

The energy independence of ψ_A for small A has been put in by hand; it therefore remains to study the case of large A. Fig. 4.3.1 shows the calculated ψ_A for uranium at 30 GeV and 300 GeV; they are for all purposes identical. Thus scaling is approximately valid for nuclear targets. The explanation is as follow. Although $\langle n \rangle^{hN}$ increases with energy rather rapidly (4.5 to 8.2 respectively, a change of over 80% from 30 GeV to 300 GeV), the KNO scaling eliminated the dependence on $\langle n \rangle^{hN}$ leaving only the dependence through $\sigma(E)$, including the implicit dependence through q. However, the increase of $\sigma(E)$ is quite slow (a change of 9% in the same energy range). Moreover, much of this energy dependence cancels, since in (4.2.5), $1-\exp(-\sigma t)$ occurs both in the numerator and the denominator, while in (4.2.6) both $\nu(b)$ and $\langle \nu \rangle$ increase with E in similar ways. This prediction of approximate scaling agrees with experiment (De Marzo, 1982).

4.3.2 Universality

It is clear that $\psi_A(\zeta, E)$ will depend on A, so universal KNO scaling does not hold. Fig.4.3.2 shows ψ_A comparing with ψ, together with experimental data where available. (Some early low-statistics emulsion experiments (Florian, 1979), whose conclusions seem to be at variance with the more recent data, (De Marzo et al.,1980) have been excluded). It is seen that the theory predicts a shift of the peak of ψ_A towards smaller ζ, which agrees with the data. This is shown more clearly in

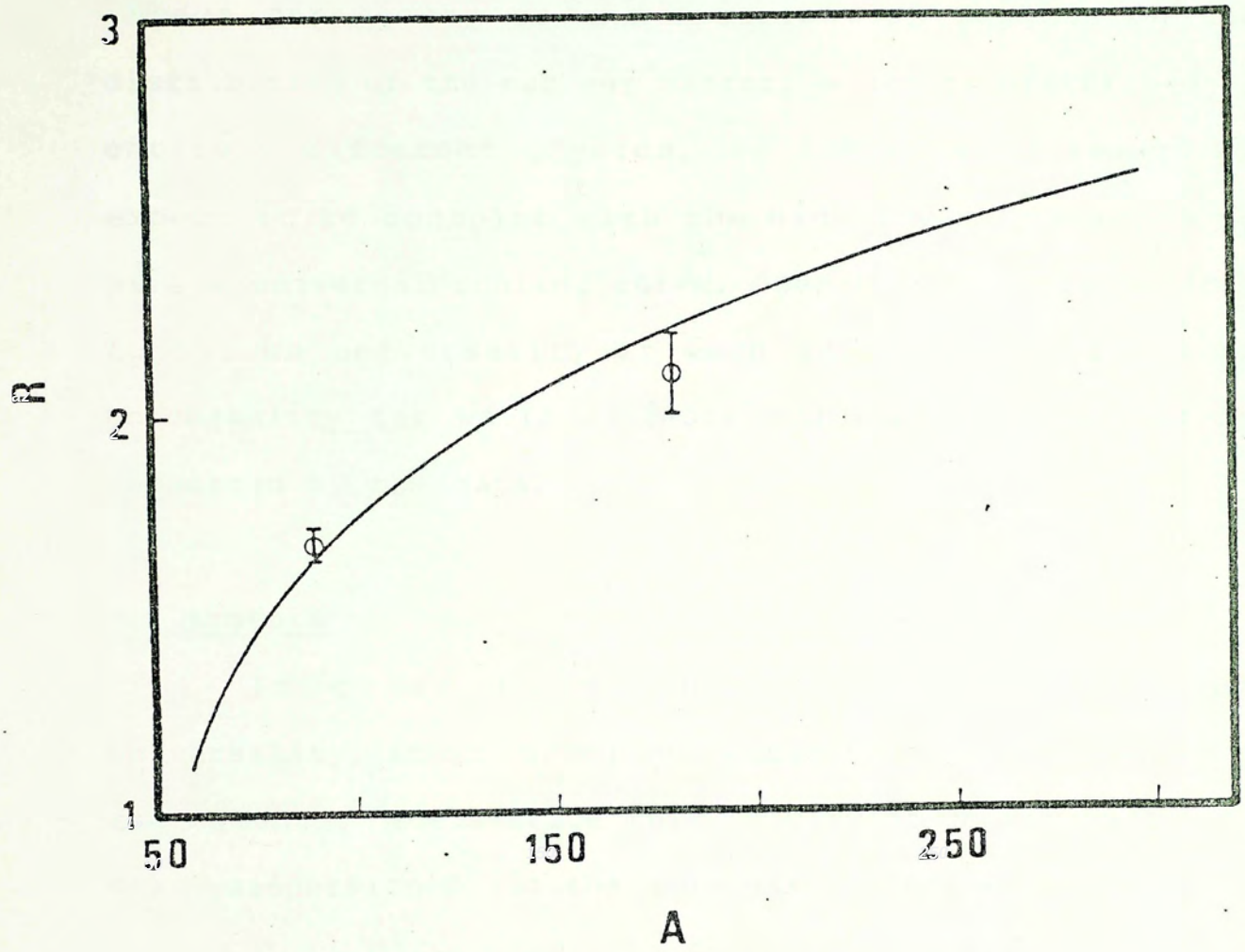

Fig.4.4.1 A dependence of R

Fig. 4.3.3.

It is not suprising that universality breaks down. Since the multiplicity distribution is the average of each impact parameter, so the distribution depends on the distribution of the nuclear matter, which is determined by entirely different physics, so there is no reason to expect it to conspire with the high energy dynamics to give a universal scaling curve. Hence it is more natural to assume universality at each impact parameter than universality for whole nucleus, and indeed the former is supported by the data.

4.4 Moments

In order to discuss the deviation from universality, it is common to consider the A dependence of the moments: the average multiplicity of shower particles $\langle n \rangle$,dispersion D and the skewness S, defined as

$$D^2 = \left\langle \left(n - \langle n \rangle^{hA} \right)^2 \right\rangle_A$$

$$S^3 = \left\langle \left(n - \langle n \rangle^{hA} \right)^3 \right\rangle_A$$

where $\langle \quad \rangle_A$ indicates average with respect to all inelastic events on nucleus A.

In order to concentrate on the A dependence, the multiplicity ratio $R = \langle n \rangle^{hA} / \langle n \rangle^{hN}$, is shown in Fig. 4.4.1. Incidentally, if a power law $R = A^{\gamma}$ is fitted, then $\gamma = 0.25$

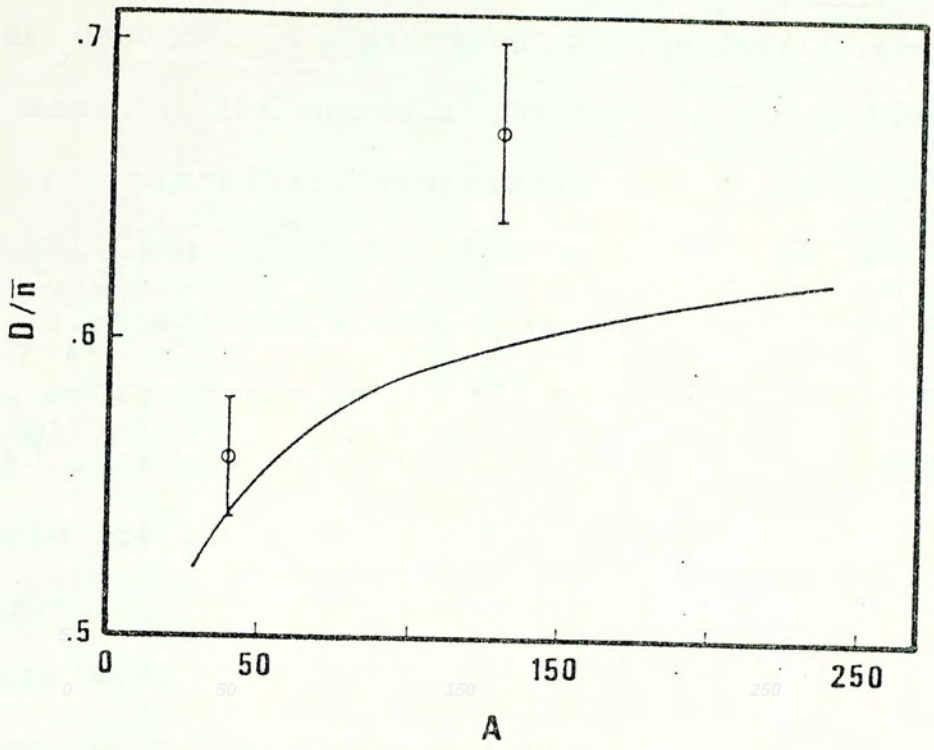

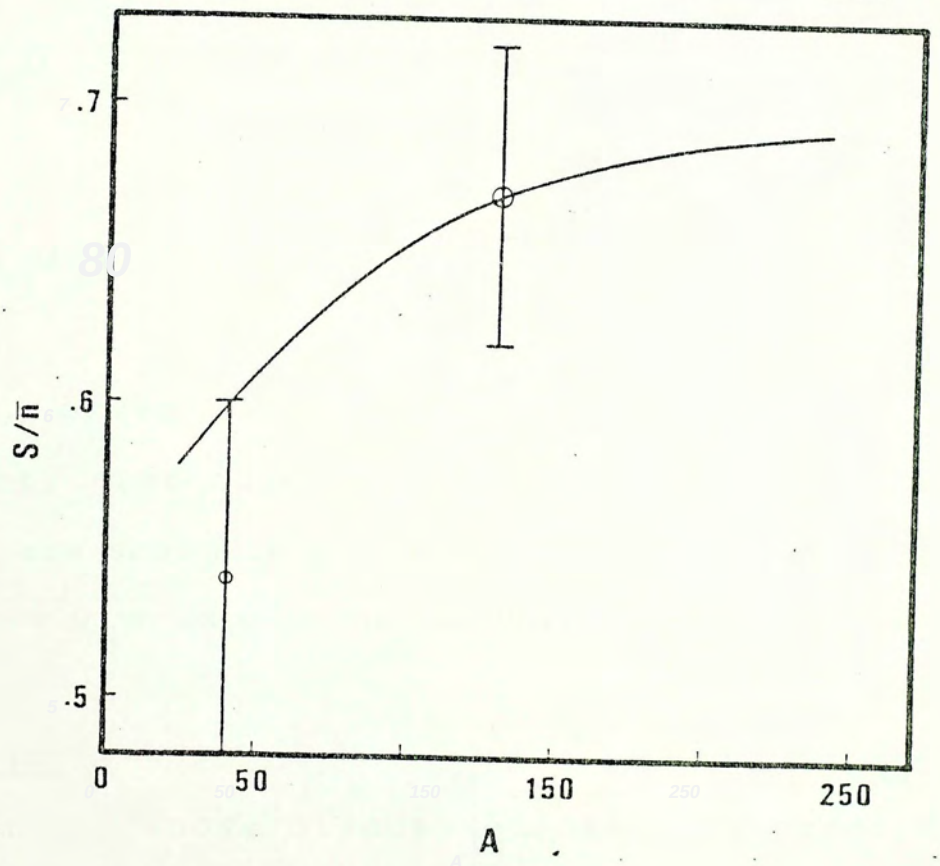

Fig.4.4.2 A dependence of normalized dispersion and skewness.

The smallness of γ both expresses the absence of internuclear cascades and provides good evidence against geometric scaling for nuclei. According to geometric scaling, all dynamics are controlled by a single length scale b (A,E). But $\sigma_{in}^{hA}(E) \propto A^{\frac{2}{3}} \sigma_{in}^{hN}(E) \propto A^{\frac{2}{3}} (\ln E)^2$ at high energies, so if all the A and E dependence enters only through b , every factor of $(\ln E)^2$ must be accompanied by a factor $A^{\frac{2}{3}}$. Since $\langle n \rangle^{hA}$ goes as $(\ln E)^2$,so geometric scaling would predict that $\langle n \rangle \propto A^{\frac{2}{3}}$, a dependence which is far too strong.

As the same reason of introducing R, the dispersion and skewness are best expressed in the normalized form

$$D/\langle n \rangle^{hA} = \left[\int (\xi - 1)^2 \psi_A(\xi) \, d\xi \right]^{1/2}$$

$$S/\langle n \rangle^{hA} = \left[\int (\xi - 1)^3 \psi_A(\xi) \, d\xi \right]^{1/3}$$

which are, given the approximate scaling, energy independent. The calculated A dependence of these quantities are shown in Fig. 4.4.2. The gentle increase with A agrees with experiment (De Marzo et al., 1982).

4.5 Conclusion

From the above discussion, the universal KNO scaling at each impact parameter seems to be in agreement with the data. The origin of KNO scaling in h-h collisons is still unclear. However, the universality would relate

the particle production in h-A collision to h-h collision, and hence provide constraints for theoretical models.

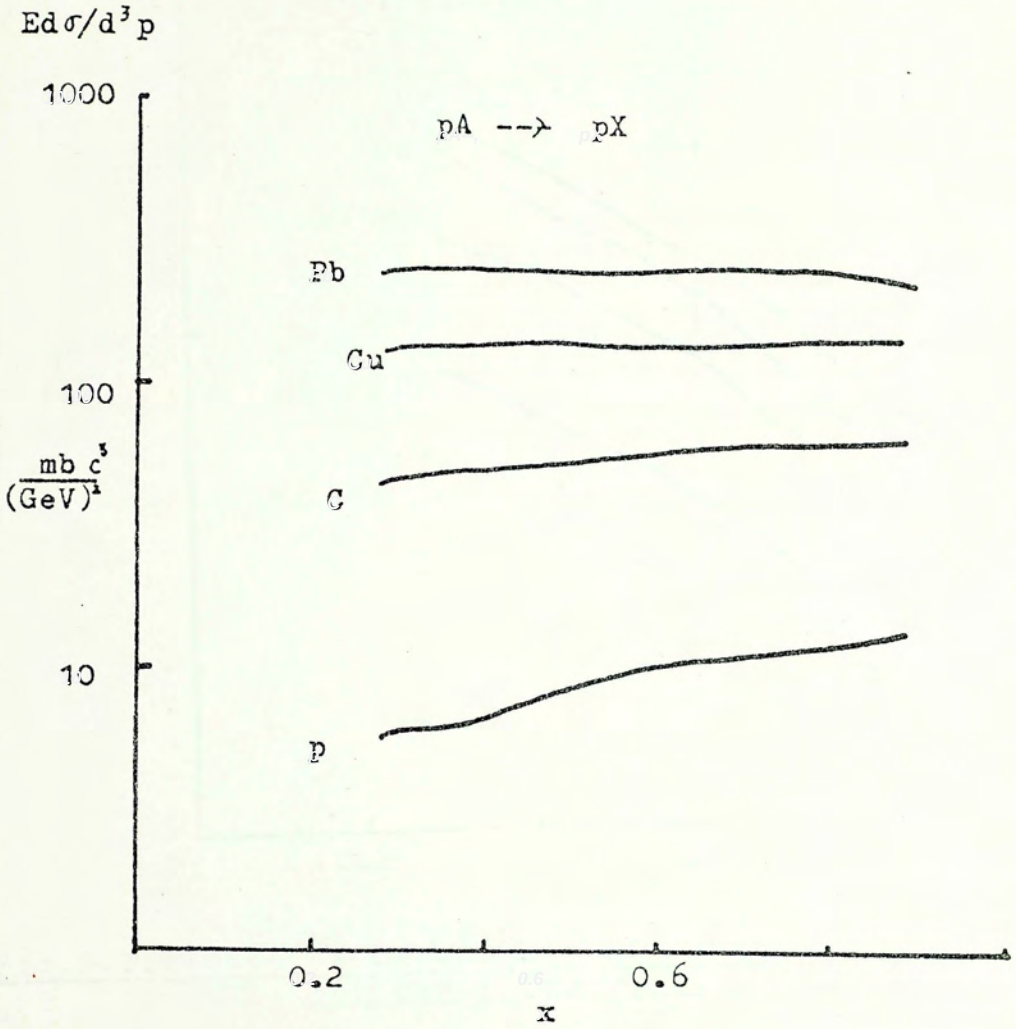

Fig.5.1.1(a) x dependence of invariant cross section for leading particle channel.

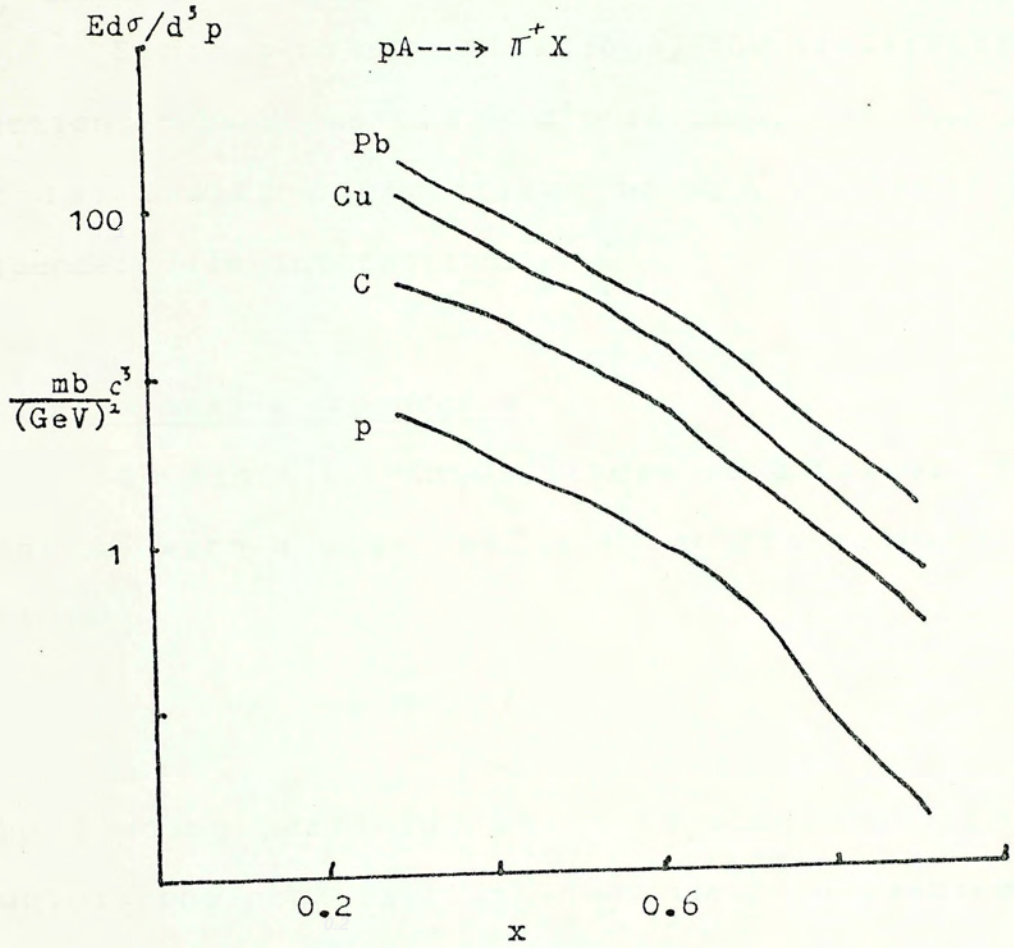

Fig.5.1.1(b) x dependence of invariant cross section for other channel.

Chapter 5

Inclusive Process in h-A Collision

5.1 Single Particle Inclusive Production

Similar to h-h collisions, the differential cross sections defined as $Ed\sigma / d^3p$ is used. In h-A collision, it is usually parametrized as $\sigma_0 A^{\alpha}$. The following dependence is interesting.

5.1.1 Feynman-x dependence

As Fig 5.1.1 shows, there is a rather flat cross section with a peak near x=1 for the leading particle channel.

$$p + A \rightarrow p + X$$

The leading particle effect is observed. For larger nuclei, the peak is flattened, i.e. the leading particle effect is reduced for larger A. The other channels, with the out-going particle different from the incoming one, show a decrease in cross section with increasing x.

5.1.2 Feynman Scaling and Factorization

After comparing the data with Eichten et al. (1973) at 24 GeV, Barton et al. (1983) pointed out that the limiting fragmentation does not hold and the fragmentation of the projectile does depend on the target. Therefore both the Feynmam scaling and the factorization break down.

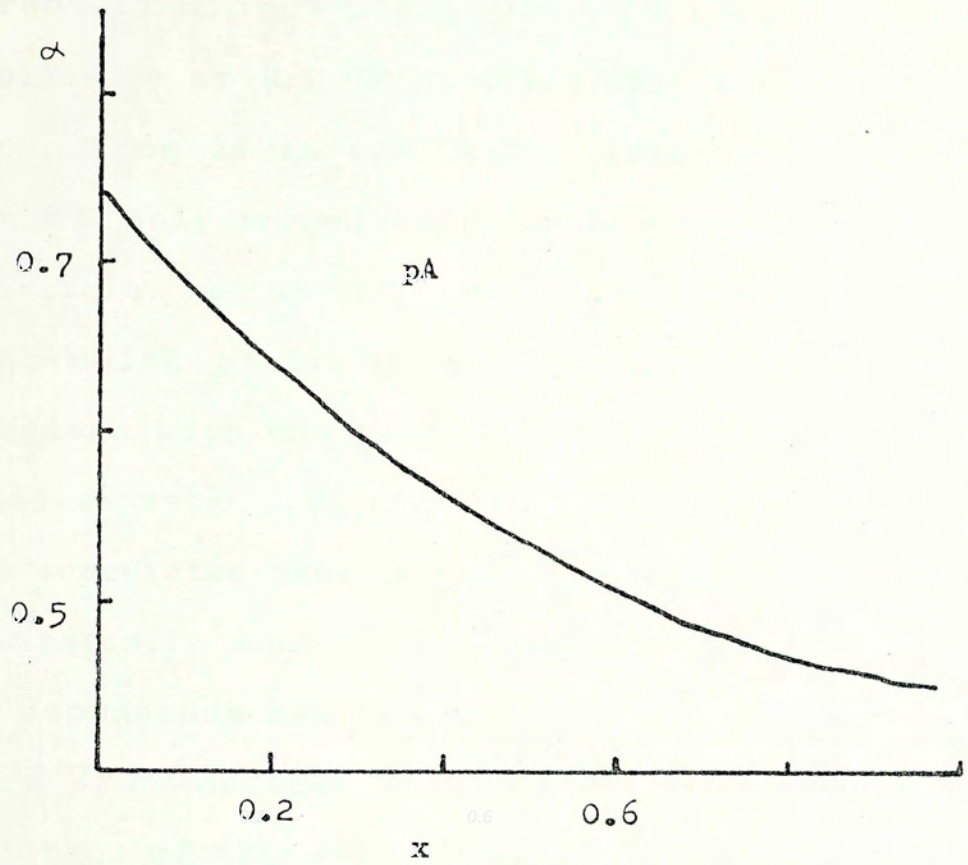

Fig.5.1.2 x dependence of α for pA collision.

5.1.3 The A Dependence

The A dependence of $Ed\sigma/d^3p$ is expressed by exponent α. After reviewing data on the inclusive production of $\pi^{\pm}$, $K^{\pm}$, p, $\bar{p}$, K°_{s}, Λ, $\bar{\Lambda}^{\circ}$, n and $\bar{\Xi}^{\circ}$ in p-A collision at 0.3 GeV/c transverse momentum with energies span from 24 to 400 GeV, Barton el at. (1983) claimed that α only depends on Feynman x and the type of incidence particle, but is independent of the energy and the type of out-going particle (Fig. 5.1.2). The exponent α decreases with the increase of x from about 0.7 at x=0.1 to 0.45 at x=0.9. If the inclusive differental cross section is integrated over x, then suming up all channels, it will essentially equal the inelastic cross section, hence the A-dependence behaves as in the inelastic cross section. Let $\bar{\alpha}$ be defined as $\sigma_{in}^{hA} = \sigma A^{\bar{\alpha}}$, then $\bar{\alpha}$ is the weighted average of $\alpha(x)$ over x, so $\alpha(x)$ lies between 1 and 0. At small x, the cross section is mainly due to the target fragmentation, hence it strongly depends on the property of the target, so $\alpha(x)$ is larger. At larger x, the cross section is mainly due to the projectile fragmentation so the A-depence is weak. The average of α is about 2/3. However, the universality of α is difficult to explain in current models. Whether the presentation of the data is completely valid is also challenged (Hwa, 1984).

5.2 Two Particle Correlation

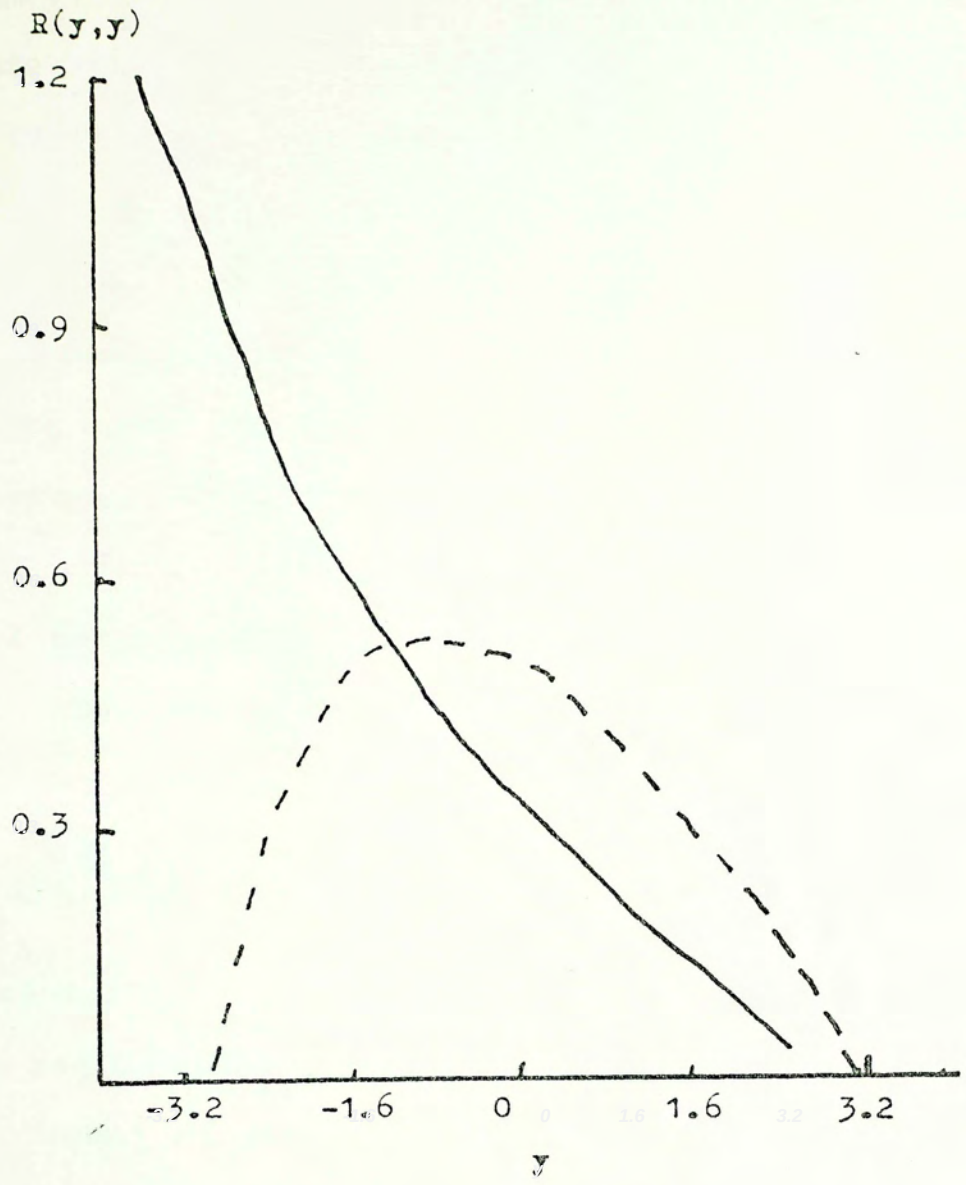

Fig.5.2.1(a) R(y,y) at 200 and 400 GeV for p-Em.

Extensive studies of correlations in h-h collision started around 1975 mainly in the second generation experiments at the ISR. An important result of the studies was the existence of clusters in the rapidity space. By 1979, various types of correlations were available, e.g. charge correlation, angle correlation etc.. However in h-A collisions, less data is presented in the study of the two particle correlation. In the following, two correlations will be discussed.

5.2.1 Rapidity Correlation

The two particle correlation function R is written as

$$R(y_1, y_2) \equiv \frac{N_T \, N_2(y_1, y_2)}{N_1(y_1) \, N_1(y_2)} - 1$$

where N_T, $N_1(y)$ and $N_2(y_1, y_2)$ denote the number of events in a sample, the number of particle with rapidity y and the number of particle pairs with rapidities y_1 and y_2. The rapidity is measured in the c.m frame of proton-nucleon system.

The data of R(y, y) and R(y, -y) are shown in Fig. 5.2.1, at 200 and 400 GeV for proton-emulsion collisions (Aggarwal, 1984). The data show the following features:

1) In the forward hemisphere ($y > 0$), the correlation R(y, y) is weak compared to the backward hemisphere ($y < 0$). That is, in the proton fragmentation region($y > 0$), it is rare to obtain two or more particles with same forward momentu[illegible] Suc[illegible] a[illegible] is similar to the

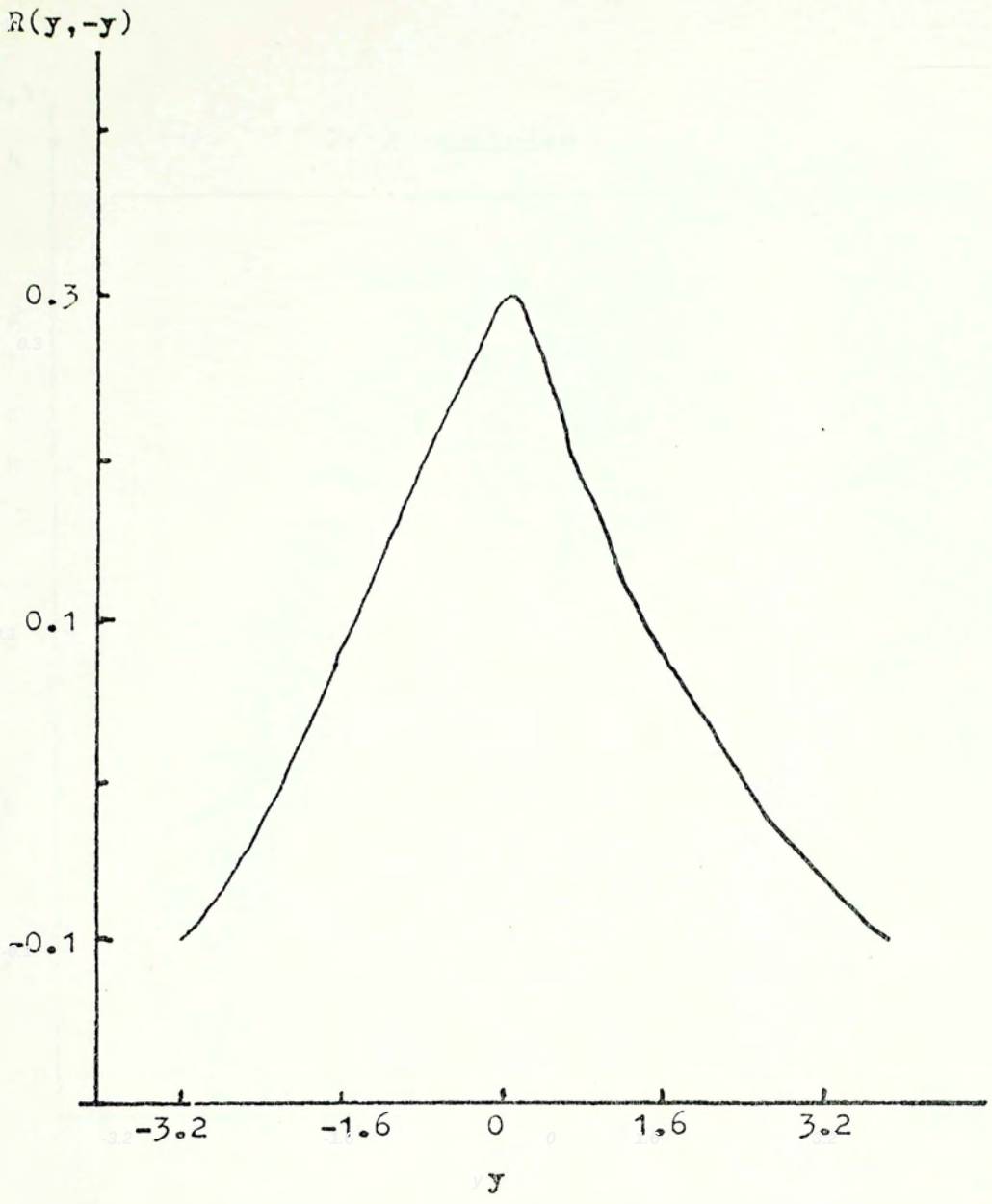

Fig.5.2.1(b) R(y,-y) at 200 and 400 GeV for p-Em.

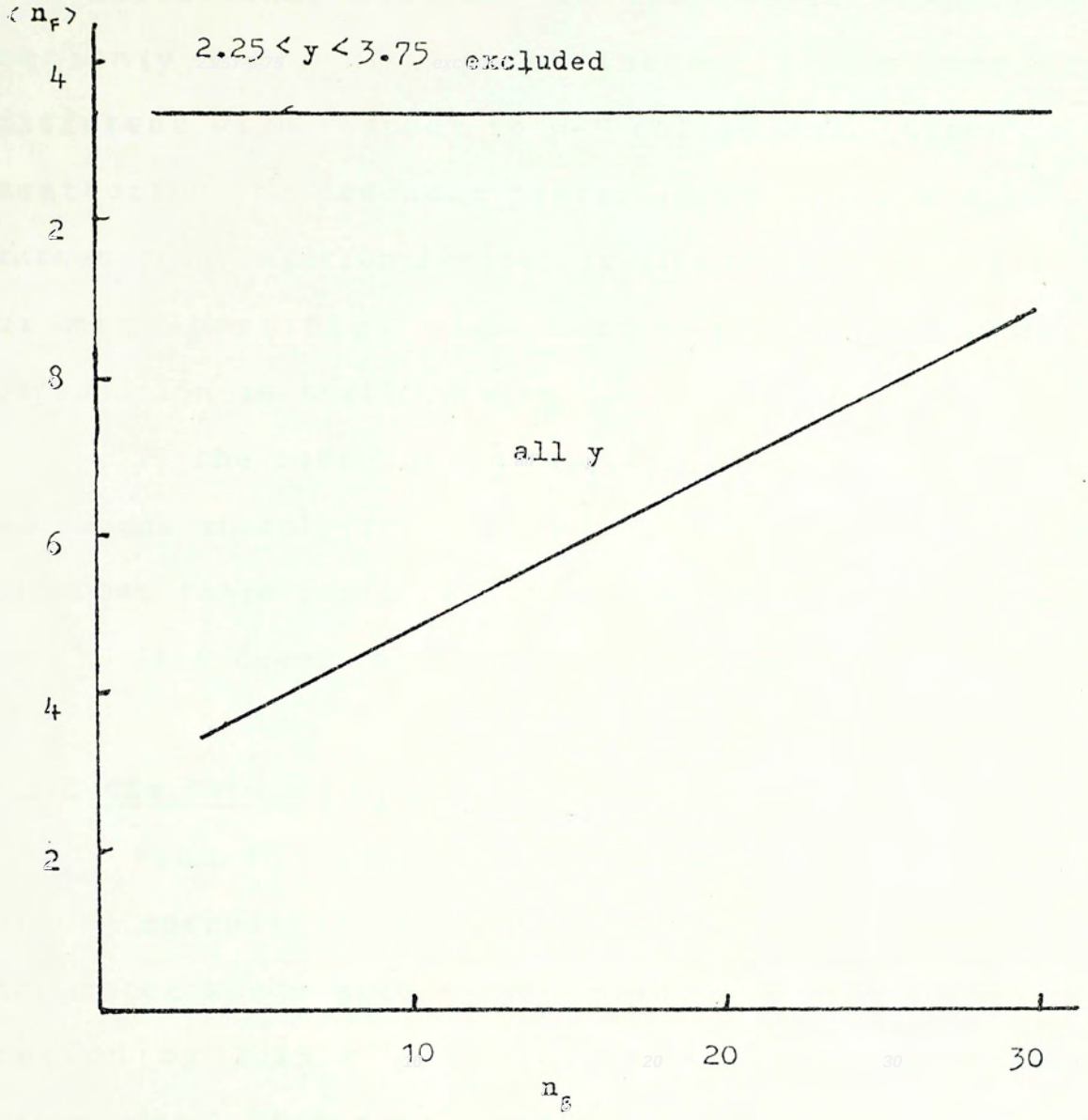

Fig.5.2.3 $\langle n_F \rangle$ vs n_β.Both the short range and long range are shown.

h-N collisions. However, in the target fragmentation region($y < 0$), $R(y_1, y_2)$ is large. It is completely different with respect to p-N collisions. Since in h-A scattering the produced particles accumulate along the target fragmentation region, it is more likely to find two or more particles with same rapidity. The detail explanation is still lacking.

2) The correlation $R(y, -y)$ is maximum for $y = 0.4$ and drops sharply for large $|y|$. This shows the existence of short range positive correlation in the central region.

3) R seems to be energy independent.

5.2.2 The Forward-backward Correlation

From Fig.5.2.3, which shows $\langle n_F \rangle$ versus n_B, a strong correlation is seen. However, after eliminating the short range effect by cutting the central rapidity region by $2.25 < y < 3.75$, the correlation almost disappears. This result indicates the presence of strong short range correlations in central region and only very weak long range correlations between the two fragmentation region.

Chapter 6

Discussions and Conclusions

In this thesis, some interesting features of soft processes in h-h scattering and in h-A scattering at high energies are discussed. The energy dependence of the usual parameters, e.g. cross sections, average multiplicity etc., are rather weak. They are usually fitted as polynomials in ln s, so it is said that they are "ln s physics".

In h-A collsions, a formalism, based on the universal KNO scaling at each parameter, is proposed to explain the multiplicity distribution. It seems to be in agreement with data. Recently, violation of KNO scaling at $\sqrt{s}$ = 540 GeV is confirmed (UA5 Collab., Alner et al., 1984). However, this discovery does not affect the results in chapter 4 because in chapter 4 the energy concerned (E_{lab} = 200 GeV, $\sqrt{s}$ = 20 GeV) is within the range of energy in which the KNO scaling holds.

So far, however, there is no rigorous and fundamental formalism to link up all the experimental data. The standard perturbation method cannot be applied to soft process in QCD. Phenomenological analysis is still the main tool in this realm. Although different models based on different physics claim to fit data, a unified and consistent model is still lacking.

What happens when the hadrons collide still has a lot of problems for us to solve.

Appendix A

Showing R=0 When the Particles Produced Independenly

When $c_1 \neq c_2$ then

$$R(y_1, y_2) = \frac{\langle n_{c_1} n_{c_2} \rangle \rho(y_1, y_2) - \langle n_{c_1} n_{c_2} \rangle \rho(y_1) \rho(y_2)}{\langle n_{c_1} n_{c_2} \rangle \rho(y_1) \rho(y_2)}$$

$$= \frac{\rho(y_1, y_2) - \rho(y_1) \rho(y_2)}{\rho(y_1) \rho(y_2)}$$

as other authors usually define. If c_1 and c_2 are produced independently

$$\rho(y_1, y_2) = \rho(y_1) \rho(y_2)$$

then

$$R(y_1, y_2) = 0$$

When $c_1 = c_2$, $n_{c_1} = n_{c_2} = n$, then some combinatoric factors come into consideration. If the particles are produced independently in y space,

$$\rho(y_1^a, y_2^b) = \rho(y_1^a) \rho(y_2^b)$$

Summing all the cases together we have

$$\sum_{(a,b)} \rho(y_1^a, y_2^b) = \sum_{\text{fix } a,b} \sum_a \rho(y_1^a) \rho(y_2^b)$$

$$\sum_{(a,b)} \rho(y_1^a, y_2^b) = n^2 \rho(y_1, y_2)$$

In $\sum_{\text{fix } a\ b} \sum_{a} \rho(y_1^a)\rho(y_2^b)$ a has n choices and b has n-1 choices, since a ≠ b

$$\therefore \sum_{\text{fix } a,b} \sum_{a} \rho(y_1^a)\rho(y_2^b) = n(n-1)\rho(y_1)\rho(y_2)$$

Therefore we have

$$n^2 \rho(y_1, y_2) = n(n-1)\rho(y_1)\rho(y_2)$$

after taken average

$$\langle n^2 \rangle \rho(y_1, y_2) = \langle n(n-1) \rangle \rho(y_1)\rho(y_2)$$

hence

$$C(y_1, y_2) \propto R(y_1, y_2) = 0$$

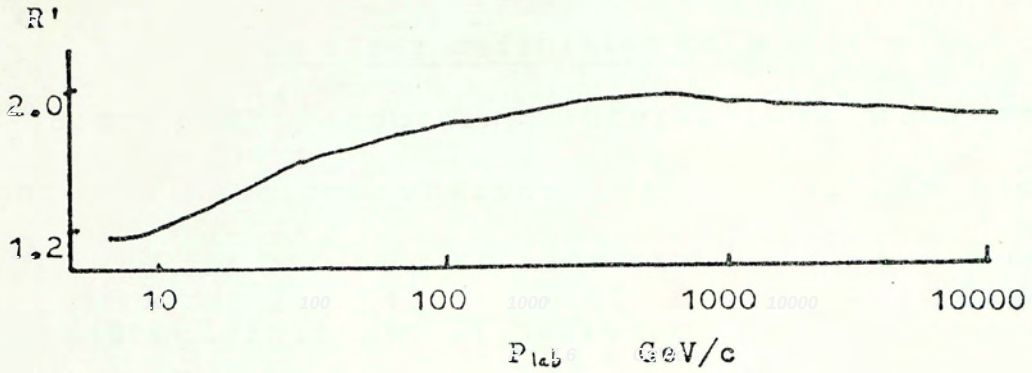

(a)

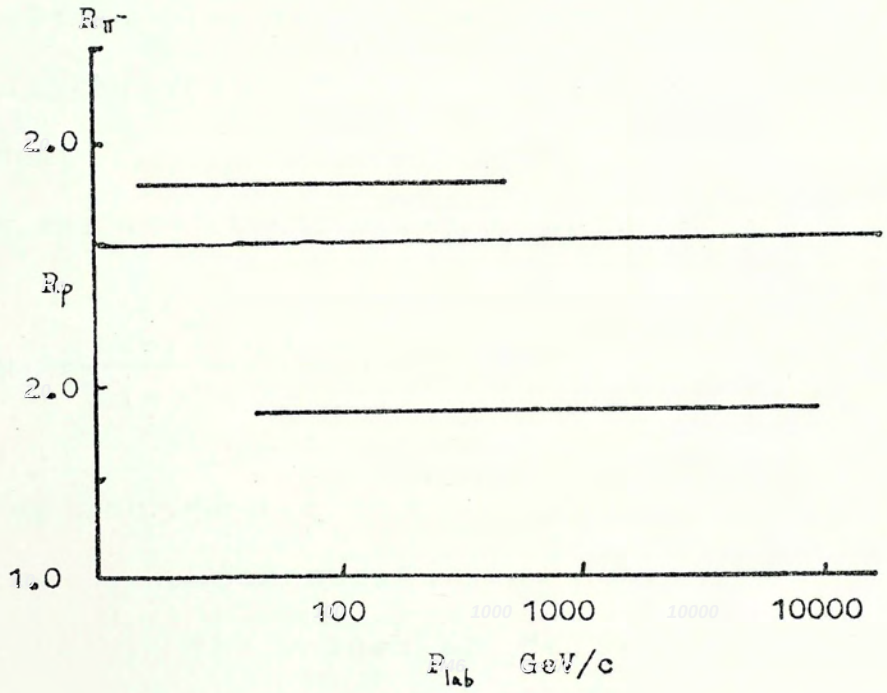

(b)

Fig.b.1 Energy dependence of different R.

Appendix B

Some other definition of R

Since $\langle n \rangle^{hA}$ contains interactions with target protons and neutrons whereas $\langle n \rangle^{hp}$ (E) is the average multiplicity for interaction with protons only. Therefore an average multiplicity of hadron-nucleon multiplicity should be used. A better ratio R' defined as

$$R' = \langle n \rangle / (\langle n \rangle - 0.5)$$

is suggested. The energy dependence of R' is shown in Fig.b.1.(a)(Aggarwal et al., 1977). It seems to be energy independent too.

Kumar (1978) has defined another R as

$$R = \frac{\langle n \rangle^{hA} - \alpha_A}{\langle n \rangle^{hp} - \alpha_H}$$

where α_A and α_H are the average number of leading particles in hadron-nucleus and hadron-proton reaction respectively. The values of α_A are 0.7 and 0 for p-Em and π^- - Em collision (Kumer et al.,1978) and the values of α_H are 0.9 and 1.2 for p-p and π^--p collisions (Buras et al.,1973). The ratio R_h is observerd to be energy independent beyond 50 GeV (Kaur et al., 1978), as Fig.b.1(b). shows.

After all, the difference between the ratios are negilible and they seem to be energy independent.

Appendix C

Some Other Parameters in h-A Collision

Some other interesting parameters are discussed by Chao (1983).

1. The variance of multiplicity

$$\sigma_n^{hA}(E,\nu) \equiv \sum_n \int d\eta \; (n - \langle n\rangle^{hA}(E,\nu))^2 \; P^{hA}(n,\eta;E,\nu)$$

where P^{hA} is the probability distribution for an event with n shower particles.

2. The mean of rapidity

$$\bar{\eta}^{hA}(E,\nu) \equiv \frac{1}{\langle n\rangle^{hA}} \int d\eta \; \eta \; \frac{d\langle n\rangle^{hA}}{d\eta}(\eta, E, \nu)$$

3. The variance of rapidity

$$\sigma_\eta^{hA}(E,\nu) \equiv \frac{1}{\langle n\rangle^{hA}} \int d\eta \; (\eta - \bar{\eta}^{hA})^2 \; \frac{d\bar{\eta}^{hA}}{d\eta}$$

The experimental data seem to suggest the following functional dependence.

$$\langle n\rangle^{hA} = \langle n\rangle(E) \; (1 + \alpha_n (\nu - 1))$$

$$\sigma_n^{hA} = \sigma_n(E) \; (1 + \beta_n (\nu - 1))$$

$$\bar{\eta}^{hA} = \bar{\eta}(E) - \alpha_n \ln \nu$$

$$\sigma_\eta^{hA} = \sigma_\eta(E) - \beta_n \ln \nu$$

Reference

Aggarwal, M.M., et al., 1977, Nucl. Phys. B131, 61.

Aggarwal, M.M., et al., 1984, Phys. Rev. D29, 150.

Alknazov, G. D. et al., 1975, Phys. Lett 57B, 47.

Baksay, L., et al., 1978, Nucl. Phys. B141, 1.

Battiston, R., et al., 1982, Phys. Lett. 115B, 333.

Baksay, L., et al., 1978, Nucl. Phys. B141, 1.

Barton, D.S., et al., 1983, Phys. Rev. D27, 2580.

Beaugpre, J. V., et al., 1971, Phys. Lett. 37B, 431.

Benecke, J., et al., 1969, Phys. Rev. 188, 2159.

Berger, Ch., et al., 1980, Phys. Lett. 95B, 313.

Bertin, A., et al., 1973, Phys. Lett. 42B, 493.

Böhm, A., et al., 1974, Phys. Lett. 49B, 491.

Buras, A.J., et al., 1973, Phys. Lett. 47B, 251.

Burq, J.P., et al., 1982, Phys. Lett. 109B, 124.

Busza, W., 1977, Acta Phys. Polon. B8, 333.

Busza, W., 1975, in High Energy Physics and Nucleus Structure (A.I.P.). p. 211.

Busza, W., 1977, in Proc. 12th Rencontre De Moriond on Deep Scattering and Hadronic Structure edited by J. Tran Thanh Van (Rencontre de Moriond). p.129.

CERN-College de France-Heidelberg-Karlsrube Collab., D.Drijard et al., 1980, Nucl. Phys. B166, 233.

Chao, W.Q., et al., 1983, Nucl. Phys. A395, 482.

Chiu, C.B. et al., 1982, Phys. Rev. D25, 2911.

Chou, T.T. and C.N. Yang, 1968, Phys. Rev. 170, 1591.

Chou, T.T. and C.N. Yang, 1983, Phys. Lett. 128B, 457.

Chou, T.T. and C.N. Yang, 1984, Phys. Lett. 135B, 175.

De Marzo, C., et al., 1982, Phys. Rev D26, 1019

DeTar, C.E., 1972, Phys. Rev D3, 128.

Eichten, T. et al.,1978, Nucl. Phys. B44, 333.

Elias, J.E., et al., 1980, Phys. Rev. D22, 13.

Feynman, R.P., 1969, Phys. Rev. Lett. 23, 1415.

Feynman, R.P.,1972, Photon-Hadron Interaction (W.A.Benjamin,Inc, New York)

Florian, J. et al., 1976, Phys. Rev. D13, 558.

Giacomelli, G. and M. Jacob, 1979, Phys. Rep. 55, 1.

Gribov, L.V. et al., 1983, Phys. Rep. 100, 1.

Gross, D. and F. Wilczek, 1973, Phys. Rev. Lett. 30, 1343.

Gottfried, K., 1974, Phys. Rev. Lett. 32, 957.

Hofstadter, R. and R. Herman, 1961, Phys. Rev. Lett. 6, 293.

Hwa, R.C., 1984, Phys. Rev. Lett., 52, 492.

Kac, M., 1973, Nucl. Phys. B62, 402.

Kaur, M., et al., 1978, Nuovo Cim. A45, 161.

Kiang, D., C. S. Lam, S. H. Ling and K. Young, 1983, Chinese University of Hong Kong Preprint.

Koba, Z., H.B. Nielson and P. Oleson, 1972, Nucl. Phys B40, 317.

Koch, W., 1982, in Proc. 13th Int. Symp. on Multiparticle Dynamics, Volendam edited by W. Kittel, W. Metzger and A. Stergiou (Singapore: World Scientific) p.543.

Kopylov, G. I., 1974, Phys. Lett. 50B, 472.

Kumar, V., et al., 1978, J. Phys. Soc. Jpn. 44, 1078.

Lam, C.S. and M. A. Walton ,1983, preprint.

Moffeit, K.C. et al., 1972, Phys. Rev. D5, 1603.

Politzer, H. D., 1973, Phys. Rev. Lett. 30, 1346.

Saleem, M. et al., 1981, Nuovo Cimento Lett. 31, 167.

Slattery, P., 1972, Phys. Rev. Lett. 29, 1624.

UA5 Collab., K. Alpgård et al., 1981, Phys. Lett. 107B,

315.

UA5 Collab., K. Alpgård et al., 1983, Phys. Lett. 123B, 361.

UA5 Collab., G. J. Alner et al., 1984, Phys. Lett. 138B, 304.

Thome, W., et al., 1977, Nucl. Phys. B129, 365.

Whitemore, J., 1974, Phys. Rep. 10C, 237.

Zieminska, D., et al., 1983, Phys. Rev. D27, 47.